
This item was submitted to [Loughborough's Research Repository](#) by the author.
Items in Figshare are protected by copyright, with all rights reserved, unless otherwise indicated.

Glucose diffusivity in tissue engineering membranes and scaffolds: implications for hollow fibre membrane bioreactor

PLEASE CITE THE PUBLISHED VERSION

PUBLISHER

© Hazwani Suhaimi

PUBLISHER STATEMENT

This work is made available according to the conditions of the Creative Commons Attribution-NonCommercial-NoDerivatives 4.0 International (CC BY-NC-ND 4.0) licence. Full details of this licence are available at:
<https://creativecommons.org/licenses/by-nc-nd/4.0/>

LICENCE

CC BY-NC-ND 4.0

REPOSITORY RECORD

Suhaimi, Hazwani. 2015. "Glucose Diffusivity in Tissue Engineering Membranes and Scaffolds: Implications for Hollow Fibre Membrane Bioreactor". figshare. <https://hdl.handle.net/2134/18297>.



Glucose Diffusivity in Tissue Engineering Membranes and Scaffolds: Implications for Hollow Fibre Membrane Bioreactor

Hazwani Suhaimi

*A doctoral thesis submitted in partial fulfillment of the requirements for
the award of Doctor of Philosophy of Loughborough University*

Department of Chemical Engineering

May 2015

© by Hazwani Suhaimi (2015)

ABSTRACT

Unlike thin tissues (e.g., skin) which has been successfully grown, growing thick tissues (e.g., bone and muscle) still exhibit certain limitations due to lack of nutrients (e.g., glucose and oxygen) feeding on cells in extracapillary space (ECS) region, or also known as scaffold in an *in vitro* static culture. The transport of glucose and oxygen into the cells is depended solely on diffusion process which results in a condition where the cells are deprived of adequate glucose and oxygen supply. This condition is termed as hypoxia and leads to premature cell death. Hollow fibre membrane bioreactors (HFMBs) which operate under perfusive cell culture conditions, have been attempted to reduce the diffusion limitation problem. However, direct sampling of glucose and oxygen is almost impossible; hence noninvasive methods (e.g., mathematical models) have been developed in the past. These models have defined that the glucose diffusivity in cell culture medium (CCM) is similar to the diffusivity in water; thus, they do not represent precisely the nutrient transport processes occurring inside the HFMB.

In this research, we define glucose as our nutrient specie due to its limited published information with regard to its diffusivity values, especially one that corresponds to cell/tissue engineering (TE) experiments. A series of well-defined diffusion experiments are carried out with TE materials of varying pore size and shapes imbibed in water and CCM, namely, cellulose nitrate (CN) membrane, polyvinylidene fluoride (PVDF) membrane, poly(L-lactide) (PLLA) scaffold, poly(caprolactone) (PCL) scaffold and collagen scaffold. A diffusion cell is constructed to study the diffusion of glucose across these materials. The glucose diffusion across cell-free membranes and scaffolds is investigated first where pore size distribution, porosity and tortuosity are determined and correlated to the effective diffusivity. As expected, the effective diffusivity increases correspondingly with the pore size of the materials. We also observe that the effective glucose diffusivity through the pores of these materials in CCM is smaller than in water. Next, we seeded human osteoblast cells (HOSTE85) on the scaffolds for a culture period of up to 3 weeks. Similar to the first series of the diffusion experiments, we have attempted to determine the effective

glucose diffusivity through the pores of the scaffolds where cells have grown at 37°C. The results show that cell growth changes the morphological structure of the scaffolds, reducing the effective pore space which leads to reduced effective diffusivity.

In addition, the self-diffusion of glucose in CCM and water has also been determined using a diaphragm cell method (DCM). The results have shown that the glucose diffusivity in CCM has significantly reduced in comparison to the water diffusivity which is due to the larger dynamic viscosity of CCM. The presence of other components and difference in fluid properties of CCM may also contribute to the decrease.

We finally employ our experimentally deduced effective diffusivity and self-diffusivity values into a mathematical model based on the Krogh cylinder assumption. The glucose concentration is predicted to be the lowest near the bioreactor outlet, or in the scaffold region, hence this region becomes a location of interest. The governing transport equations are non-dimensionalised and solved numerically. The results shown offer an insight into pointing out the important parameters that should be considered when one wishes to develop and optimise the HFMB design.

Keywords: Glucose; Diffusivity; Cell culture medium; Membrane; Scaffold; Osteoblast cell; Mathematical modelling; Hollow fibre membrane bioreactor; Tissue engineering

ACKNOWLEDGEMENT

In the name of Allah, the Most Gracious and the Most Merciful

I would like to begin with by thanking and praising Allah for His countless blessings and strengths He has bestowed upon me in completing this thesis.

My deepest and sincerest thanks go to my supervisor, Dr Diganta Bhusan Das, who has helped me to see the end of this PhD journey through his valuable suggestions, comments and advice. His patience and diligence in guiding me is greatly appreciated. Under his supervision, I am able to develop my skills as a researcher and an individual.

I would also like to thank Dr John Ward from the Department of Mathematical Sciences for sharing his insights on the mathematical model. I also want to thank Professor Victor Starov for giving valuable suggestions and recommendations especially in the beginning of my research. A special mention goes to David Smith, who is now enjoying his retirement, for rendering assistance a lot of times during the course of my biological experiments. Many thanks to Tim Coles, Monika Pietrzak and Sean Creedon for their technical assistance in the biological lab. The help of Tony Eyre, Steve Bowler and Mark Barron from the mechanical workshop in the construction of the diffusion cell is greatly appreciated. My thanks also go to Paul Izzard for IT support. My appreciation extends to Shaun Fowler and Dr Keith Yendall from the Department of Materials for giving me access to the benchtop SEM for material characterisation. I am very grateful to the finance and administrative staff for their help in purchasing chemicals and equipment.

I am grateful to Ministry of Education of Brunei for a scholarship and financial support throughout my studies here starting from first degree and all the way to PhD. Unit Penuntut-Penuntut in London is highly acknowledged for looking after my welfare here.

I would like to thank my lab mates in room S128 and my office mates in room S130 as well as friends from the department for their kind friendship and helping me to get

through some tough times and making my stay here a memorable one. Special thanks go to Shuai Wang, who is also now a fellow PhD student, for her help in the experiments and chats about China which I have always enjoyed. A special mention goes to my friends back in Brunei, old and new, whom have always believed in me. Not to forget Dr Adibah, a friend since childhood, who has always listened to my worries and assisted me a lot in biological terms. To Azan and Pla, we started at the same time and we almost finish at the same time too. Pla, thank you for being my PhD buddy and listening to my daily ramblings and I hope our friendship will last for life. Azan, my housemate of 4 years and travel buddy, know that I am always grateful for the random chats and trips to keep us sane. A big thank you to Rahimah for the late night lab sessions together as well as Kak Shikin and Manal for sharing their insights and quick lunches at tea room.

For my family who always stands behind my back, words cannot describe how much I appreciate the support you have given me. A very special gratitude goes to my parents, Haji Suhaimi Haji Tuah and Hajah Norhanney Abdullah for always supporting my decision to embark on this journey and for making me a person of who I am today, for the sacrifices they have made throughout my 7 years of study here as well as the silent prayers they have made for me. To my sisters, Norhamizah and Nurul Najibah, for always believing in me, sharing the most of my anxiety and happiness, seeing me through the difficult times, countless sacrifices made for my benefit and being an inspiration to me, I am forever indebted. To my family who will be the most happiest to see the completion of this thesis, I am dedicating this to you.

TABLE OF CONTENTS

ABSTRACT	ii
ACKNOWLEDGEMENT.....	iv
TABLE OF CONTENTS	vi
LIST OF PUBLICATIONS	ix
ABBREVIATIONS	xi
NOMENCLATURE.....	xiv
LIST OF TABLES	xvi
LIST OF FIGURES	xviii
CHAPTER 1 INTRODUCTION	1
1.1 Background	1
1.2 Objectives	3
1.3 Thesis structure	4
CHAPTER 2 LITERATURE REVIEW	6
<i>Chapter overview</i>	<i>6</i>
2.1 Introduction.....	6
2.2 Measurements of glucose concentration or diffusivity	18
2.2.1 Needle enzyme electrodes.....	19
2.2.2 Diffusion cell	20
2.2.3 Refractive index method	21
2.2.4 Dispersion model method	23
2.2.5 Six cross-flow cell unit method	24
2.3 Porosity and tortuosity of tissue engineering membranes and scaffolds ...	29
2.4 Microstructure and diffusion.....	32
2.5 Glucose diffusivities in liquids	35
2.6 Chapter summary	39
CHAPTER 3 GLUCOSE DIFFUSIVITY IN CELL CULTURE MEDIUM... 42	
<i>Chapter overview</i>	<i>42</i>
3.1 Introduction.....	42
3.2 Experimental	44
3.2.1 Materials.....	44

3.2.2 Diffusion cell design	44
3.2.3 Experimental process	45
3.2.3.1 Calibration of the diffusion cell	45
3.2.3.2 Methodology for diffusion experiments	48
3.3 Results and discussions	49
3.4 Chapter summary	53
CHAPTER 4 GLUCOSE DIFFUSIVITY OF TISSUE ENGINEERING MEMBRANES AND SCAFFOLDS.....	54
<i>Chapter overview</i>	54
4.1 Introduction	55
4.2 Materials and methods	62
4.2.1 Membranes	62
4.2.2 Scaffolds	62
4.2.3 Other materials	63
4.2.4 Determination of pore size distribution of the membrane and scaffold materials	66
4.2.5 Evaluation of the porosity (ϵ) and tortuosity (τ) of the membrane and scaffold materials	66
4.2.6 Measurement of glucose diffusion coefficient.....	68
4.2.6.1 Diffusion cell for measurement of glucose diffusion coefficient	68
4.2.6.2 Measurements of glucose diffusivities of the samples saturated in water	69
4.2.6.3 Measurements of glucose diffusivities of the samples saturated in CCM	70
4.2.7 Determination of glucose diffusion coefficient in liquid.....	71
4.3 Results and discussions	72
4.3.1 Material characterization	72
4.3.2 Atomic force microscopy (AFM) observation for surface roughness	74
4.3.3 Glucose diffusion analysis	76
4.3.4 Relationship between porosity (ϵ) and tortuosity (τ).....	81
4.4 Chapter summary	83
CHAPTER 5 GLUCOSE DIFFUSIVITY IN CELL-SEEDED TISSUE ENGINEERING SCAFFOLDS.....	85
<i>Chapter overview</i>	85
5.1 Introduction	85

5.2 Materials and methods	87
5.2.1 Materials	87
5.2.2 Pore size distribution determination and morphological structure of scaffolds	90
5.2.3 Scaffold preparation.....	90
5.2.4 Cell culture and seeding.....	90
5.2.5 Glucose diffusivity measurement	92
5.3 Results and discussions.....	93
5.3.1 Cell proliferation on scaffolds	93
5.3.2 Glucose diffusion analysis	96
5.4 Chapter summary	101
CHAPTER 6 GLUCOSE TRANSPORT IN HOLLOW FIBRE MEMBRANE BIOREACTOR FOR TISSUE ENGINEERING: MATHEMATICAL MODELLING USING EXPERIMENTAL MEASUREMENTS OF GLUCOSE DIFFUSIVITY	102
<i>Chapter overview</i>	102
6.1 Introduction.....	103
6.2 Mathematical model development.....	104
6.2.1 Glucose transport equations.....	107
6.2.2 Non-dimensionalisation	109
6.2.3 Numerical procedure.....	111
6.3 Results and discussions.....	112
6.3.1 Effect of fibre spacing on glucose concentration.....	112
6.3.2 Effect of bioreactor length on glucose concentration	115
6.3.3 Effect of cell density on glucose concentration	117
6.4 Chapter summary	119
CHAPTER 7 CONCLUSIONS AND FUTURE WORK	120
7.1 Conclusions.....	120
7.2 Future work.....	121
REFERENCES.....	124
APPENDIX.....	A1

LIST OF PUBLICATIONS

Journal

- Suhaimi H, Das DB (2015) Glucose diffusion in tissue engineering membranes and scaffolds: a review, *Reviews in Chemical Engineering* (revised version resubmitted) (Chapter 2)
- Suhaimi H, Wang S, Das DB (2015) Glucose diffusivity in cell culture medium, *Chemical Engineering Journal*, Vol. 269, 323-327, DOI: 10.1016/j.cej.2015.01.130 (Chapter 3)
- Suhaimi H, Wang S, Thornton T, Das DB (2015) On glucose diffusivity of tissue engineering membranes and scaffolds, *Chemical Engineering Science*, Vol. 126, 244-256, DOI: 10.1016/j.ces.2014.12.029 (Chapter 4)
- Suhaimi H, Das DB (2015) Glucose diffusivity in cell-seeded tissue engineering scaffolds, *Biotechnology letters* (revised version resubmitted) (Chapter 5)
- Suhaimi H, Ward J, Das DB (2015) Glucose transport in hollow fibre membrane bioreactor for tissue engineering: mathematical modelling using experimental measurements of glucose diffusivity, *Chemical Engineering Science* (under preparation) (Chapter 6)

Conference

- Suhaimi H, Wang S, Thornton T, Das DB (2013) Transport properties of membranes and scaffolds for tissue engineering bioreactors, *Davis Swindin Memorial Lecture Conference*, Loughborough, UK, 24 June 2013
- Suhaimi H, Wang S, Das DB (2014) Glucose transport properties of tissue engineering membranes and scaffolds, *The 2014 Tissue Engineering Congress Conference*, London, UK, 2-4 June 2014

- Suhaimi H, Wang S, Das DB (2014) Glucose transport properties of tissue engineering membranes and scaffolds, Research Challenges in Focus Conference, Loughborough, UK, 18 June 2014
- Suhaimi H, Wang S, Das DB (2014) Glucose transport properties of tissue engineering membranes and scaffolds, Tissue and Cell Engineering Society (TCES) 2014 Annual Meeting Conference, Newcastle, UK, 2-4 July 2014
- Wang S, Suhaimi H, Das DB (2015) Glucose diffusivity in cell culture medium used in tissue engineering bioreactor, The 6th APS International PharmSci 2015, Nottingham, UK, 7-9 September 2015

Presentation

- Title of presentation: Glucose transport properties of tissue engineering membranes and scaffolds, Seminar room S173, Department of Chemical Engineering, Loughborough University, UK, 18 March 2014

ABBREVIATIONS

AF	Annulus fibrosus
AFM	Atomic force microscopy
AP	Anterior-posterior
BSA	Bovine serum albumin
BTE	Bone tissue engineering
CCM	Cell culture medium
CDE	Convection-diffusion equation
CG	Chitosan-gelatin
CN	Cellulose nitrate
CS	Chondroitin sulfate
DCM	Diaphragm cell method
DE	Diffusion equation
Dex-TA	Dextran-tyramine
DMEM	Dulbecco's modified eagle medium
ECM	Extracellular matrix
ECS	Extracapillary space
FBS	Foetal bovine serum
FESEM	Field emission scanning electron microscopy
FRAP	Fluorescence recovery after photobleaching
FTIR	Fourier transform infrared microscopy
GAG	Glycosaminoglycan
GEL	Gelatin
HA	Hydroxyapatite

HFMB	Hollow fibre membrane bioreactor
HOSTE85	Human osteoblast cell
HPCTS	Hydroxypropyl chitosan
HRF	High resonant frequency
IAF	Inner annulus fibrosus
ICC	Inverted colloidal crystal
MAF	Middle annulus fibrosus
MAPLE	Mathematical problem-solving and programming environment
MATLAB	Matrix laboratory
ML	Medial-lateral
MSD	Mean square displacement
NEAA	Non-essential amino acid
NiPAAm	<i>N</i> -isopropylacrylamide
NMR	Nuclear magnetic resonance microscopy
OAF	Outer annulus fibrosus
OECM	Open-end capillary method
PAI	Poly(amide-imide)
PBS	Phosphate buffered saline
PCL	Poly(caprolactone)
PES	Polyethersulfone
PGA	Polyglycolic acid
PGS	Poly(glycerol sebacate)
PLGA	Poly(lactic-co-glycolic acid)
PLLA	Poly(L-lactide)
PSf	Polysulfone
PTFE	Polytetrafluoroethylene

PTT	Poly(trimethylene terephthalate)
PU	Polyurethane
PVA	Polyvinyl alcohol
PVDF	Polyvinylidene fluoride
RDE	Reaction-diffusion equation
RPM	Revolution per minute
RTD	Residence time distribution
SEM	Scanning electron microscopy
SI	Superior-inferior
SPEKK	Sulfonated poly(ether ether ketone ketone)
ssDNA	Single-stranded deoxyribonucleic acid
TE	Tissue engineering
TEM	Transmission electron microscopy
TFC	Thin film composite
TIRF	Total internal reflection fluorescence microscopy
TMJ	Temporomandibular joint
β -CD	β -cyclodextrin
β -TCP	β -tricalcium phosphate
3D	Three dimensional

NOMENCLATURE

Symbol	Description	Unit
D_e	Effective diffusivity	m^2/s
D	Self-diffusivity	m^2/s
ε	Porosity	-
τ	Tortuosity	-
β	Cell calibration constant	m^{-2}
t	Diffusion time	s
i	Initial	-
f	Final	-
k_B	Boltzmann's constant	J/K
T	Temperature	K
η	Dynamic viscosity	$\text{kg}/\text{m}/\text{s}$
r	Stokes radius	m
\emptyset	Association factor	-
M	Relative molecular mass	g/mol
V	Molar volume	cm^3/mol
v_d	Donor volume	m^3
v_m	Solid volume	cm^3
v_t	Total volume	cm^3
ρ_w	Water density	g/cm^3
m_1	Dry membrane/scaffold mass	g
m_2	Pycnometer mass with water	g
m_3	m_2 and membrane/scaffold contained inside	g
c_d	Donor concentration	mg/ml
c_r	Receptor concentration	mg/ml

R_a	Average surface roughness	nm
R_{rms}	Root mean squared	nm
N	Number of sample points	-
a	Fibre inner radius	m
m	Fibre membrane thickness	m
l	Fibre length	m
A	Krogh cylinder radius	m
U_0	Average axial flow velocity	m/s
ν	CCM kinematic viscosity	m ² /s
D_l	Lumen diffusivity	m ² /s
D_m	Membrane diffusivity	m ² /s
D_s	Scaffold diffusivity	m ² /s
D_s^{cell}	Cell-seeded scaffold diffusivity	m ² /s
C_0	Inlet concentration	mol/m ³
n	Cell seeding density	cells/m ³
k_0	Uptake rate per cell	mol cell ⁻¹ s ⁻¹
nk_1	Consumption rate coefficient	s ⁻¹
ϵ	Fibre lumen aspect ration	-
δ	Dimensionless membrane thickness	-
R	Dimensionless Krogh cylinder radius	-
D_m^*	Normalized membrane diffusivity	-
D_s^*	Normalized scaffold diffusivity	-
Pe	Péclet number	-
Da	Damköhler number	-
Re	Reynolds number	-
λ	Effective mass transfer coefficient	m/s

LIST OF TABLES

Table 2.1: Some examples of membranes showing different morphological structures. Different morphological structure of these materials affect the glucose diffusivity though the materials	15
Table 2.2: Effective diffusivities of glucose in swelling N-isopropylacrylamide (NiPAAm) gel (Andersson et al., 1997)	24
Table 2.3: Glucose diffusivities in mixed-matrix membranes (Adams et al., 2013)	25
Table 2.4: Examples of measured glucose diffusivity values for typical tissue engineering membranes and scaffolds	26
Table 2.5: Porosity-tortuosity relations for idealised porous materials	31
Table 2.6: Porosity and tortuosity values in TE membranes and scaffolds (Suhaimi et al., 2015b).....	31
Table 2.7: Fabrication details of SPEKK membranes (Li et al., 2007).....	34
Table 2.8: Typical diffusing solutes and their respective diffusivities	38
Table 3.1: Self-diffusivities of glucose in CCM and water	51
Table 4.1: Some examples of commonly used support porous materials and their characteristics	57
Table 4.2: Summary of the commercial membrane and scaffold properties	64
Table 4.3: Material thicknesses as measured a surface profiling instrument (Talysurf CLI 2000, Taylor Hobson Ltd, Leicester, UK), and their respective swelling percentage. Please note that the average thicknesses we have measured vary slightly from the values of average thickness that the manufactures provide for the same samples (Table 4.2)	65
Table 4.4: Dynamic viscosities of liquids at different temperatures (determined in-house using a U-tube viscometer)	71
Table 4.5: Roughness parameters of Cellulose Nitrate and Polyvinylidene Fluoride (PVDF) membranes.....	76
Table 4.6: Effective diffusion coefficients with standard deviations for glucose across membranes/scaffolds saturated in water and CCM	79
Table 4.7: Comparison of the diffusion coefficient values for liquid only calculated from Stokes-Einstein's equation and found in previous papers as well as experimentally determined diffusion coefficient values	80
Table 4.8: Experimentally-calculated porosity and tortuosity for all materials.....	82
Table 4.9: Porosity-tortuosity relations for ideal porous materials saturated with water.....	82

Table 5.1: Summary of the commercial scaffold properties.....	89
Table 5.2: Effective diffusion coefficients with standard deviations for glucose across blank and cultured scaffolds saturated in CCM.....	100
Table 6.1: Values of dimensional parameter used in the present model	106
Table 6.2: Values of non-dimensional parameter used in the present model	110

LIST OF FIGURES

Figure 2.2: Schematic diagram showing a single hollow fibre.....	10
Figure 2.3A: Overview of the number of papers published with regard to tissue engineering membranes and scaffolds during the last 18 years (key words: membranes and scaffolds for tissue engineering; search engine: www.scopus.com).....	11
Figure 2.3B: Overview of the number of papers published with regard to glucose transport in tissue engineering materials during the last 18 years (key words: glucose transport in tissue engineering membranes and scaffolds, tissue bioreactors; search engine: www.scopus.com)	12
Figure 2.4: Overview of the number of patients on the waiting list, received transplants and the donor statistics from 2000 to 2014.....	12
Figure 2.5: A representation of liquid diffusional pathway in porous media	17
Figure 2.6: SEM micrographs showing surface morphology of (a) PVDF membrane, (b) cellulose nitrate membrane, (c) poly(caprolactone) scaffold, (d) poly(L-lactide) scaffold and (e) collagen scaffold (Suhaimi et al., 2015b)	21
Figure 2.7: SEM micrographs showing surface morphology of (a) PSf membrane, (b) PSf 5% β -CDPU membrane, (c) PSf 8% β -CDPU membrane and (d) PSf 10% β -CDPU membrane (Adams et al., 2013)	24
Figure 2.8: SEM micrographs showing the AP-ML orientation of the collagen fibre in all five regions of the TMJ disc (Shi et al., 2013).....	33
Figure 2.9: SEM micrographs showing axial sections of (a) IAF, (b) MAF, (c) OAF and radial sections of (d) IAF, (e) MAF and (f) OAF (Travascio et al., 2009)	34
Figure 2.10: TEM micrographs of (a ₁) SPEKK-1, (a ₂) SPEKK-2 and (a ₃) SPEKK-3 and AFM micrographs of (b ₁) SPEKK-1, (b ₂) SPEKK-2 and (b ₃) SPEKK-3 (Li et al., 2007)	35
Figure 2.11: The TIRF technique consisted of: (a) optical system, (b) sealing sample solution and (c) penetration of light (Uehara et al., 2014)	37
Figure 3.1: (A) Front section of cell design used in diffusion experiments; (B) Schematic drawing of the diaphragm cell set-up used for glucose diffusion experiments	46
Figure 4.1: Schematic drawing of a diffusion cell	68
Figure 4.2: SEM micrographs showing surface morphology of the selected sample materials: (a) PVDF membrane, (b) Cellulose Nitrate membrane, (c) PCL scaffold, (d) PLLA scaffold and (e) Collagen scaffold.....	73

Figure 4.3: Average pore size distribution of membrane/scaffold as determined by us; x-axis scales are referred as follows: (a) Cellulose Nitrate membrane, (b) PVDF membrane, (c) PCL and PLLA scaffolds and (d) Collagen scaffold. The pore sizes have been manually obtained using ImageJ.....	74
Figure 4.4: AFM topographic images of (A) CN and (B) PVDF membranes.....	75
Figure 4.5: Diffusion cell experiment with 8 mg/ml glucose for both PCL and PLLA scaffolds saturated in CCM at 37°C	78
Figure 4.6: Comparison of porosity-tortuosity relations for all materials which are determined from the experiments in this work and four models of ideal porous material. The equations for the relationship between tortuosity and porosity for ideal porous media saturated with water (Eq. 4.12 – Eq. 4.15) are shown in Table 4.9	83
Figure 5.1: The cell growth curve for HOSTE85 as a function of time where the doubling time of HOSTE85 cells is 1.49 days. The cells were cultured for 5 days and cell number was calculated on each day using a haemocytometer where trypan blue was added into the cell suspension to differentiate between live and dead cells	91
Figure 5.2: Schematic drawing of a diffusion cell to measure the glucose diffusivity across the seeded scaffolds saturated in cell culture medium at 37°C (dimensions of the cell are shown in the figure)	93
Figure 5.3: SEM micrographs showing morphological changes on the surface of collagen, PLLA and PCL scaffolds from no cells attached (blank scaffold) to cells cultured on week 1, week 2 and week 3	94
Figure 5.4: SEM images showing the cross-sectional cell distribution in collagen, PLLA and PCL scaffolds where cells have migrated into on the time points of week 1, week 2 and week 3 of culture period.....	95
Figure 5.5: The approximate number of cells grown on collagen, PLLA and PCL scaffolds at culture time periods of week 1, week 2 and week 3. The difference between cell number contained inside the control well and cell number contained inside the wells that initially were present with scaffold specimens, represents the number of cells that have grown on the scaffolds	96
Figure 5.6: Diffusion cell experiment with 8 mg/ml glucose for cultured collagen scaffold saturated in CCM at 37°C. Both PLLA and PCL scaffolds show similar patterns as collagen scaffold and are not shown in the figure	96
Figure 5.7: Effective diffusion coefficient of glucose in different TE scaffolds at different culture time: (A) collagen scaffold, (B) PLLA scaffold and (C) PCL scaffold	98
Figure 5.8: The relationship between effective diffusivity and seeded cell number for PLLA scaffold. The percentage difference for both cell number and effective diffusivity at different culture time were calculated at the time points of 1, 2 and 3 weeks of culture time with reference to initial time (at 0 week)	101

Figure 6.1: Schematic diagram of a single hollow fibre showing the lumen, membrane and scaffold	105
Figure 6.2: A representation of the Krogh cylinder problem with the relevant governing equations and boundary/interfacial conditions for first-order cell kinetics	110
Figure 6.3: Glucose concentration profile for PVDF-PLLA (without cell) system at 37°C	113
Figure 6.4: Glucose concentration profile for PVDF-PLLA (without cell) system at 37°C for $R = 2.5, 3.2$ and 5 at $z = 1$	114
Figure 6.5: Glucose concentration profile for PVDF-cell-seeded PLLA system at 37°C	114
Figure 6.6: Glucose concentration profile for PVDF-cell-seeded PLLA system at 37°C for $R = 2.5, 3.2$ and 5 at $z = 1$	115
Figure 6.7: Glucose concentration profile for PVDF-PLLA (without cell) system at 37°C for $Pe = 1, 8.06$ and 20 at $z = 1$	116
Figure 6.8: Glucose concentration profile for PVDF-cell-seeded PLLA system at 37°C for $Pe = 1, 8.06$ and 20 at $z = 1$	116
Figure 6.9: Glucose concentration profile for PVDF-cell-seeded PLLA system at 37°C for change in cell density within the scaffold at $z = 1$ for zeroth-order cell kinetics	117
Figure 6.10: Reynolds and Péclet numbers effects on changing the average flow velocity at different fibre length	118
Figure 6.11: The glucose concentration within the scaffold region at different radial position in terms of two dimensionless numbers, Re and Pe	119

CHAPTER 1

INTRODUCTION

1.1 Background

The notion of growing cells *in vitro* was first suggested by Loeb in 1897 (Loeb, 1897). This was followed by numerous experiments where researchers were only able to show cell survival, not growth, until the breakthrough came when Harrison (1907) successfully grew frog ectodermal cells *in vitro*. Up to the mid 1980s, the term tissue engineering was not defined as what it is now. Instead, it was seen as changes of tissues and organs through surgeries as well as the use of biomaterials or prosthetics (Skalak and Fox, 1988). In 1988, tissue engineering was defined as has been used since then:

‘Tissue engineering is the application of the principles and methods of engineering and life sciences toward the fundamental understanding of structure-function relationships in normal and pathologic mammalian tissue and the development of biological substitutes to restore, maintain, or improve function’ (Skalak and Fox, 1988).

Tissue engineering is a relatively new field of regenerative medicine aiming at growing artificial tissues and organs both *in vitro* and *in vivo*. This includes bone cells. Bone diseases such as osteosarcoma, osteoporosis and osteoarthritis and bone defects such as fractures have caused an impact on the health of millions of people and traditional bone defects management mechanisms would require bone grafts (Kim et al., 2014). Autologous bone graft has been widely used and referred to as the ‘gold standard’ but due to several disadvantages (e.g., donor site morbidity and limited availability (Nauth et al., 2011; Starecki et al., 2014)), an alternative treatment is being sought after that is envisioned to be a long lasting cure. This treatment is defined as bone tissue engineering (BTE) approach.

To put it simply, BTE involves harvesting living tissues from a patient's body of relative excess and expansion of these cells *in vitro*, followed by loading of cells on tissue engineering scaffolds in a process known as cell seeding. Once these cells have reached physiologically relevant standards for bone tissue engineering, surgical implantations are performed in reconstructive surgeries and finally evaluation of *in vivo* results is carried out to observe the functionality of the regenerated tissues (Vindigni et al., 2011).

Cell growth chamber, or a bioreactor, is an integral part of *in vitro* cell expansion in providing an optimized cell environment. Before the emergence of bioreactors, cell expansion had been traditionally performed in shake flasks. However, temperature, light condition and media composition were the only parameters that were able to support the growth of cells inside the shake flasks (Chin et al., 2014). Further researches have suggested other essential parameters for optimum cell growth conditions including gaseous composition, mixing, efficient nutrient transfer, pH, hydrodynamic forces and shear stress which can be conveniently controlled in a bioreactor (Hossain et al., 2012; Dong et al., 2013). Hence, the need of a bioreactor system is essential.

Cells are similar to human beings in terms of growth and development. Humans need regular intake of food that contains necessary nutrients such as carbohydrates, proteins and vitamins for healthy growth and robust development. The same principle applies to cells where they require substantial nutrients to grow, multiply and form functional tissues. The distribution and availability of nutrients to living cells is one of the important factors that ensure successful tissue formation, growth and survival. Glucose, oxygen and carbon dioxide are examples of necessary nutrients that pertains the viability and metabolism of cells (Simon et al., 2014).

In a human body, oxygen and nutrients are supplied to cells by the naturally formed blood vessels which are made tailored to deliver enough nutrients but this is not the case for cells grown *in vitro*. Due to the absence of the blood vessels, artificial network of fibres has been suggested to mimic the blood capillary system and this is made possible in the design of a hollow fibre membrane bioreactor (HFMB). The HFMBs is unique in such a way that it allows better nutrient transport and therefore provides a desired nutrient concentration to be maintained inside the HFMBs. Cells are grown on a scaffold and the transport of nutrients within the scaffold is mainly

dominated by diffusion. Although many studies have reported the advantages of growing functional bone tissues (Abdullah and Das, 2007; Pearson et al., 2013; De Napoli et al., 2014; Misener et al., 2014) in HFMBs, one cannot ignore one major problem that persists along with its numerous advantages. To measure the nutrient concentration during tissue formation is not an easy task and proven to be challenging (Chesnick et al., 2007) and with this reason alone, researchers have tried to develop a computational modelling framework that enables the nutrient concentration profiles to be generated (Galban and Locke, 1999; Abdullah et al., 2006; Mohebbi-Kalhari et al., 2012).

Various computational modelling frameworks have been developed and studied to determine the nutrient concentration profiles inside the HFMBs as well as the effect of increasing cell mass grown on the scaffold within the extracapillary space (ECS) of the HFMBs on the transport of nutrients by diffusion. However, as far as we are aware, none of these studies used experimentally determined glucose diffusion coefficient values in cell culture medium (CCM) with tissue engineering membranes and scaffolds imbibed with CCM, which is the typical media for cell/tissue culture experiments. This is applicable to both cell-free and cell-seeded tissue engineering materials. Therefore, we propose in this work, the investigation of glucose diffusion experiments with both cell-free and cell-seeded tissue engineering materials imbibed with CCM as well as the self-diffusion of glucose in CCM at 37-38°C of which diffusivity values will be used for modelling glucose transport.

1.2 Objectives

The overall aim of this research is to analyse the glucose diffusivity in tissue engineering membranes and scaffolds and the implications they have in hollow fibre membrane bioreactors for bone tissue growth. Glucose is chosen in this research as it represents one of the most crucial nutrients for cell growth as well as due to the lack of its diffusivity data in CCM in the literature. As previously mentioned, the diffusivity values of glucose determined experimentally will be employed to generate glucose concentration profiles from the already existed computational modelling framework via MATrix LABoratory (MATLAB) in order to observe any changes with the new values obtained experimentally, instead of the assumed glucose diffusivity values in previous studies.

This research specifically aims to:

- Investigate the self-diffusion of glucose in CCM and water (reference fluid)
- Quantify the relationship between glucose diffusion coefficient and membrane morphology by engaging typical membrane and scaffold materials for tissue engineering in diffusion experiments
- Relate the diffusivity values to the quantitative information of the pore morphology of the tissue engineering materials
- Determine the effects of micro-structural properties of tissue engineering seeded-scaffolds and transport properties of glucose by diffusion
- Link processes at various scales in HFMBs for growing bone tissues by changing the dimensionless groups of variables and numbers in the multiscale modelling framework based on experimentally deduced diffusivity values
- Observe any changes on the glucose concentration profiles based on diffusivity values obtained in-house and determine effective mass transport behaviour in HFMBs

1.3 Thesis structure

This thesis is divided into seven main chapters as discussed briefly below.

Chapter 1 gives a brief background to the work in this thesis as well as the objectives of this research.

Chapter 2 introduces a detailed background of BTE which include a review of measurements of glucose concentration or diffusivity, some techniques used to determine porosity and tortuosity of tissue engineering membranes and scaffolds, microstructure and diffusion and typical methods used to investigate glucose diffusivities in liquids.

Chapter 3 presents the self-diffusion of glucose in CCM and water (reference fluid). In this chapter, glucose diffusion experiments are performed using a diffusion cell based on the diaphragm cell method (DCM) principle. The results of glucose diffusion in CCM and water are discussed and compared with diffusivity values

obtained from Stokes-Einstein's equation as well as from empirical corrections such as Wilke-Chang's correlation.

Chapter 4 discusses a series of well-defined laboratory diffusion experiments to measure the glucose diffusion coefficient across a number of tissue engineering membranes and scaffolds imbibed with water and CCM. A total of five different membranes and scaffolds are outlined in this chapter namely cellulose nitrate membrane, polyvinylidene fluoride membrane, poly(L-lactide) scaffold, poly(caprolactone) scaffold and collagen scaffold of different pore size and thickness. Pore size distribution, porosity and tortuosity evaluation as well as the relationship between diffusivity and membrane microstructure are discussed.

Subsequently, Chapter 5 mimics the work done in Chapter 4 by seeding the scaffolds employed in Chapter 4 with osteoblast cells with an estimated range of size between 20-30 microns. This chapter aims to observe any changes on the mass transfer rate by diffusion and to deduce if the microstructure is changed by cells grown on the surface as well as migrated cells into the scaffold (e.g. pore volume).

Chapter 6 models the mass transfer behaviour in HFMB using the experimental values obtained in Chapters 3, 4 and 5. This chapter illustrates the effect of changing the dimensionless groups of variables and numbers has on the glucose concentration profiles. The dimensionless numbers include Peclet, Damköhler and Reynolds numbers.

Chapter 7 concludes this research as well as recommendations for future work is listed in this chapter.

Finally, references act as a closing part of this thesis.

CHAPTER 2

LITERATURE REVIEW

Chapter overview

Tissue engineering has evolved into an exciting area of research due to its potential in regenerative medicine. The shortage of organ donor as well as incompatibility between patient and donor pose an alarming concern. This has resulted in an interest in regenerative therapy where the importance of understanding the transport properties of critical nutrients such as glucose in numerous tissue engineering membranes and scaffolds is crucial. This is due to its dependency on successful tissue growth as a measure of potential cure for health issues that cannot be healed using traditional medical treatments. In this regard, the diffusion of glucose in membranes and scaffolds which act as templates to support cell growth must be well grasped. Keeping this in mind, the review aims to discuss the glucose diffusivity of these materials. This chapter reviews four interconnected issues, namely, (i) the glucose diffusion in tissue engineering materials, (ii) porosity and tortuosity of these materials, (iii) the relationship between microstructure of the material and diffusion and, (iv) estimation of glucose diffusivities in liquids, which determine the effective diffusivities in the porous membranes or scaffolds. It is anticipated that the review would help improve the understanding of the transport properties of glucose in membranes and scaffolds used in tissue engineering applications.

2.1 Introduction

Organ shortage and failures due to accidental and illness incidences have been a concern in almost every part of the world. Organ transplantation has been a common practice in clinical settings and has been reported to be successful as early as the 1960s (Couch et al., 1966). Although it has been perceived to be successful, it also has its limitations, e.g., long patient waiting time and death of organ donors (Liu et al., 2013; Guo and Ma, 2014). To overcome these limitations, engineers, biologists,

chemists and material experts have come together to create the tissue engineering (TE) approach as an alternative to organ transplantation which provides a cost-effective permanent treatment, resulting in improved health care and quality of lives of the patients. TE is therefore defined as a multidisciplinary field that helps to repair, replace and restore the original functions of damaged tissues (Langer and Vacanti, 1993; Liu et al., 2013). A simple illustration of TE principles is shown in Figure 2.1. As the figure shows, TE approach aims to mimic the *in vivo* environment to help in cell proliferation and differentiation into tissues and consequently tissue regeneration (Tabata, 2014). In brief, living cells are harvested from a patient's body of relative excess followed by expansion of these cells *in vitro*. The cells are then loaded on tissue engineered scaffolds which act as a template for cell growth in a process known as cell seeding. The cells are grown, with the supply of nutrients (e.g., glucose and oxygen), and monitored for its physiologically relevant standards for bone tissue engineering (BTE) in terms of cell-cell and cell-matrix interactions as well as possessing the nanostructural and chemical extracellular matrices (ECM) (Zhu et al., 2015) as found in the native ECM of the body. Surgical implantations into the host body are carried out and finally the functionality of the regenerated tissue is observed *in vivo*.

Due to its numerous successes, TE has become the leading choice in the field of regenerative medicine (Khaled et al., 2011). The main goal of TE is to produce an alternative that can overcome the limitations of traditional treatments and possess a good potential to eventually form an 'artificial' organ that resembles the original organ in terms of function and ability. Furthermore, it is envisaged that a TE approach presents a permanent cure without the need for follow-up therapies (Langer and Vacanti, 1993; Patrick et al., 1998). For example, bone tissue engineering (BTE), which has been reported since the early 1980s (Amini et al., 2012), has become a substitute for bone grafting.

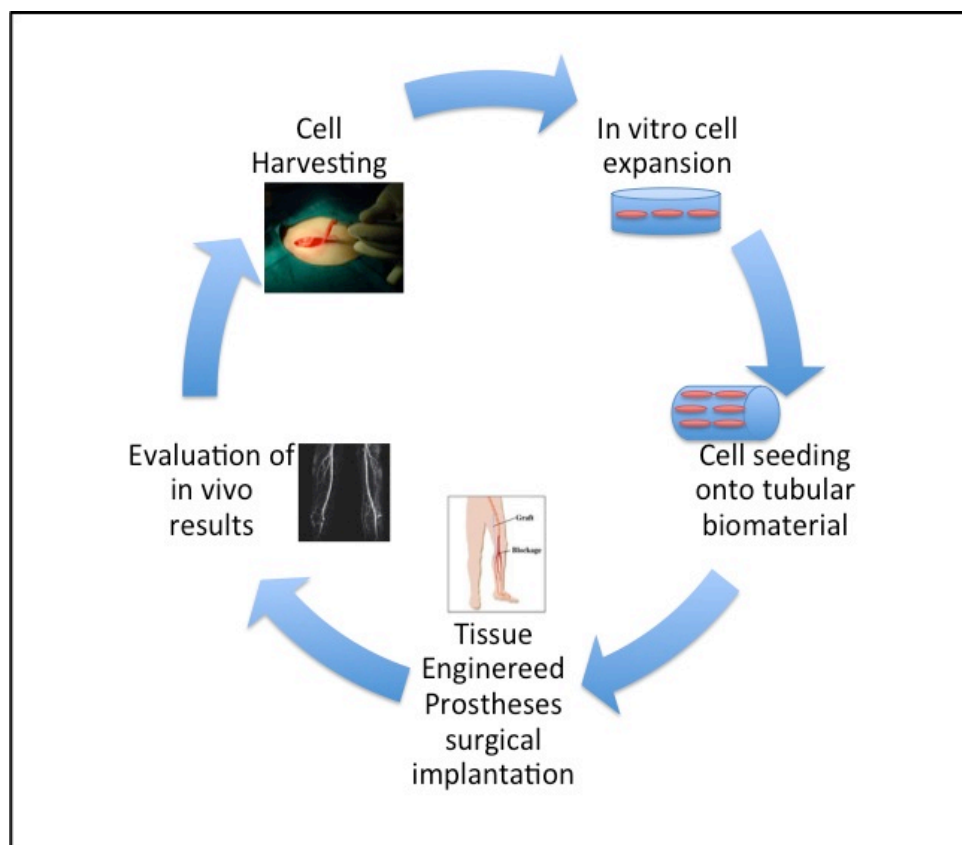


Figure 2.1: Basic principles of tissue engineering (Vindigni et al., 2011)

Tissue engineering researchers have shown the possibility of growing artificial tissues both *in vitro* and *in vivo*, e.g., bone, cartilage, tendon and blood vessel tissues (L'Heureux et al., 2007; Schulz et al., 2008; Abousleiman et al., 2009; Grayson et al., 2010; Kimelman-Bleich et al., 2011; Omae et al., 2012). However, it is proven difficult to grow tissues *in vitro* than *in vivo* due to the absence of a natural capillary network that supplies nutrients (e.g., glucose) and removes waste products (e.g., lactic acid) as well as the inaccessibility of a controlled environment during cell cultivation (Li et al., 2014). Hence, the idea of growing artificial tissues in bioreactors has been introduced.

Bioreactors are defined as a growth kit that helps to monitor and control necessary conditions for cell growth (e.g., pH, pressure, temperature, nutrient supply and removal of waste product) as well as synchronising both biological and biochemical processes involved in cell culture (Gardel et al., 2014). There have been several reported studies that show the development of these bioreactors to grow 3D tissues, such as spinner flasks (Page et al., 2013), rotating vessels (Nishi et al., 2013; Chao and Das, 2015) and flow perfusion systems (Baptista et al., 2013). Although these

bioreactors satisfy tissue engineers to the extent of improved tissue growth, they may still not be able to sustain the cell culture environments (Li et al., 2014). One of the reasons is due to the limited nutrient diffusion in the scaffold and membrane in the bioreactor.

An example of a bioreactor where the issues with limited mass transfer have largely been overcome is hollow fibre membrane bioreactors (HFMBs) (Abdullah et al., 2006; Das and Jones, 2006; Ye et al., 2006; Das, 2007; De Napoli et al., 2011; Mohebbi-Kalhari et al., 2012). The presence of a network of hollow fibre membranes in the bioreactor allows nutrients (e.g., glucose) to diffuse into the scaffolding matrix and membrane, and remove waste products produced by the cells (e.g., lactic acid) (Ye et al., 2006). This therefore allows a nutrient circulation system identical to that in the natural tissue to be generated, consequently creating better mass transfer behaviour and allowing high nutrient concentration to be maintained in HFMBs (Abdullah and Das, 2007; Pearson et al., 2013; De Napoli et al., 2014; Misener et al., 2014).

Mass transfer behaviour in TE bioreactors is generally governed by one or more than one of the following processes, namely, convection, diffusion and reaction. Convection refers to the coupled mass transport due to fluid flow (i.e., advection) and diffusive transport while diffusion refers to the transport of molecules due to concentration gradient alone. Reaction is illustrated by the formation of a new product (for e.g., C) as a result of a chemical or metabolic reaction. An example of a bioreactor that involves all three processes is the HFMBs. Figure 2.2 shows a schematic drawing which reveals the three main sections mainly the extracapillary space (ECS) which can be referred as scaffold, membrane and lumen. In the figure, R_1 refers to the fibre lumen radius while R_2 illustrates R_1 and the thickness of the membrane wall. R_3 represent R_2 and the ECS thickness while L refers to the fibre length. As for A_1 , A_2 and A_3 , they refer to the lumen, membrane wall and half of the ECS, respectively.

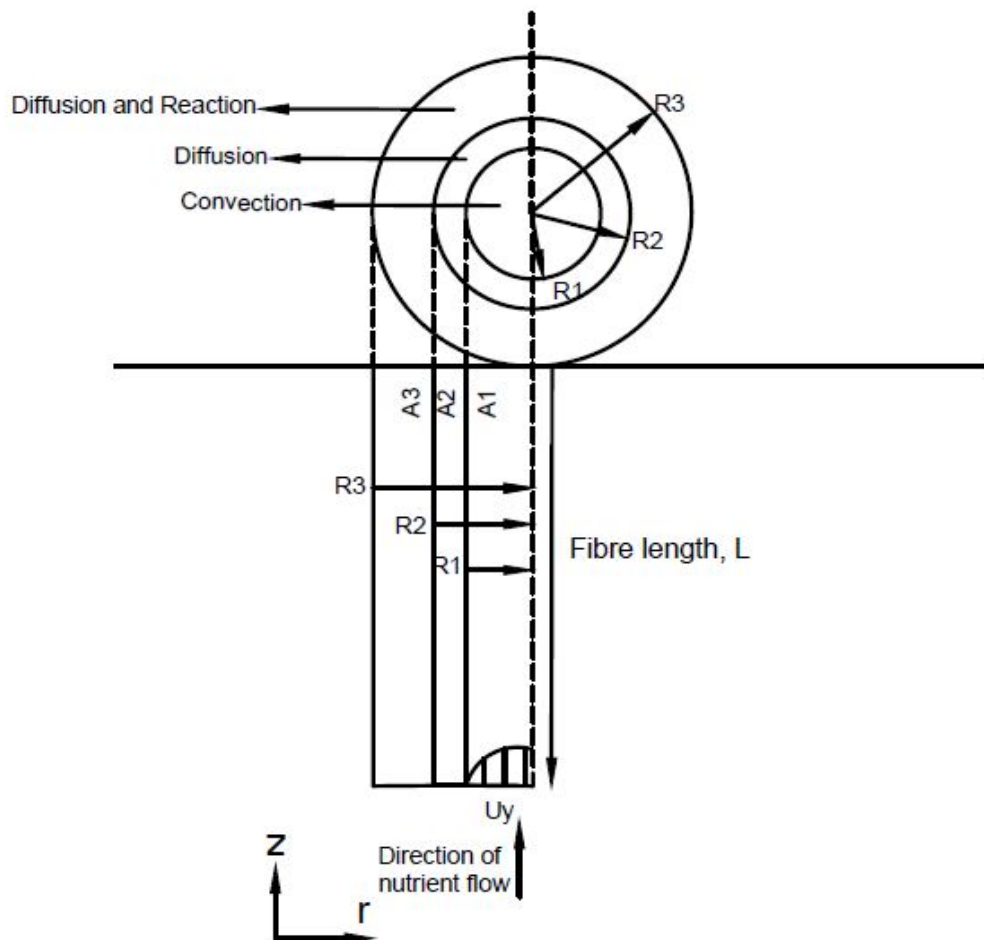


Figure 2.2: Schematic diagram showing a single hollow fibre

According to Ye et al. (2006), Das (2007) and Abdullah et al. (2009), the transport of a solute in the fibre lumen region is governed by advection and diffusion, but the advective process dominates the diffusive process. In the membrane region, solute transport is governed by diffusion only. In the ECS, the solute transport is governed by reaction and diffusion processes; however, reaction process dominates the diffusive transport.

A surge of interest has been observed in trying to understand the mass transfer behaviour in tissue engineering bioreactors (Khaled and Vafai, 2003; Khanafer and Vafai, 2006; Wang et al., 2009; Laatikainen, 2011; Podichetty et al., 2014). In the last two decades, the use of membranes and scaffolds as a synthetic extracellular matrix (ECM) for tissue engineering studies has also gained popularity, which is evidenced from the increasing number of publications (Figure 2.3A and 2.3B). The tissue engineering discipline has grown remarkably and the significance of

understanding the importance of tissue engineering applications is demonstrated by the fact that the number of patients waiting for transplants is almost doubled to those who actually received the transplants, as shown in Figure 2.4 (Regional data, United Network for Organ Sharing). This trend continues where only 27,036 people received transplants while 77,917 people were on the waiting list, from January 2014 to November 2014.

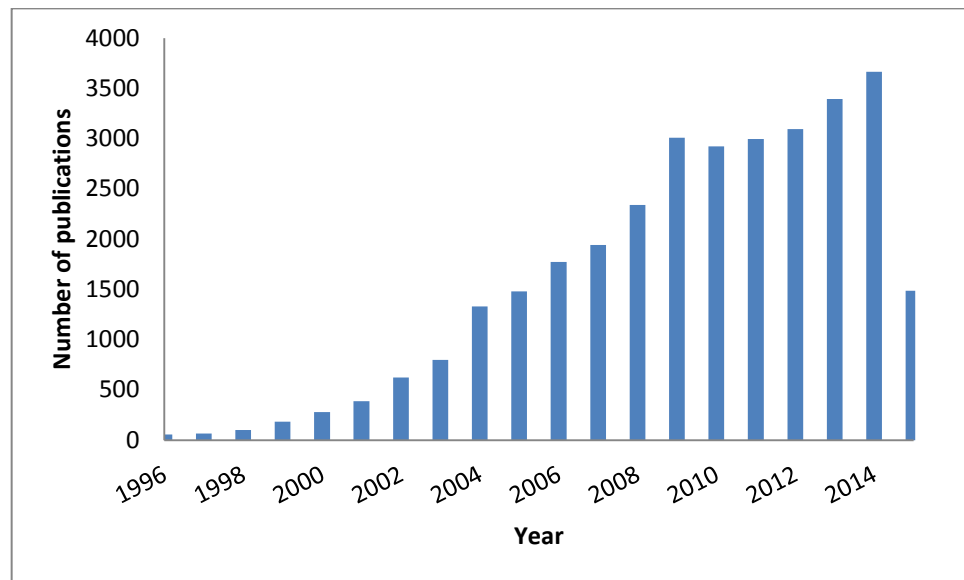


Figure 2.3A: Overview of the number of papers published with regard to tissue engineering membranes and scaffolds during the last 18 years (key words: membranes and scaffolds for tissue engineering; search engine: www.scopus.com)

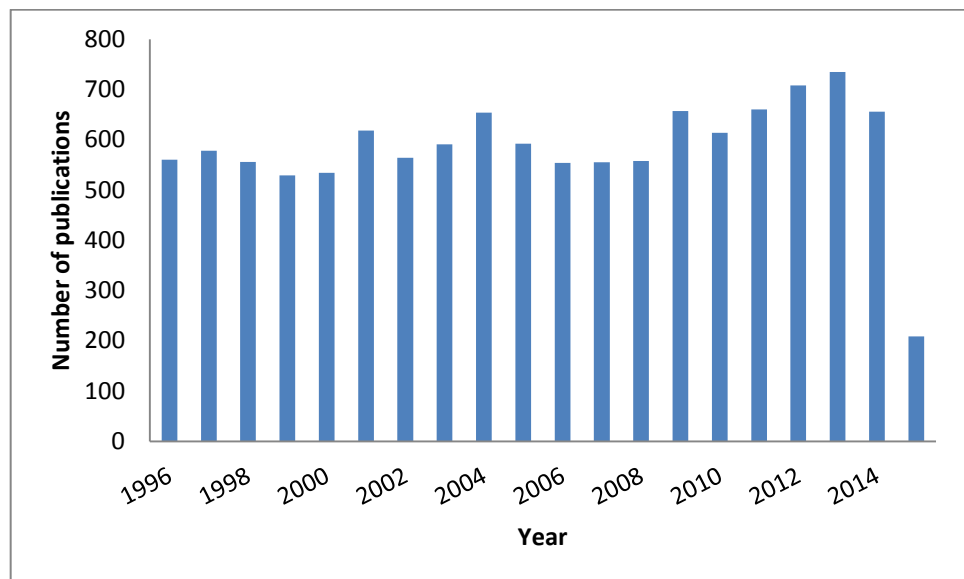


Figure 2.3B: Overview of the number of papers published with regard to glucose transport in tissue engineering materials during the last 18 years (key words: glucose transport in tissue engineering membranes and scaffolds, tissue bioreactors; search engine: www.scopus.com)

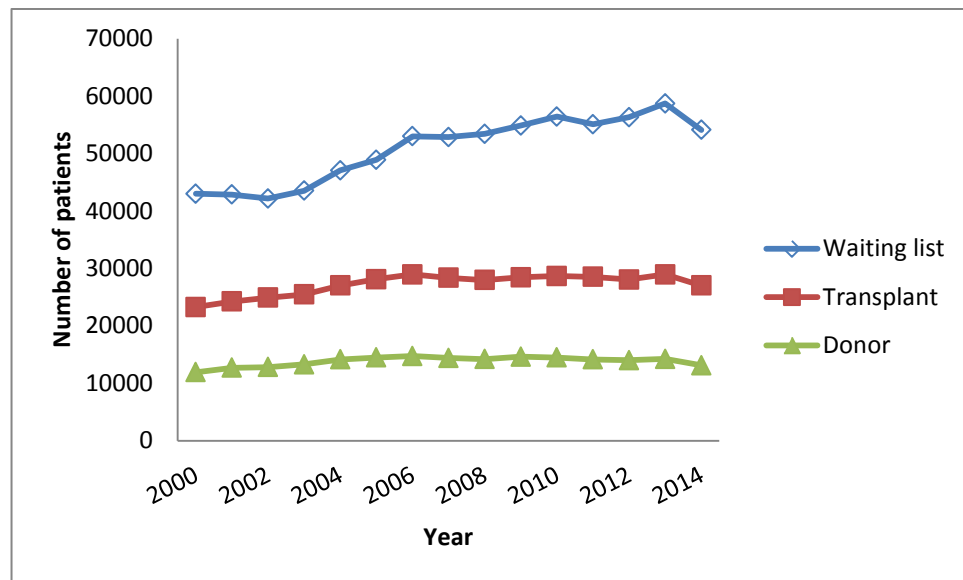


Figure 2.4: Overview of the number of patients on the waiting list, received transplants and the donor statistics from 2000 to 2014

To combat this challenge, numerous studies have been conducted to enhance the understanding of the field of regenerative medicine, more specifically, in the field of tissue engineering and research has already indicated the necessity of a bioreactor system which is essential for a controlled environment during cell cultivation (Li et al., 2014).

One of the key features of most tissue engineering bioreactors is the use of membrane and scaffold which acts as a support for cells to grow into new tissues before being implanted into the host tissue. One of the important criteria of this support system is the highly porous structure for ease of nutrient diffusion, particularly glucose, to produce a 3D structure of new tissues (Deans et al., 2012; Florczyk et al., 2013; Guan et al., 2013). Table 2.1 shows some typical examples of morphological structures of membrane/scaffold materials that can have an effect on the nutrient diffusion for cell growth. These will be discussed later in the chapter. Please note that the materials presented in Table 2.1 might not be necessarily used in tissue engineering applications. The objective here is to show the variation of

morphological structure of various kinds of membranes/scaffolds, which can affect the solute diffusivity.

Since solute diffusion is dependent on the material morphology, there is not a particular membrane structure for better glucose diffusion, however, based from extensive literature studies, hollow fibre membranes seem to illustrate a promising indication for enhanced glucose delivery into the cells (Abdullah and Das, 2007; Bettahalli et al., 2011; Diban and Stamatialis, 2014; Wung et al., 2014). Hollow fibre membranes have a large surface area to volume ratio therefore allowing a relatively high flow rate of culture medium containing glucose to be maintained. The basic building blocks of any membrane material are usually non-periodic and display heterogeneity in nature as they vary within the same material, or from one material to another, which defines the non-linear and non-monotonic relationship between membrane material and glucose transport. If the membrane/scaffold material is less tortuous and more porous, the glucose diffusion is predicted to be smoother and faster than one in a more tortuous structure which limits the glucose diffusion. However, there is a possibility that the glucose diffusion may be enhanced especially in hydrophilic materials but the results of Suhaimi et al. (2015b) indicated no difference between hydrophobic and hydrophilic materials with regard to diffusivity data. In this work, they investigated the glucose diffusion in both hydrophobic and hydrophilic materials and results showed that instead of a difference in diffusivity data due to hydrophobic and hydrophilic nature, the difference in the morphological structure of the materials was deduced as the primary factor for the different diffusivity data presented in their work.

In a tissue engineering process, the supporting template for cell growth plays a crucial role in cell attachment, differentiation and proliferation (Guo and Ma, 2014). Researchers have identified several important characteristics which scaffolds must have, e.g., (1) biocompatibility and biodegradability (2) high porosity and connectivity of pores for diffusion, (3) appropriate surface chemistry and surface topography for cellular interaction, (4) good mechanical properties for regeneration and (5) low/no adverse response (Hutmacher, 2001; Yang et al., 2001; Holzwarth et al., 2011). Due to the importance in tissue engineering processes, several different materials have been investigated to develop potential scaffolds such as ceramics (e.g., hydroxyapatite and tricalcium phosphate) and polymers (Sachlos and

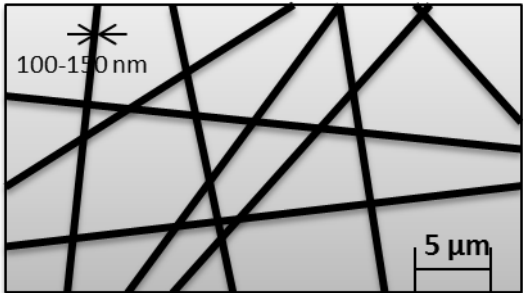
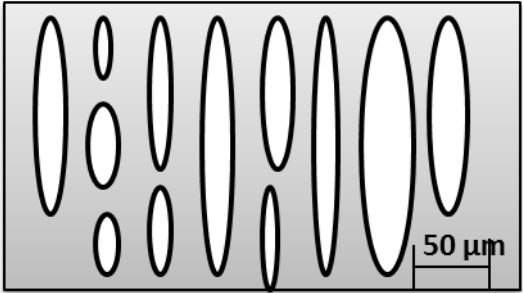
Czernuszka, 2003; Guo and Ma, 2014). For example, polymers have been reported to have a greater potential as scaffolds for tissue engineering purposes due to its processing flexibility and biodegradability (Nair and Laurencin, 2007). Synthetic polymers such as aliphatic polyester (e.g., polyglycolic acid (PGA), polylactic acid (PLLA) and polycaprolactone (PCL)), polyanhydrides, polyphosphazenes (e.g., alanine and phenylalanine alkyl ester), polyurethanes (PUs) and poly(glycerol sebacate) (PGS) and natural polymers such as collagen are some of the most commonly used polymers as scaffolds for TE (Freed and Vunjak-Novakovic, 1998; Agrawal and Ray, 2001; Hutmacher, 2001; Sachlos and Czernuszka, 2003; Nichol et al., 2013; Guo and Ma, 2014; Suhaimi et al., 2015b, 2015c). Melt moulding, solution casting, phase separation, solvent-casting particulate-leaching, emulsion freeze drying, fibre meshes/fibre bonding, freeze drying and gas foaming are some conventional scaffold fabrication techniques cited in the literature (Sachlos and Czernuszka, 2003).

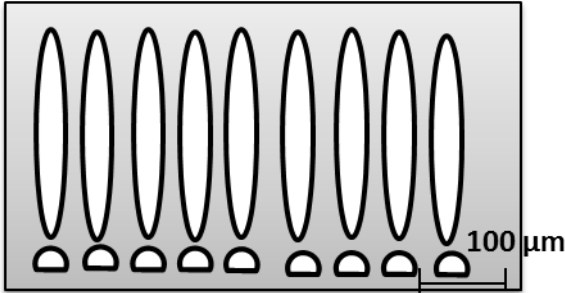
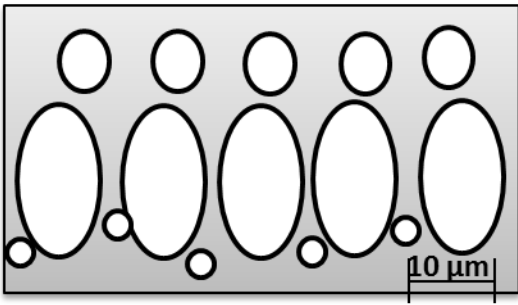
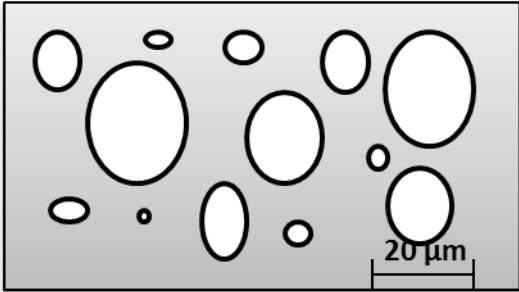
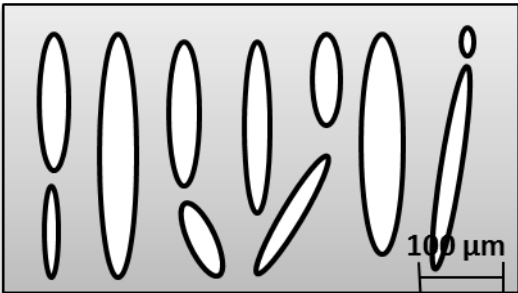
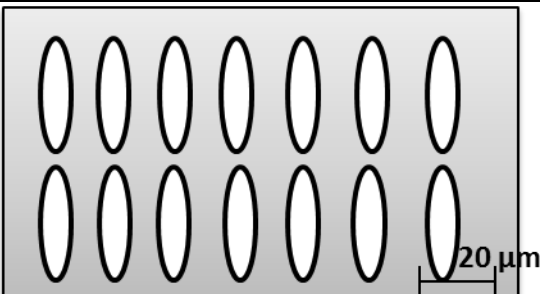
Meneghello et al. (2009) fabricated poly(lactic-co-glycolic acid)/polyvinyl alcohol (PVA) blended hollow fibre membranes where the results demonstrated that 5% (w/w) addition of PVA helped to better transport the cell culture medium and its constituents. Bettahalli et al. (2011) developed poly(L-lactic acid) (PLLA) hollow fiber membranes to test the delivery capability of these membranes to diffuse nutrients to the cells. Results showed that the transport of nutrients was high at a rate of 1963 L/(m² h bar). In the same year, De Napoli and coworkers (De Napoli et al., 2011) investigated cell growth in layers of medical microporous polypropylene hollow fibre membranes and the results showed cells formed thick multilayer among the membranes. More recently, Bettahalli et al. (2014) developed a multilayer scaffold by rolling PLLA electrospun sheets with a multibore hollow fibre membrane and the results showed that the concept illustrated a good potential for developing complex and thicker tissues. Diban et al. (2014) developed a biodegradable poly(ϵ -caprolactone) scaffold and results indicated good cell attachment, proliferation and penetration into the scaffold. Permeance tests also indicated high water permeabilities which is a positive indication of nutrient delivery into the cells.

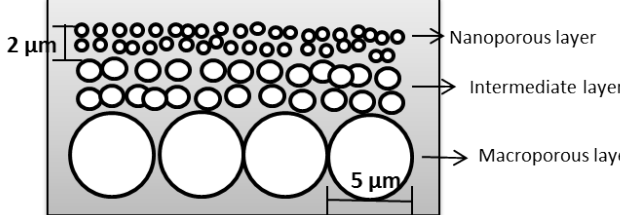
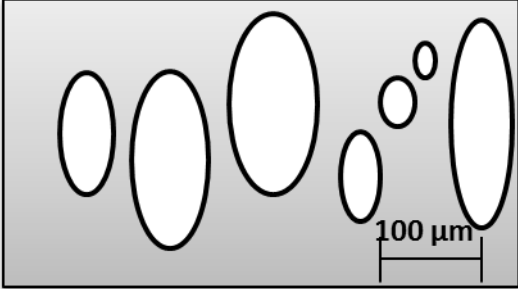
Earlier, Ellis and Chaudhuri (2007) developed a hollow fibre membrane scaffold based on poly(lactide-co-glycolide) (PLGA) sheets. Their results showed that

varying the air gap and spinning temperature significantly changed the morphology of the hollow fibre membrane scaffold, allowing larger macrovoids and thicker skin formed. This is a one step forward in addressing the size limitations in tissue engineered constructs for clinical practice. Chaudhuri et al. (2008) fabricated honeycomb-structured poly(DL-lactide) and poly[(DL-lactide)-co-glycolide] films using water droplet templating method. Osteoblast cells were able to attach and proliferate on these films, suggesting the potential of its application as tissue engineering scaffold. In the same year, Ellis and Chaudhuri (2008) studied the combination of three different lactide:glycolide ratios and results showed that any ratio was able to support bone regeneration *in vitro*. Freed et al. (1993) and Galban and Locke (1999) considered the diffusion of nutrients such as glucose and oxygen in porous scaffolds and both indicated that restriction diffusion of nutrients did limit cell growth, though it may not be the only limiting factor.

Table 2.1: Some examples of membranes showing different morphological structures. Different morphological structure of these materials affect the glucose diffusivity though the materials

Membrane type	Schematic of cross-section	Reference
Poly(trimethylene terephthalate) (PTT) nanofiber membrane		Li et al. (2013) Xue et al. (2010)
Thin film composite (TFC) membrane		Han (2013)

Polysulfone (PSf) membrane		Crock et al. (2013) Zhao et al. (2011)
Poly(vinylidene fluoride) (PVDF) hollow fibre membrane		Sukitpaneenit and Chung (2009) Zhang et al. (2013) Liu et al. (2009)
PVDF membrane		Lin et al. (2002) Li et al. (2012)
Polyethersulfone (PES) membrane		Madaeni and Bakhtiari (2012) Rahimpour et al. (2012) Daraei et al. (2013)
Poly(amide-imide) (PAI) hollow fiber membrane		Setiawan et al. (2011) Zhang et al. (2011)

Ceramic asymmetric membrane		Kim and der Bruggen (2010) DeFriend et al. (2003) Tsuru et al. (2001)
Cellulose acetate blend membrane		Han et al. (2013) Mohammadi and Saljoughi (2009)

Since by definition a porous medium consists of a network of open spaces, in which a network of pores and fibres for membranes and scaffolds exists, the molecular diffusion is interrupted by the tortuous channels and the combination of both porosity and tortuosity characterizes the morphological structure of the porous media (Figure 2.5). A relationship which takes into account the mass transport by diffusion, porosity, as well as the tortuosity, is summarized in Eq. (2.1):

$$D_e = D \frac{\varepsilon}{\tau} \quad (2.1)$$

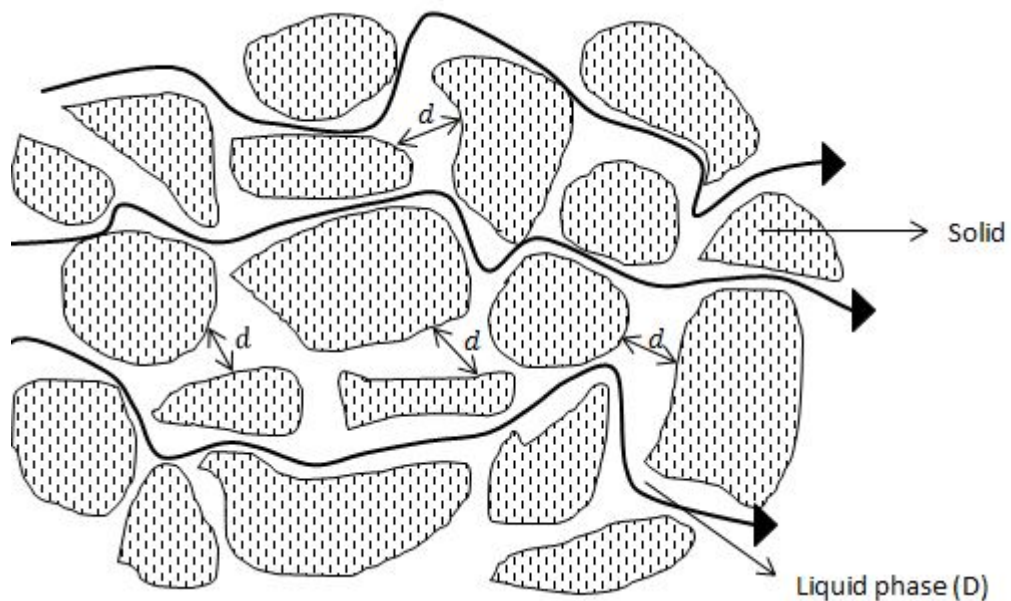


Figure 2.5: A representation of liquid diffusional pathway in porous media

where D_e is the effective diffusion coefficient of the solute in membranes or/and scaffolds, D is the self-diffusion coefficient of the solute in the liquid which fills the pores while ε and τ are porosity and tortuosity of the material, respectively, with the assumption that the average pore diameter, d , is much greater than the mean free path of the solute diffusing in the given liquid.

Keeping these aspects in mind, the present review aims to give an overview of the diffusion of glucose in membranes and gels/scaffolds for tissue engineering applications as well as the self-diffusion of glucose in liquid. In effect, the review is divided into sections, which represent the four terms in Eq. (2.1). Firstly, the review will discuss the measurements of diffusion of glucose in membranes/scaffolds using various methods available. Secondly, it will deal with the techniques available to measure porosity and tortuosity of the porous media. Thirdly, the review will cover the effects of microstructure on the diffusion process. Lastly, the different methods available for the estimation of glucose self-diffusion in liquids will be reviewed briefly, given that their understanding is also required to quantify the effective diffusion of glucose in the membranes/scaffolds.

The field of tissue engineering holds a promising future in such a way that there are some health conditions that cannot be cured just by prescribing some medicines and drugs such as liver failure and spinal cord failure (Langer, 2009). When this happens, apart from organ transplants which induce immunological responses to name a few, tissue engineering is the only hope that remains. It is greatly hoped that the present review will help in understanding the diffusion of nutrient and its effects on the membrane and scaffold microstructure, specifically, and in the field of tissue engineering, generally.

2.2 Measurements of glucose concentration or diffusivity

Numerous glucose diffusion studies have been reported for a vast number of applications ranging from tissue engineering (Hannoun and Stephanopoulos, 1986; Sternberg et al., 1988; Weng et al., 2005; Rong et al., 2006; Papenburg et al., 2007; Wang et al., 2009; Jin et al., 2010; Podichetty et al., 2014), diabetes management (Bindra et al., 1991; Maier et al., 1994; Atanasov and Wilkins, 1996; Wang and Musameh, 2003; Boss et al., 2012), modern laser medicine (Chance et al., 1995; Liu et al., 1996; Tuchin et al., 1997; Wang, 2000; Vargas et al., 2001; Yao et al., 2002;

Bashkatov et al., 2003), pharmaceuticals (Andersson et al., 1997), chemical engineering (Laatikainen, 2011), filtration (Yaroshchuk et al., 2011; Adams et al., 2013), oil and fat industry (Miyagi et al., 2012) and water desalination (Lonsdale et al., 1965; Sherwood et al., 1967). A review of these studies suggests that a number of different techniques could be applied to measure glucose concentration or diffusivity as discussed below.

2.2.1 Needle enzyme electrodes

A number of papers have been reported on the use of needle enzyme electrode to observe glucose diffusion. For example, Rong et al. (2006) presented an interesting work to measure directly the transient glucose concentration at the centre of a specially compressed and rolled collagen gel using needle enzyme electrodes. They first stabilised and calibrated the needle electrodes. Glucose was then oxidised by glucose oxidase enzyme solution to hydrogen peroxide which was further oxidised to form an amperometric current. The current was read by an AUTOLAB PGSTAT10 potentiostat instrument. They also proposed a computational model to fit the simulated concentration profile to the experimental results. The glucose diffusion coefficient was estimated to be $1.3 \times 10^{-10} \text{ m}^2/\text{s}$ (Table 2.4) in the chosen gel and the authors concluded that potential errors sourced from noise, baseline and zero time determination were able to be kept as minimum as possible and consequently resulted in higher accuracy. Wang and Musameh (2003) conducted a study on needle enzyme electrodes to observe the potential of this technique for continuous monitoring of glucose and results demonstrated positive response for future use. Fang et al. (2014) fabricated a glucose electrode coated with poly lactic-co-glycolic acid (PLGA) biodegradable membrane to test the long-term stability of the electrode in bovine serum at 37°C. The condition was to mimic the *in vivo* environment and their results showed 80% of its sensitivity was retained after 44 days inside the serum. They concluded that glucose sensors exhibited a good potential for real time measurements of glucose concentrations inside the body. Glucose biosensors have been developed for over 50 years with the aim of continuous measuring of glucose level. An error of <20% for glucose concentrations ranging between 1.65 and 22 mmol/L should be followed as recommended by U.S.FDA (Yoo and Lee, 2010). Needle enzyme electrode is seen as a good and reliable biosensor for measuring glucose concentration both *in vitro* and *in vivo*.

2.2.2 Diffusion cell

Diffusion cell technique has been regularly used since Hannoun and Stephanopoulos (1986) measured both ethanol and glucose diffusivities in calcium alginate membranes, both seeded and not seeded with cells. More recently, Jin et al. (2010) studied the diffusion of glucose in different molecular weights of dextran-tyramine (Dex-TA) hydrogels to determine the ability of these hydrogels as injectable scaffolds for tissue engineering applications. They used a diffusion cell consisted of two chambers with identical volumes. Both chambers were filled with glucose solution and distilled water, respectively. The diffusion cell was subjected to a 37°C water bath. The concentration of glucose in both chambers were analysed using a UV spectrophotometer at a wavelength of 450 nm. Jin et al. (2010) also employed an enzyme based system to help measure the glucose concentration. As what can be expected of diffusion work in similar cases, the glucose concentration in glucose solution-filled chamber decreased while that of distilled water-filled chamber increased accordingly before reaching a plateau after three days. They also concluded that different molecular weights and degree of substitution of TA groups work well with glucose diffusion where in all cases over 70% of glucose diffused was observed.

Papenburg et al. (2007), in an attempt to observe the glucose diffusion in their own fabricated PLLA micropatterned sheets, also employed a diffusion cell. The glucose diffusion coefficient was measured to be $0.8\text{--}0.1 \times 10^{-10} \text{ m}^2/\text{s}$ (Table 2.4). Boss et al. (2012) used the diffusion cell to measure the glucose diffusion coefficient across nanoporous alumina membrane and results showed a value of $1.35 (\pm 0.31) \times 10^{-10} \text{ m}^2/\text{s}$ (Table 2.4). More recently, Suhaimi et al. (2015b) adopted the diffusion cell method to determine the glucose diffusion coefficient in typical tissue engineering membranes and scaffolds (Figure 2.6) saturated with water and cell culture medium (CCM). Their results demonstrated reduced glucose diffusivities in materials saturated with CCM (e.g., from $1.20 \pm 0.38 \times 10^{-10} \text{ m}^2/\text{s}$ to $0.728 \pm 3.37 \times 10^{-10} \text{ m}^2/\text{s}$ for polyvinylidene fluoride (PVDF) membrane). Diffusion cell method is valid under the assumption of steady state systems which make use of Fick's first law to measure the glucose diffusivity.

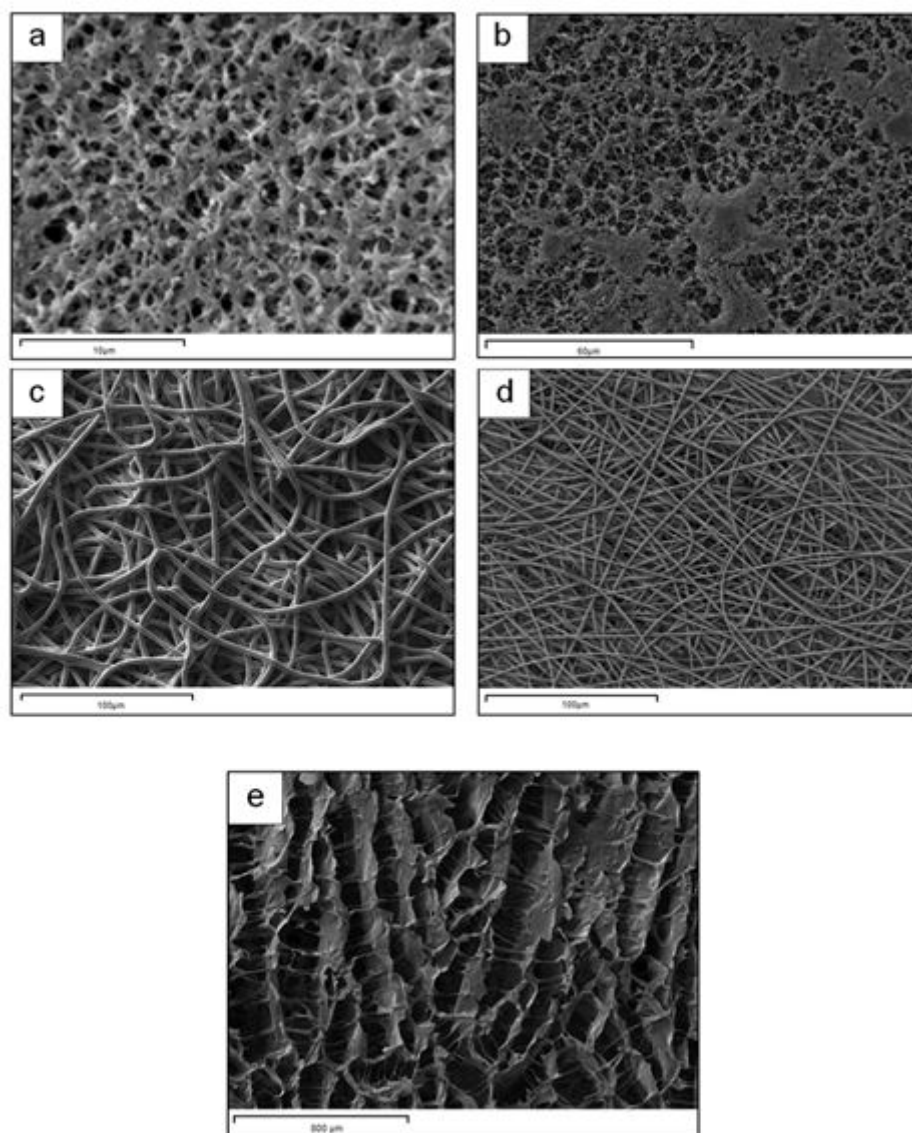


Figure 2.6: SEM micrographs showing surface morphology of (a) PVDF membrane, (b) cellulose nitrate membrane, (c) poly(caprolactone) scaffold, (d) poly(L-lactide) scaffold and (e) collagen scaffold (Suhaimi et al., 2015b)

2.2.3 Refractive index method

A group of researchers (Weng et al., 2005) attempted to further understand the glucose behaviour in agarose gel which has a significant effect in molecular diffusion research in general and tissue engineering in particular. For this particular work, they adopted a refractive index method as a means to measure the glucose diffusion coefficient in the agarose gel. The gel was contained inside a triangular cell where it was later immersed into the glucose solution. When this happened, the change of light was captured by a CCD camera and post processed with specific

software. The source of light came from a He-Ne laser. This method presents some advantages over others due to its capability to measure concentration in situ without interrupting the process as well as the simple post processing work thereafter. As such, the method has been used since in the early 1990s up until recently (Maier et al., 1994; Chance et al., 1995; Liu et al., 1996; Tuchin et al., 1997; Wang, 2000; Vargas et al., 2001; Yao et al., 2002; Bashkatov et al., 2003; Zhang et al., 2013; Trichet et al., 2014 Ullah et al., 2014; Pleitez et al., 2015).

In general, when light passes through a prism, some if not all, will be refracted back in what is known as refractive angle. This refractive angle resembles refractive index of the prism. Weng et al. (2005) indicated in their work the success of monitoring glucose transport in the agarose gel as well as determining the diffusion coefficients using the method. They deduced $5.73 \times 10^{-10} \text{ m}^2/\text{s}$ (Table 2.4) as the diffusivity in 1.5% agarose gel at 25°C. This figure is comparable to the value of Andersson and Oste (1994) whose work monitored the glucose diffusion in 1.2-3.6% agarose gel at 25°C using a steady-state diaphragm cell. The obtained diffusion coefficients were around $4.25\text{-}6.15 \times 10^{-10} \text{ m}^2/\text{s}$ which is close to what Weng et al. (2005) obtained. Another pertinent work by Li et al. (1996) can be taken as a comparison where they observed the glucose diffusion in 0.197% agarose gel at 37°C. The comparison indicated that the obtained glucose diffusivity was at least 50% more than what Weng et al. (2005) obtained. They also compared the diffusivities of glucose in 0.5% and 1.5% agarose gel and as expected, 0.5% agarose gel showed a slightly higher diffusion coefficient of $6.26 \times 10^{-10} \text{ m}^2/\text{s}$ due to lower polymer content resulting in higher glucose mobility.

In 2006, Liang and coworkers attempted to improve the in situ refractive index method with temperature-controlled capability (Liang et al., 2006). They used protein instead of glucose to measure the diffusion coefficient in agarose gel. Results proved that this improved method was reliable in measuring the protein diffusion at different temperatures. There seems to be no recent study reported on the use of refractive index method to monitor the glucose diffusion in tissue engineering materials. However, this method has been used recently to measure glucose level in tissue sample and one such study is reported by Ullah et al. (2014) where they used the refractive index method to measure the glucose level in mouse blood. The aim of their study was to further understand the use of laser applications

to determine blood glucose levels without incision. Their results showed a positive indication for future applications. This technique is suitable for materials such as transparent gel-like scaffolds since it involves light transmission from and to the solute molecules in the gel to capture the speed.

2.2.4 Dispersion model method

Apart from the polymer content of a gel matrix, the working temperature of the diffusion process also has an impact on the diffusing solute molecules. Andersson et al. (1997) conducted a temperature dependent study on the effect of glucose diffusion at 10, 20 and 30°C in a swelling *N*-isopropylacrylamide (NiPAAm) gel using a dispersion model method. They noted in their report that due to dispersion and time delay during the actual experiment, the concentration recorded by the detector was different to the in situ concentration in the diffusion cell. For these reasons, they fitted the experimental concentration profiles into a mathematical model that corrected both the dispersion and time delay factors. The calculated diffusion coefficients of glucose at 10, 20 and 30°C are summarized in Table 2.2. They concluded that the glucose diffusivity agreed with Wilke-Chang temperature correlation (Wilke and Chang, 1955) suggesting the change in diffusivity was mostly due to the change in temperature, not due to the degree of gel swelling. On the other hand, Podichetty et al. (2014) reported the use of dispersion model coupled with residence time distribution (RTD) analysis to observe the distribution of glucose in polycaprolactone (PCL) scaffold and chitosan-gelatin (CG) scaffold. Their results showed the surface properties of scaffolds had an effect on the glucose distribution and concluded that the combined approach gave useful insights to designing bioreactors for tissue regeneration. Since this method combines both experimental and modelling approaches, the mathematical model is validated by experimental measurements and it is also valid for small diffusants in diluted and uncharged gel systems.

Table 2.2: Effective diffusivities of glucose in swelling N-isopropylacrylamide (NiPAAm) gel (Andersson et al., 1997)

Temperature (°C)	Effective diffusivity (m ² /s)
10	$2.70 (\pm 0.13) \times 10^{-10}$
20	$3.74 (\pm 0.20) \times 10^{-10}$
30	$4.65 \pm 0.57) \times 10^{-10}$

2.2.5 Six cross-flow cell unit method

A number of studies of glucose transport through different types of membranes have been carried out but no or little work has been reported on the glucose diffusion in polymeric/cyclodextrin mixed-matrix membranes. Thus, Adams et al. (2013) presented a noble work on the transport of glucose through polysulfone (PSf)/ β -cyclodextrin (β -CD) polyurethane (PU) mixed-matrix membranes of three different PSf concentrations. The surface morphology of the mixed-matrix membranes showed uniformly sized circular voids of a smooth structure (Figure 2.7).

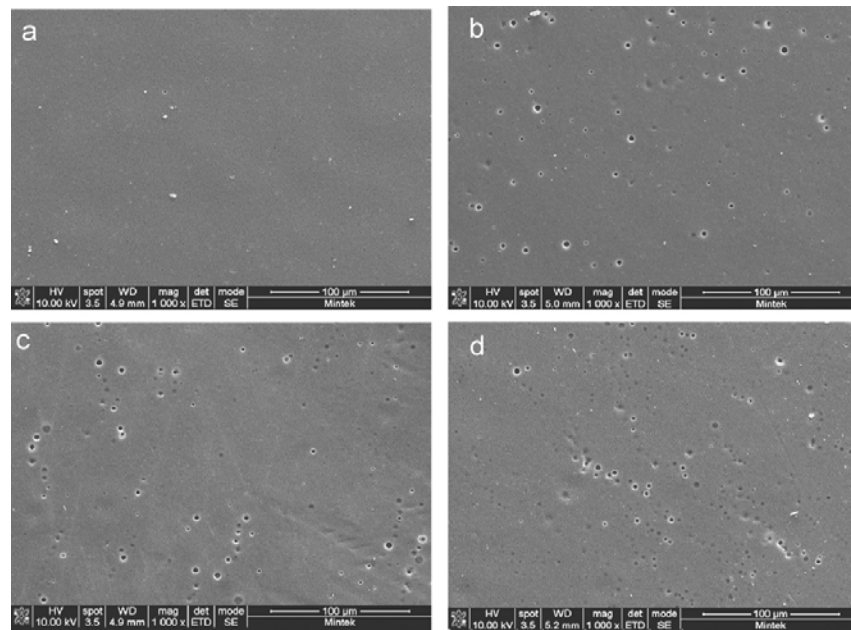


Figure 2.7: SEM micrographs showing surface morphology of (a) PSf membrane, (b) PSf 5% β -CDPU membrane, (c) PSf 8% β -CDPU membrane and (d) PSf 10% β -CDPU membrane (Adams et al., 2013)

Before conducting the investigation, the membranes were subjected to a pressure of 3.10 MPa for a period of 2 hours and, specifically for diffusion experiments, they were conditioned to a pH of 6.89 and a temperature of 20°C. The diffusion coefficients of glucose were calculated based on Fick's diffusion law assuming the concentration difference was the sole driving force. The corresponding diffusion coefficients are shown in Table 2.3. The authors concluded that mixed-matrix membranes performed well in diffusing glucose due to its increased hydrophilicity as well as its crystal structure. This method which applies solution-diffusion system is typically validated with non-porous membranes in which the difference between solubility and diffusivity leads to separation of permeates. Table 2.4 summarises the different methodologies used for measurements of glucose diffusion in various membranes and scaffolds as well as the corresponding effective diffusion coefficients values from these studies.

Table 2.3: Glucose diffusivities in mixed-matrix membranes (Adams et al., 2013)

Membrane type	Effective diffusivity (m^2/s)
Polysulfone (PSf)	0.0793×10^{-10}
PSf 5% β -cyclodextrin polyurethane (β -CDPU)	0.0290×10^{-10}
PSf 8% β -CDPU	0.1833×10^{-10}
PSf 10% β -CDPU	0.1717×10^{-10}

Table 2.4: Examples of measured glucose diffusivity values for typical tissue engineering membranes and scaffolds

Scaffold/membrane		Temperature (°C)	Porosity (%)	Methodology	Effective diffusivity (10 ⁻¹⁰ m ² /s)	Reference
Poly(L-lactic acid) (PLLA) scaffold	Ethanol	23	84.3 ± 2.1	Diffusion cell – samples were analysed using a UV spectrophotometer at λ = 450 nm	0.15 ± 0.5	Papenburg et al. (2007)
		23	82.6 ± 0.7		0.33 ± 0.1	
		4	75.2 ± 1.6		1.04 ± 4.5	
	Isopropanol	23	86.0 ± 0.8		0.26 ± 0.2	
		23	86.0 ± 1.2		0.64 ± 1.7	
		4	83.0 ± 2.6		0.86 ± 1.5	
Inverted colloidal crystal (ICC) scaffold		25	NA	Computer simulation	3	Shanbhag et al. (2005)
Hydroxypropyl chitosan/gelatin/chondroitin sulfate (HPCTS/GEL/CS) scaffold		37	NA	Diffusion cell – samples were reacted with dinitrosalicylic (DNS) acid at 540 nm	1.16 ± 0.11	Wang et al. (2009)
Poly(caprolactone) (PCL) scaffold		37	80	Diffusion cell	1.78 ± 0.50	Suhaimi et al. (2015b)
Poly(L-lactide) (PLLA) scaffold			80		1.39 ± 0.28	

Collagen scaffold		72		37.1 ± 2.78	
Polyvinylidene fluoride (PVDF) membrane	37	69	Diffusion cell	0.768 ± 2.78	Suhaimi et al. (2015b)
Cellulose nitrate membrane		64		0.891 ± 0.80	
Nanoporous polyethylene membrane	37	28.9 ± 0.7	Diffusion cell – samples were analysed using a refractometer at 589.3 nm	0.18	Boss et al. (2012)
Asymmetric alumina membrane				1.39	
Polysulfone (PSf) membrane	20	NA	Diffusion was analysed based on a solution-diffusion model using a six cross-flow cell unit	0.07933	Adams et al. (2013)
PSf 5% β -cyclodextrin polyurethane (CDPU) membrane				0.029	
PSf 8% β -CDPU membrane				0.183	
PSf 10% β -CDPU membrane				0.172	
Collagen scaffold	NA	NA	Needle enzyme electrodes	1.33	Rong et al. (2006)
Dextran-tyramine (Dex-TA) scaffold	NA	NA	Diffusion cell	3.2	Jin et al. (2010)
0.5% Agarose scaffold	25	NA	Refractive index	6.26	Weng et al. (2005)

1.5% Agarose scaffold				5.73	
<i>N</i> -isopropylacrylamide (NiPAAm) scaffold	10	NA	Diffusion cell connected to a computer	2.7 ± 0.13	Andersson et al. (1997)
	20			3.74 ± 0.20	
	30			4.65 ± 0.57	

2.3 Porosity and tortuosity of tissue engineering membranes and scaffolds

Besides the interactions between the diffusing solute and the porous network in membranes and scaffolds, the amount of void spaces (porosity) and the tortuous path length (tortuosity), which increases the distance a molecule has to traverse through the pore network, also have significant effects on the mass transport.

Porosity can be determined either using indirect or direct techniques. Examples of indirect techniques include liquid permeability (Palacio et al., 1999), permporometry (Mey-Marom and Katz, 1986), air-liquid porometry (Hernandez et al., 1996), liquid-liquid porometry (Bechhold et al., 1931), SEM (Riedel and Spohr, 1980), transmission electron microscopy (TEM) (Nakao, 1994), atomic force microscopy (AFM) (Binnig et al., 1986), field emission scanning electron microscopy (FESEM) (Dietz et al., 1992), thermoporometry (Brun et al., 1977) and gas adsorption-desorption (Dollimore and Heal, 1964; Gregg and Sing, 1982). On the other hand, pycnometric methods, mercury intrusion and apparent density estimation are some examples of direct techniques for measuring porosity (Palacio et al., 1999).

Comparisons between using direct and indirect techniques will be highlighted here. While pycnometric method appears to be easy and simple, it can lead to hydration problem which will have a significant effect on the porosity determination. Instead of wetting the porous material with water, mercury as the wetting agent has been proven to be more precise (Liabastre and Orr, 1978). However, only certain pore sizes are able to work well with Hg-porosimetry due to a considerable amount of pressures needed to infuse mercury into very fine pores. Apparent density estimation is also another simple and easy method to comprehend, yet it tends to overestimate porosities which may be due to hydration and the presence of contaminants as well as non-pure materials whose densities are unaccountable for in the calculation of porosity. A common setback of using these direct techniques is the ability to detect non-active pores or dead-end pores in the porous materials.

Microscopic methods such as scanning electron microscopy (SEM), transmission electron microscopy (TEM), atomic force microscopy (AFM) and field emission scanning electron microscopy (FESEM) present surface and cross section micrographs of the porous material and these images can be uploaded onto a computer and analysed using special software which enable surface porosity to be determined easily. However, the bulk porosity requires the cross section images to

be captured at certain angles which will eventually distort the overall structure. The air-liquid and liquid-liquid porometry techniques require two steps: the first one is to produce a flow graph against pressure or the resulting pore diameter which can be deduced using Washburn equation (Washburn, 1921). This step requires a suitable air and liquid to be pressurised in order to diffuse into the pores while the second step involves integrating the cross section area of the pore diameter which results to porosity determination.

Palacio et al. (1999) reported the outcome of using a gas penetration method in view of experimental and nominal porosities and they acknowledged the difference between these two. This may be due to a lack of information from the manufactures on the techniques used to obtain the nominal values therefore comparisons of using the same method to confirm the porosity values are not possible. The nominal values are merely a representative for the same batches of the same membrane material and therefore cannot be truly justified. This method is preferred if all voids are to be investigated and also benefits from minimising structure distortion as only minimal pressures are required.

Tortuosity is defined by the increased distance the diffusing solution has to travel due to pore bending and curves. Porosity, diffusion coefficient and tortuosity are correlated together (van Cappellen and Gaillard, 1996) and the latter can be determined experimentally, theoretically and empirically. Shen and Chen (2007) reviewed two experimental methods: one is the work of Sweerts et al. (1991) aimed at determining the ratio of diffusivity in free media to the diffusivity in a porous material of known porosity while the other one is the work of McDuff and Ellis (1979) aimed at determining diffusivities of marine sediments. They linked tortuosity to a formation factor obtained via electrical resistivity measurements. The former is time consuming while the latter needs electrical resistivity probes.

Theoretical methods of correlating porosity and tortuosity are generally based on the assumption of an idealised porous medium with the absence of adjustable parameters. Examples of such models can be seen in the works of Bhatia (1985), Dykhuizen and Casey (1989) and Petersen (1958). In contrast to the theoretical method, empirical method encompasses adjustable parameters which differ in values in traditional literatures. The first reported work involving the empirical method is

the work of Archie (1942). Some examples of the relationship between porosity and tortuosity for idealised porous material can be found in Table 2.5.

Table 2.5: Porosity-tortuosity relations for idealised porous materials

Relation	Reference
$\tau = 1 - 0.41 \ln \varepsilon$	Comiti and Renaud (1989)
$\tau = 1 - 0.49 \ln \varepsilon$	Mauret and Renaud (1997); Barrande et al. (2007)
$\tau = 1/\varepsilon^{0.33}$	Bear (1972); Dullien (1975)
$\tau = 1 + 0.8 (1 - \varepsilon)$	Koponen et al. (1996)
$\tau^2 = 1 - \ln (\varepsilon^2)$	Boudreau (1996)
$\tau = \frac{\varepsilon}{1 - (1 - \varepsilon)^{1/3}}$	Beeckman (1990)

Suhaimi et al. (2015b) determined both porosity and tortuosity values for tissue engineering membranes and scaffolds experimentally. All materials were saturated with both water and CCM at temperatures of 27 and 37°C. Porosity was evaluated using a pycnometric method while tortuosity was derived from the determination of the ratio of diffusivity in free media to the effective diffusivity in the porous network (i.e. TE membranes and scaffolds). The corresponding porosity and tortuosity values are shown in Table 2.6. They concluded that tortuosities varied with temperature as what has been reported previously (Gao et al., 2014; Sadighi et al., 2013; Sharma and Chellam, 2005).

Table 2.6: Porosity and tortuosity values in TE membranes and scaffolds (Suhaimi et al., 2015b)

Material	Porosity (%)	Tortuosity (dimensionless)			
		Water at 27°C	Water at 37°C	CCM at 27°C	CCM at 37°C
Polyvinylidene fluoride membrane (PVDF)	69	4.0	3.5	5.4	5.6
Cellulose nitrate	64	2.4	3.1	4.8	4.4

membrane (CN)					
Poly(L-lactide) scaffold (PLLA)	80	2.7	3.0	3.3	3.5
Poly(caprolactone) scaffold (PCL)	80	1.6	1.9	2.8	2.8

2.4 Microstructure and diffusion

The relationship between nutrient diffusion (i.e., glucose) and membrane/scaffold morphology or tissue morphology is crucial for better understanding the transport behaviour of the nutrients. In addition, it will help to further improve the computational modelling work with regard to nutrient supply to the cells. An example of the relationship between solute diffusivity and tissue morphology is shown in the work of Shi et al. (2013). Temporomandibular joint (TMJ) disc, a fibrocartilaginous tissue, was taken as their tissue sample and five regions namely anterior, medial, intermediate, lateral and posterior in three orthogonal orientations; medial-lateral (ML), anterior-posterior (AP) and superior-inferior (SI) were subjected to fluorescein diffusion. The diffusion process was analysed by a fluorescence recovery after photobleaching (FRAP) technique. All the tissue samples were examined using SEM for the purpose of observing the tissue morphology, that is, the collagen fibre structure (Figure 2.8).

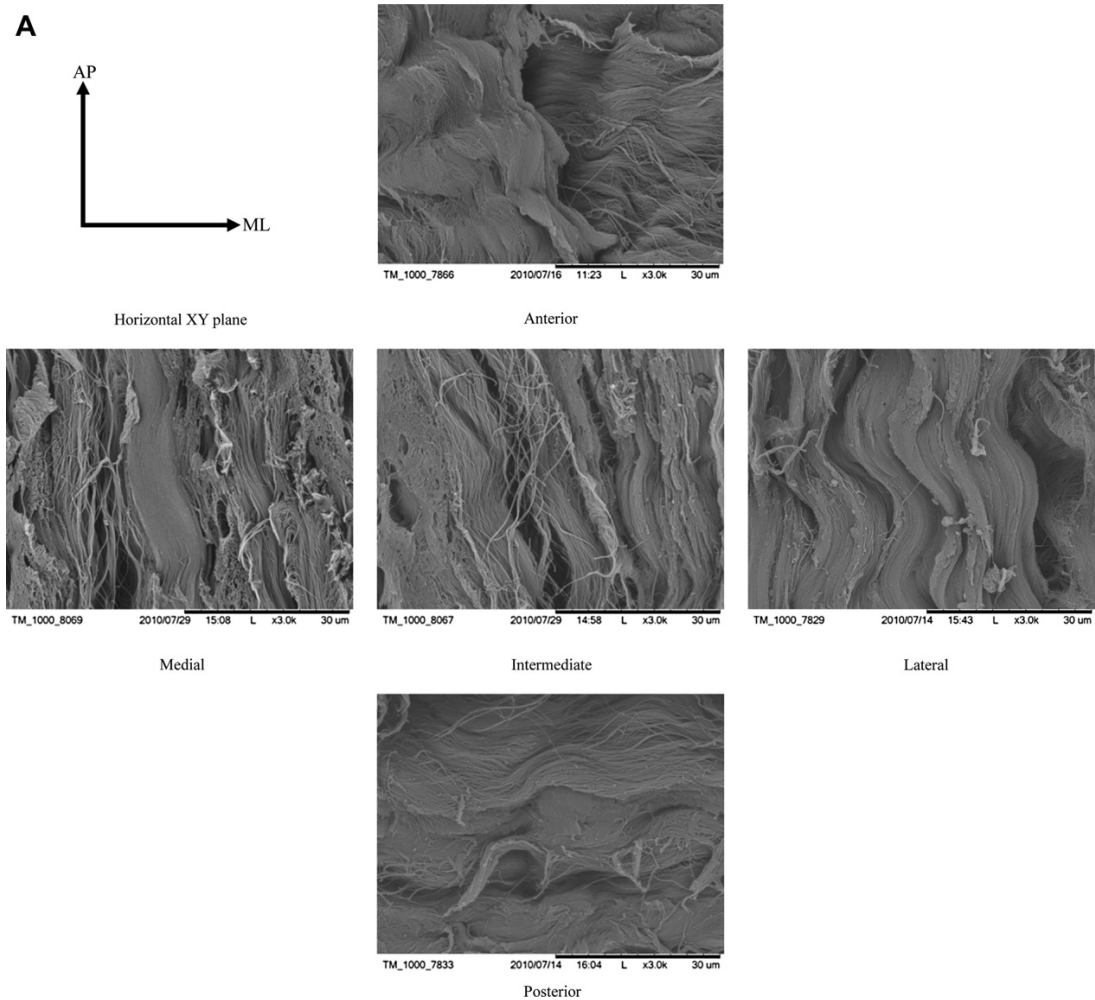


Figure 2.8: SEM micrographs showing the AP-ML orientation of the collagen fibre in all five regions of the TMJ disc (Shi et al., 2013)

Shi et al. (2013) stated that the collagen fibre orientation may influence the fluorescein (a molecule that is similar to glucose in terms of molecular weight) diffusion based on the inhomogeneous and anisotropic diffusion style of the fluorescein in the TMJ tissue. Furthermore, both the anisotropic diffusion and collagen fibre orientation showed same degrees of similarity and trends in all five regions investigated. They demonstrated that the fluorescein diffusion was dependent on the composition of the region.

Another similar example can be seen in the work of Travascio et al. (2009) where they observed the diffusion of fluorescein in human annulus fibrosus (AF) via the fluorescence recovery after photobleaching (FRAP) technique. The diffusion process spanned across three regions namely inner AF (IAF), middle AF (MAF) and outer AF (OAF) in two directions, axial and radial, respectively. They concluded that their findings in a similar fashion to Shi et al. (2013) stating a relationship

between solute diffusivity in the human AF and the morphological structure and content of the tissue existed. This hypothesis was drawn based on the similar trend of both diffusivity values and water content whereby higher water content as well as higher diffusivity value were determined in IAF region compared to the OAF region. The morphological structure of the tissue samples were analysed using SEM (Figure 2.9).

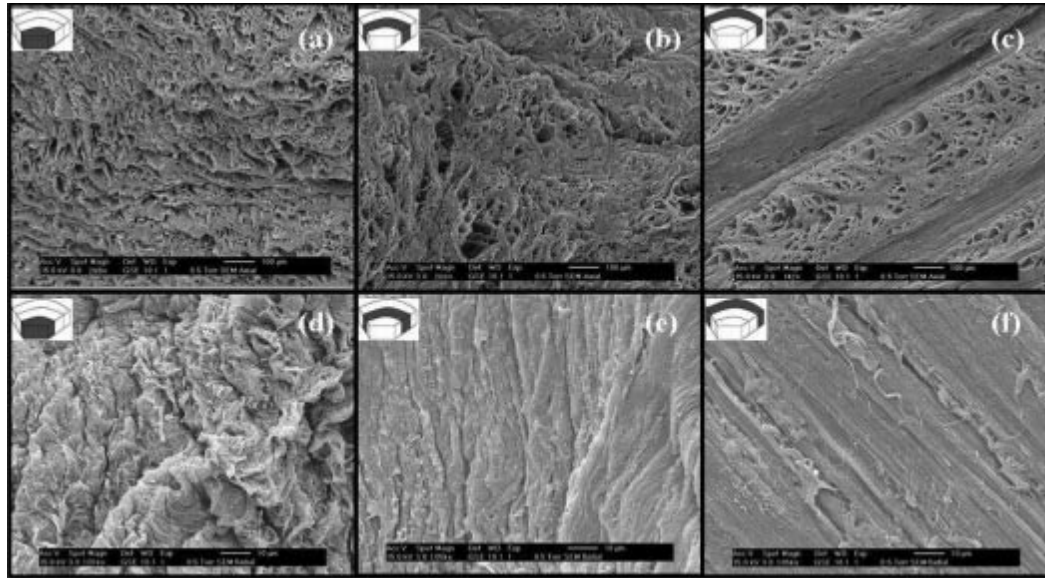


Figure 2.9: SEM micrographs showing axial sections of (a) IAF, (b) MAF, (c) OAF and radial sections of (d) IAF, (e) MAF and (f) OAF (Travascio et al., 2009)

An additional example that verified the relationship between transport property and morphological structure of the porous material is illustrated in the work of Li et al. (2007). They fabricated sulfonated poly(ether ether ketone ketone)s (SPEEKK) membranes (Table 2.7) and observed the morphologies using TEM and AFM (Figure 2.10).

Table 2.7: Fabrication details of SPEEKK membranes (Li et al., 2007)

Membrane	Sulfonated degree (D_s)
SPEEKK-1	0.78
SPEEKK-2	0.97
SPEEKK-3	1.23

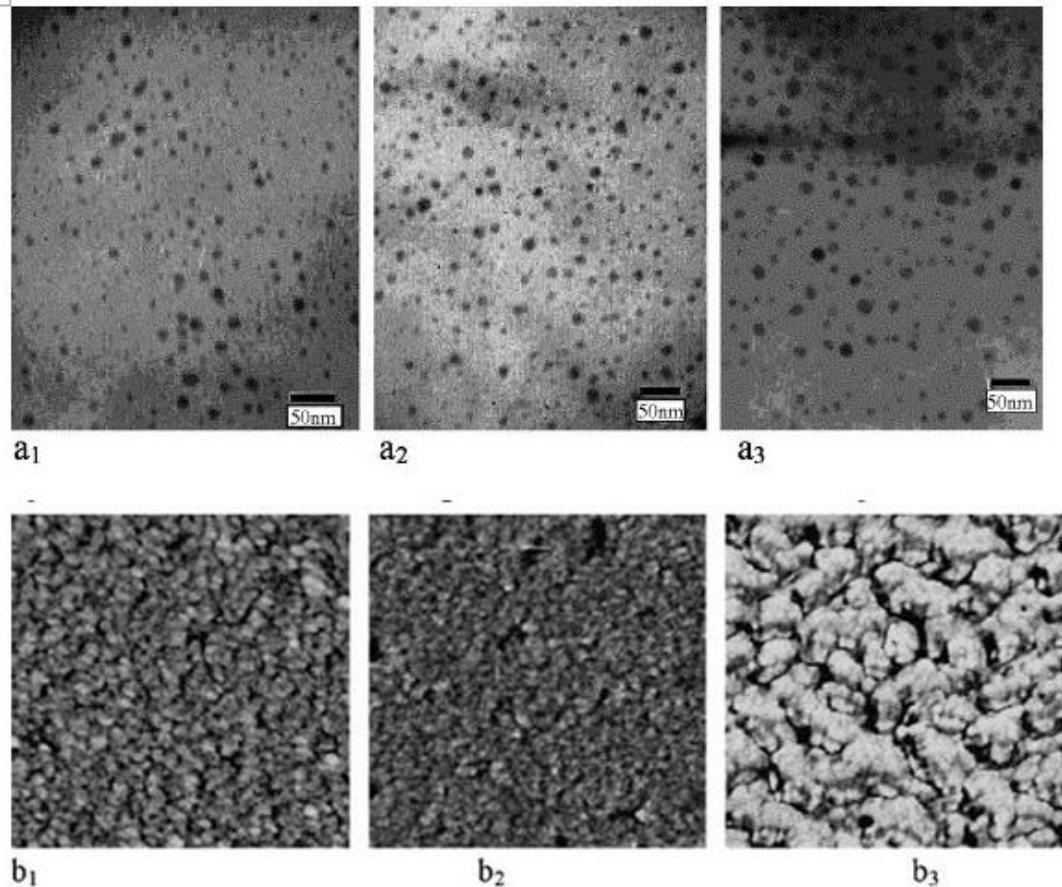


Figure 2.10: TEM micrographs of (a₁) SPEEKK-1, (a₂) SPEEKK-2 and (a₃) SPEEKK-3 and AFM micrographs of (b₁) SPEEKK-1, (b₂) SPEEKK-2 and (b₃) SPEEKK-3 (Li et al., 2007)

2.5 Glucose diffusivities in liquids

Attempts to deduce liquid diffusivities have been ongoing dated back over many decades ago and by far, the most frequently used method is a diaphragm cell method (DCM). The DCM has been used as early as some 60 years ago up until now (Mills, 1957; Wendt and Shamim, 1970; Choy et al., 1973; Tham et al., 1973; Turhan et al., 1995; Breer et al., 2014; Buzier et al., 2014) due to its precise and accurate measurements. Other methods have surfaced recently such as Taylor dispersion method using a long capillary tube (Ribeiro et al., 2006 and 2014), static and dynamic light scattering (Soraruf et al., 2014), open-end capillary method (OECM) (Ouerfelli et al., 2014) and total internal reflection fluorescence microscopy (TIRF) (Uehara et al., 2014).

Generally, the DCM is consisted of two half glass compartments with stirrers attached to both and a diaphragm in the middle to separate the content of the compartments. The diaphragm differs in every experiment, ranging from track-etched membrane, porous disk, dialysis paper and to glass sinter membrane depending on the molecular size of the diffusing solutes. Both compartments are filled with the diffusing solution and distilled water, respectively. Samples are withdrawn from both compartments at allocated time intervals for measurement of concentration. The whole experimental set-up is conditioned to a working temperature.

The corresponding diffusion coefficient by the DCM method is given by:

$$D = \frac{1}{\beta t} \ln \left(\frac{C_{lower}^0 - C_{upper}^0}{C_{lower} - C_{upper}} \right) \quad (2.2)$$

where β is the cell calibration constant which must be determined before the start of the diffusion experiment. The diaphragm cell is calibrated by performing a diffusion experiment of solute of known diffusivity at the same experimental conditions.

The Taylor dispersion method is typically used to investigate mutual diffusion coefficients of aqueous solutions. It involves a long capillary tube where it houses a number of ports for inlet point. The diffusing solution is injected into the ports and a metering pump is used to keep the flow consistent. The concentration of the dispersed injected sample is analysed by a differential refractometer and the equivalent diffusion coefficient is calculated via the dispersion equation which followed the Gaussian concentration profile:

$$D = \frac{R^2}{48\bar{t}} \left[\frac{(1+4K^2)^{1/2} + 3}{(1+4K^2)^{1/2} + 2K^2 - 1} \right] \{1 + (1 - \delta_a)^{1/2}\} \quad (2.3)$$

where R and \bar{t} are capillary tube radius and mean residence time, respectively while K and δ_a are defined as follow:

$$K = \sigma/\bar{t}, \bar{t} = L/\bar{u}, \delta_a = (768)^2 \Theta \zeta_0 \text{ and } \zeta_0 = \frac{2\sigma^2 - \bar{t}^2 + (\bar{t}^4 + 4\bar{t}^2\sigma^2)^{1/2}}{8\bar{t}^2 - 4\sigma^2} \quad (2.4)$$

where σ , L , \bar{u} and Θ are variance, capillary tube length, mean flow velocity and a constant of 2.17014×10^{-5} , respectively.

Ouerfelli et al. (2014) in their report presented the OECM for the purpose of investigating the diffusion of trivalent lanthanide and actinide ions in aqueous

electrolyte solutions. They attached radioactive tracer to these solutions and deduced the diffusivity by the following equation:

$$D = 0.4053 \frac{l^2}{t} \ln \left(\frac{0.8106}{\Gamma} \right) \quad (2.5)$$

where l , t and Γ are capillary length, diffusion time and ratio of final average activity to total activity in the capillary tube at initial time ($\Gamma = A(t)/A(0)$), respectively. Eq. (2.5) is only valid for concentrations up to 0.114 mol/l. Uehara et al. (2014) reported the diffusion of single-stranded DNA molecules (ssDNA) in aqueous solutions by the TIRF technique (Figure 2.11).

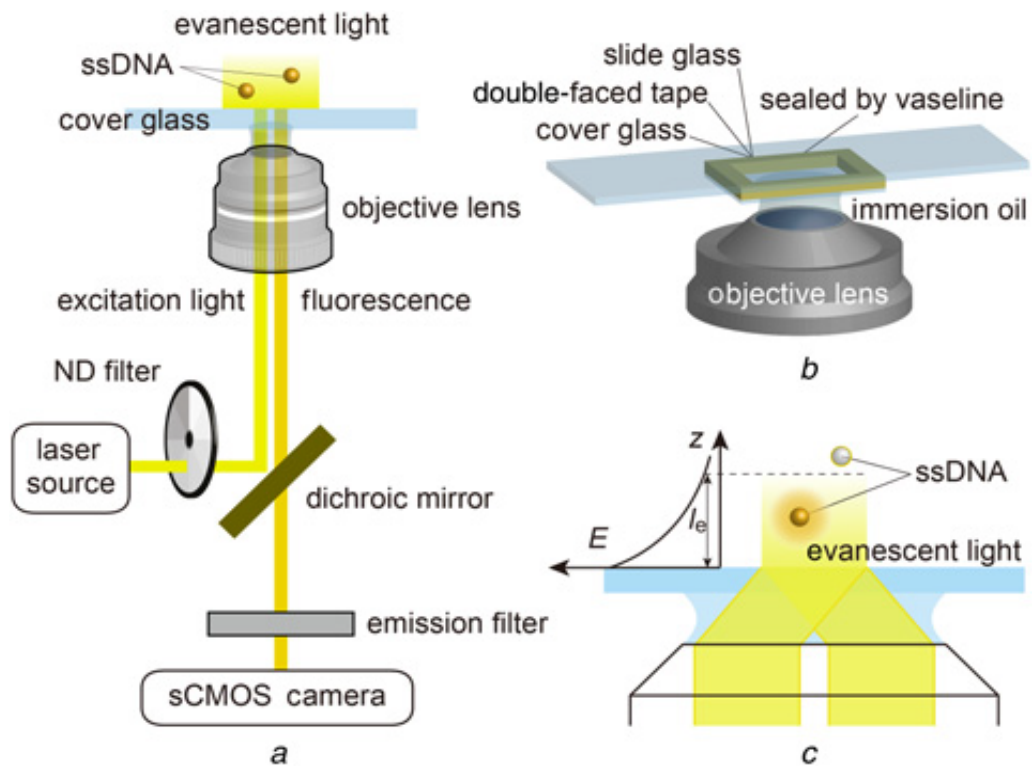


Figure 2.11: The TIRF technique consisted of: (a) optical system, (b) sealing sample solution and (c) penetration of light (Uehara et al., 2014)

The corresponding diffusion coefficients were evaluated based on their mean square displacements (MSDs):

$$D = \lim_{t \rightarrow \infty} \frac{1}{2n_{dim}t} \langle |r(t) - r(0)|^2 \rangle \quad (2.6)$$

where $r(t)$, n_{dim} and $\langle \rangle$ are the ssDNA molecules' vector position at time t , dimension of $r(t)$ and ensemble average, respectively.

More recently, Suhaimi et al. (2015a) measured glucose diffusivity in both CCM and water (as reference fluid) using the DCM principle and they concluded that the glucose diffusion coefficients in CCM were significantly reduced than the ones in water. This was attributed to the higher dynamic viscosity of CCM compared to water as well as the multi-component interactions present in CCM, though the latter is believed not to be as significant as the former. While many authors assumed the diffusivity in cell culture media to be equal to that in water (Li, 1982; Das and Abdullah, 2007; Clark et al., 2011; Van Winkle et al., 2012), Suhaimi et al. (2015a) highlighted the significant differences between the diffusivities in both media. Table 2.8 summarises some examples of diffusing solutes and the corresponding diffusivity values that have been reviewed in this section.

Table 2.8: Typical diffusing solutes and their respective diffusivities

Diffusing solute	Temperature (°C)	Methodology	Diffusivity ($10^{-10} \text{ m}^2/\text{s}$)	Reference
Chloride ion	25	Diaphragm cell method (DCM)	20.33	Mills (1957)
Water-magnesium chloride-sodium chloride	25	DCM	0.3	Wendt and Shamim (1970)
Sodium ion	25	DCM	7.4	Choy et al. (1973)
Sodium chloride	25	DCM	14.6	Turhan et al. (1995)
Potassium chloride			18.7	
Glucose			6.6	
L-tryptophan			6.52	
Lysozyme			1.09	
Bovine serum albumin (BSA)			6.44	
Aqueous lactose	25	Taylor dispersion	5.68 ± 0.035	Ribeiro et al. (2006)
Aqueous sucrose			5.25 ± 0.009	

Aqueous glucose		method using a long capillary tube	6.78 ± 0.020	
Aqueous fructose			6.89 ± 0.030	
Aspartic acid	25	Taylor dispersion method using a long capillary tube	8.20 ± 0.010	Ribeiro et al. (2014)
Monosodium salt			9.35 ± 0.007	
Single stranded DNA (ssDNA) molecule	NA	Total internal reflection fluorescence microscopy (TIRF)	2.73	Uehara et al. (2014)
Aqueous glucose in water	37	NA	9	Buchwald (2011)
Aqueous glucose in cell culture media (CCM)	37	Stokes-Einstein equation	5.926	Provin et al. (2008)
Glucose in water	27	DCM	6.98 ± 0.60	Suhaimi et al. (2015a)
	37		9.58 ± 0.13	
Glucose in CCM	27		5.67 ± 0.74	
	37		6.16 ± 1.25	

2.6 Chapter summary

Various different techniques have been used and applied to determine the effective diffusion coefficient of small solutes (e.g., glucose) in the porous material such as needle enzyme electrodes, refractive index method, dispersion model method, six cross-flow cell unit method and diffusion cell. The suitability of each technique depends on the materials' properties to be investigated as well as the validity of each method. For example, the refractive index method is only suitable for transparent materials as light needs to transmit across the transparent gel to capture its speed of which refractive indexes are translated into concentration measurements. Needle enzyme electrodes, refractive index method and dispersion model method are shown

to require indirect and complicated methods for the concentration measurements of the diffusant across the materials. On the other hand, six cross-flow cell unit and diffusion cell methods are simple and easy to use. We recommend diffusion cell as a way to investigate glucose diffusion in tissue engineering materials as it has been widely used and accepted. Moreover, this method works under the assumption of steady state systems which is usually the case for glucose diffusion across tissue engineering materials, as compared to six cross-flow cell unit which involves the use of non-porous membranes. For some methods, there is only one or two studies reviewed for the particular method. As the aim of this chapter is to analyse and study methods that have been developed and used over the years in concentration measurements, it is still worth mentioning even though there seems to be fewer studies reported using the methods as they can also be a potential technique for concentration determination.

There have been a number of equations developed and produced by various authors based on the methods studied. As such, the equations are used in different applications. For example, diaphragm cell method will use Eq. (2.2) while Taylor dispersion method will employ Eq. (2.3) and Eq. (2.4). As the aim of this chapter is not to discuss which equation is the most appropriate one as the equation used for estimating the liquid diffusivity depends on the method used, we will therefore not state in this chapter. However, due to its simple, precise and accurate measurements, diaphragm cell method (DCM) has been widely used, and hence, Eq. (2.2). In addition, with reference to Table 2.8, DCM seems to be the most frequently used method in determining the liquid diffusivity in free medium. The range of concentration used for DCM is also larger than other methods (Table 2.8); therefore, we can conclude that DCM is more applicable in wider applications.

Apart from pore size, porosity and tortuosity also affect the diffusion of a molecule through the porous material. Both direct and indirect approaches have been discussed with regard to its respective advantages and disadvantages and we conclude that there is no general procedure to determine both porosity and tortuosity of the porous media. For example, while pycnometric method seems to be straightforward, it can also result in hydration. Mercury has also been proposed as a better wetting agent instead of water for pycnometric technique, however it is only valid for certain pore sizes. Hence, we conclude that the most appropriate method

depends on the materials to be characterized itself. Sufficient studies have proven that there exists a relationship between the property of transport of solute and morphological structure and these findings are crucial in better and improved understanding of the nutritional supply to extra cellular matrix and cells for tissue engineering applications. Despite a number of literature works, the relationship between membrane morphology and solute diffusion is not fully understood yet as the building blocks of the material varies within the same material, and from one material to another. The temperature and fluid that saturates it may also affect the microstructure and this in turn affects the diffusion.

CHAPTER 3

GLUCOSE DIFFUSIVITY IN CELL CULTURE MEDIUM

Chapter overview

The diaphragm cell method (DCM) was applied to determine the self-diffusion of glucose in cell culture media (CCM) and water (reference fluid). For this purpose, a diffusion cell based on the DCM principle was constructed and the cell was calibrated with ethanol prior to carrying out the diffusion experiments. The results show that the diffusion coefficients of glucose in CCM are significantly smaller as compared to those for water which are due to the larger dynamic viscosity of CCM. This may also account for the presence of extra components and difference in fluid properties of CCM. The obtained diffusivity values are compared to values estimated from Stokes-Einstein equation and it appears that the agreement is fairly good.

3.1 Introduction

Diffusion is one of the primary mechanisms for transport of solutes in media of biological importance. For example, glucose diffusion in tissue engineering fluids is fundamental in growing successful three dimensional (3D) tissues. Glucose is a small biomolecule which plays an important part as a source of nutrient for growing these tissues. For many years now, numerous efforts have been made to understand glucose diffusion behaviour in various chemical, biomedical and tissue engineering applications (e.g., Khanafer and Vafai, 2006; Wang et al., 2009; Laatikainen, 2011; Podichetty et al., 2014). In particular, glucose transport has been studied in the context of tissue engineering bioreactors as it determines their performance for growing artificial tissues (Chapman et al., 2012; Baptista et al., 2013; Nishi et al., 2013; Napoli et al., 2014). From the point of view of mathematical modelling of glucose transport in these bioreactors, values of glucose diffusivity in liquids (e.g., cell culture media, CCM) and porous materials (e.g., membranes, scaffolds) are essential to solve the diffusion equations (Mauck et al., 2003a; Ye et al., 2006;

Khademi et al., 2014; Chao and Das, 2015). These data are also needed to verify theories of mass transport (e.g., Chen et al., 1992) and to enhance our understanding of the diffusion processes, e.g., how fast and slow the molecular transport is in a liquid medium in a bioreactor (Suhaimi et al., 2015b).

While a number of studies have reported the diffusion coefficients of glucose in aqueous solutions (Longsworth, 1952; Dionne et al., 1996; Phanthong and Somasundrum, 2003; Curcio et al., 2005), none of these studies seem to have reported the glucose diffusivity in tissue engineering fluids (e.g., CCM). They have mainly focused on glucose diffusion in water and other fluids (e.g., poly-ether-sulphone, poly-sulphone and polyvinyl alcohol). There are also a number of studies which have reported the influence of some compounds usually found in biological media on the diffusion of oxygen as well as the effect of different solutes have on the liquid mass transfer coefficients (Hebrard et al., 2009; Jamnongwong et al., 2010; Garcia-Abuin et al., 2013). But as far as we are aware, there is a serious lack of data in the literature for the glucose diffusion in CCM. Consequently, most previous studies have assumed that the glucose diffusivities in CCM are similar to those in water (e.g., Li, 1982; Abdullah and Das, 2007; Clark et al., 2011; van Winkle et al., 2012). The extent to which this assumption is correct or wrong is not certain at the moment. The purpose of our study is therefore to measure glucose diffusivities in CCM and water (as a reference fluid).

A number of methods have been studied and developed to estimate the liquid diffusion coefficients such as Taylor dispersion method using a long capillary tube (Ribeiro et al., 2006, 2014), static and dynamic light scattering (Soraruf et al., 2014), open-end capillary method (OECM) (Ouerfelli et al., 2014) and total internal reflection fluorescence microscopy (TIRF) (Uehara et al., 2014). However, the most commonly used method is a diaphragm cell method (DCM) due to its precise and accurate measurements. The DCM has been used dated back from some 60 years ago up until now (Mills, 1957; Wendt and Shamim, 1970; Choy et al., 1973; Tham et al., 1973; Turhan et al., 1995; Breer et al., 2014; Buzier et al., 2014). The apparatus consists of two well-stirred compartments separated by a diaphragm. One of the compartments is filled with a solute solution from where the solute diffuses through the pores of the diaphragm into the other compartment with a lower or zero solute concentration. Typical diaphragm cell diffusion experiments are conducted

over a period of 1-3 days where the contents of both the compartments are analysed for concentration determination at the end of the experimental period (Tyrrell and Harris, 2013).

We propose in this chapter the use of a diffusion cell based on the DCM principle. By adopting the DCM method, we have investigated the self-diffusion of glucose in CCM and water (reference fluid) at 27 and $37 \pm 1^\circ\text{C}$. 37°C is chosen as most cell culture or tissue engineering experiments are conducted at $37\text{--}38^\circ\text{C}$. On the other hand 27°C is chosen as a control and typical ambient condition. It is envisaged that the diffusivity values as determined in this work will provide improved tool for designing and modelling nutrient transport in tissue engineering bioreactors.

3.2 Experimental

3.2.1 Materials

The solute used in this study was glucose of analytical grade powder D-glucose-anhydrous (Fisher Scientific UK Ltd, Loughborough, UK) of molecular weight 180.16 g/mol. The cell culture medium (CCM) used was Dulbecco's Modified Eagle Medium (DMEM) (Life Technologies Ltd, Paisley, UK). It typically contains inorganic salts (e.g., potassium chloride and sodium chloride), amino acids (e.g., glycine), vitamins (e.g., folic acid and riboflavin) and other components (e.g., phenol red and sodium pyruvate).

As the diaphragm, polyvinylidene fluoride (PVDF) membranes with pore size of 0.1 μm and thickness of 125 μm were used in the diffusion cell. These membranes were wetted overnight in deionised water in order to remove any remaining preservative on the membrane surface, prior to conducting the diffusion experiments (Suhaimi et al., 2015b).

3.2.2 Diffusion cell design

Two glass cylindrical diffusion cells were made to estimate the liquid diffusivities of glucose in both CCM and water (reference fluid). The cells consisted of identical volumes of 52.5 ml each with an internal geometry of length 60 mm x height 38 mm (Figure 3.1B). A membrane was placed in between two membrane holders belonging to each cell and clasped together when in use. Each cell had a stirrer shaft

which was clamped to a polytetrafluoroethylene (PTFE) seal of a motor. The motors were sealed by motor seal units and plugged into a diffusion cell motor control which controlled the rotational speed of the stirrer shafts (Figure 3.1A). The stainless steel impeller-like stirrer shafts had a rotational speed of 40 RPM. The radial flow impellers were used to simply maintain good mixing in each compartment. The whole apparatus was placed in a transparent temperature-controlled box with a thermocouple attached to it to regulate the experimental temperature at either 27 or $37 \pm 1^\circ\text{C}$. Both cells were assembled by tightly screwing the stainless steel rods into the standing holder which kept the whole apparatus together.

3.2.3 Experimental process

3.2.3.1 Calibration of the diffusion cell

Prior to conducting the diffusion experiments, the diffusion cell was calibrated with a calibration solute. Ethanol was chosen based on its reliable diffusivity value in water, i.e., $1.28 \times 10^{-9} \text{ m}^2/\text{s}$ which can be found in the International Critical Tables (Washburn, 1926). A diffusion experiment was performed in the diffusion cell to determine a cell constant, β , which is essential for the determination of glucose diffusion coefficient in both water and CCM. The method of calculation for DCM is presented below.

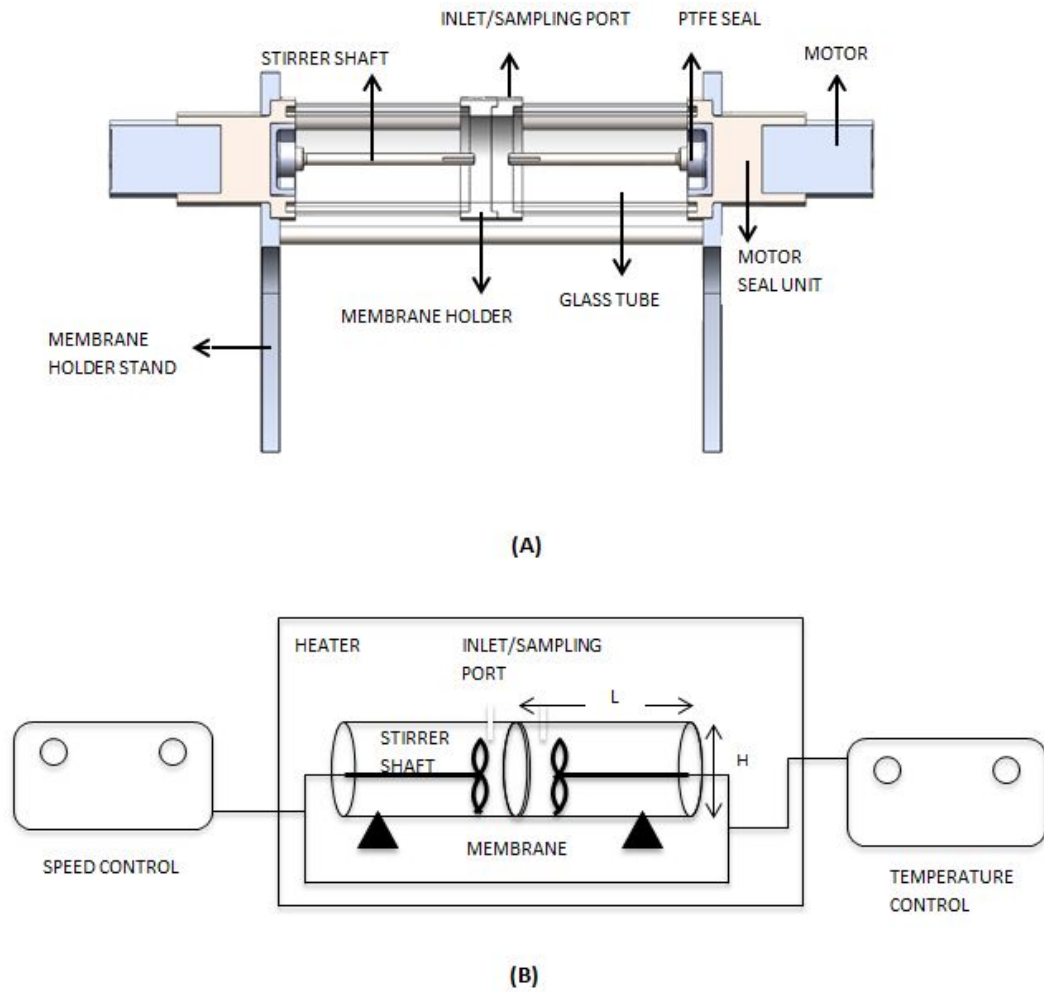


Figure 3.1: (A) Front section of cell design used in diffusion experiments; (B) Schematic drawing of the diaphragm cell set-up used for glucose diffusion experiments

To calibrate the DCM, one of the compartments was filled with ethanol solution while the other with deionized water. The diffusion of ethanol was monitored by withdrawing samples using a plastic syringe from both the compartments, at intervals of 1 h for a period of 5 h. The samples were placed in a glass cuvette and analysed by a UV spectrophotometer (UV Mini 1240, Shimadzu, Japan) at a wavelength of 196.5 nm. The samples were poured back into the compartments almost immediately after analysing, in order to keep the volume constant.

The rate of flow of liquid through the membrane is proportional to the difference of concentration in solute and it is given by:

$$j = \frac{D}{\tau \delta} (C_{\text{glucose-CCM/water}} - C_{\text{CCM/water}}) \quad (3.1)$$

where D is the solute diffusivity, τ is the tortuosity across the membrane and δ is the thickness of the membrane.

The overall mass balance of the compartment containing the glucose-CCM/water solution is defined by:

$$V_{\text{glucose-CCM/water}} \frac{dC_{\text{glucose-CCM/water}}}{dt} = -Aj \quad (3.2)$$

while for the other compartment containing CCM/water is defined by:

$$V_{\text{CCM/water}} \frac{dC_{\text{CCM/water}}}{dt} = -Aj \quad (3.3)$$

where A is the membrane surface area and t is the diffusion time.

Substituting Eq. (3.1) in Eq. (3.2) and Eq. (3.3) provides Eq. (3.4) and Eq. (3.5), respectively:

$$V_{\text{glucose-CCM/water}} \frac{dC_{\text{glucose-CCM/water}}}{dt} = -A \frac{D}{\tau\delta} \left(C_{\text{glucose-CCM/water}} - C_{\text{CCM/water}} \right) \quad (3.4)$$

$$V_{\text{CCM/water}} \frac{dC_{\text{CCM/water}}}{dt} = -A \frac{D}{\tau\delta} \left(C_{\text{glucose-CCM/water}} - C_{\text{CCM/water}} \right) \quad (3.5)$$

Dividing Eq. (3.4) by $V_{\text{glucose-CCM/water}}$ and Eq. (3.5) by $V_{\text{CCM/water}}$ we obtain Eq. (3.6) and Eq. (3.7), respectively:

$$\frac{dC_{\text{glucose-CCM/water}}}{dt} = -A \frac{D}{\tau\delta} \left(C_{\text{glucose-CCM/water}} - C_{\text{CCM/water}} \right) \frac{1}{V_{\text{glucose-CCM/water}}} \quad (3.6)$$

$$\frac{dC_{\text{CCM/water}}}{dt} = -A \frac{D}{\tau\delta} \left(C_{\text{glucose-CCM/water}} - C_{\text{CCM/water}} \right) \frac{1}{V_{\text{CCM/water}}} \quad (3.7)$$

Eq. (3.8) is derived by subtracting Eq. (3.7) from Eq. (3.6):

$$\frac{d}{dt} \left(C_{\text{glucose-CCM/water}} - C_{\text{CCM/water}} \right) = D\beta \quad (3.8)$$

where β is $-\frac{AV_{\text{CCM/water}} - AV_{\text{glucose-CCM/water}}}{\tau\delta V_{\text{CCM/water}} V_{\text{glucose-CCM/water}}}$

Finally, Eq. (3.8) is integrated with the following initial conditions:

$$t = 0$$

$$C_{f,\text{glucose-CCM/water}} - C_{f,\text{CCM/water}} = C_{i,\text{glucose-CCM/water}} - C_{i,\text{CCM/water}} \quad (3.9)$$

to give

$$\frac{C_{f,\text{glucose-CCM/water}} - C_{f,\text{CCM/water}}}{C_{i,\text{glucose-CCM/water}} - C_{i,\text{CCM/water}}} = e^{-\beta Dt} \quad (3.10)$$

By rearranging Eq. (3.10), D is defined as below (Robinson and Stokes, 1959; Cussler, 1997):

$$D = \frac{1}{\beta t} \ln \left(\frac{C_{i, \text{glucose-CCM/water}} - C_{i, \text{CCM/water}}}{C_{f, \text{glucose-CCM/water}} - C_{f, \text{CCM/water}}} \right) \quad (3.11)$$

where D is the diffusion coefficient of ethanol in water, t is the diffusion time, C is the concentration of the diffusing solute molecule and i and f denote the initial and final, respectively. β was calculated by dividing the slope of the line with the diffusion coefficient of ethanol in water. The cell constant, β , was then determined by Eq. (3.11).

It is worth pointing out that the cell constant, β , is a characteristic of the diffusion cell. Littel et al. (1992) concluded in their calibration experiment of the same principle of diffusion cell that the effect of temperature on the value of the cell constant was negligible within experimental accuracy. In addition, Sanni and Hutchison (1968) calibrated their diffusion cell at 25°C only despite having diffusion measurements at temperatures up to 60°C. They also reported in their work that there was no effect on medium change. Hence, we define in the current study that the cell constant is not dependent on temperature and/or fluid.

3.2.3.2 Methodology for diffusion experiments

One compartment was filled with glucose solution while the other compartment contained either CCM or water. The glucose powder was dissolved without further purification in a beaker with either CCM or water prior to the start of the diffusion experiment. Both solutions were allowed to reach thermal equilibrium at either 27 or 37°C in the heated water bath for 60 min before the apparatus was assembled. The whole apparatus was placed in a transparent temperature-controlled box at both temperatures. Both compartments were stirred at 40 RPM and maintained at this speed for the complete duration of the experiment.

An YSI glucose analyser (YSI 2300 STAT PLUS, YSI UK Ltd, Hampshire, UK) was used to measure the glucose concentration at initial and final conditions. The operation principle of the glucose analyser was described in detail in section 4.2.6.3. Both compartments were filled with 52.5 ml of CCM/water and the other compartment also contained 8 mg/ml of glucose solution. The glucose-in-water diffusion experiments were run for 24 and 22 h at 27 and 37 ± 1°C, respectively,

while the glucose-in-CCM diffusion experiments were run for a period of 7-11 h for both temperatures. The latter was run for a much shorter period than the former due to contamination of CCM that typically occurred beyond 11-12 h. There were two possible causes of the contamination: (i) contact with air during sampling procedure and (ii) formation of gaseous substances was observed at the inlet/sampling port which may be due to an enhanced reaction of CCM content. The latter persisted after several experiments and, hence, we concluded that the duration of the experiments was justified through repeated experiments. The samples were withdrawn simultaneously from both compartments using a plastic syringe and placed in a glass cuvette for concentration determination. 25 μl were aspirated by the sipper of the analyser. Immediately after being analysed, the samples from both compartments were poured back. This was the case for initial concentration determination only. All diffusion experiments were repeated three times. The corresponding diffusion coefficients were calculated according to Eq. (3.11) where β is the cell constant determined experimentally from cell calibration process.

3.3 Results and discussions

The self-diffusion of glucose in both CCM and water was determined for 27 and $37 \pm 1^\circ\text{C}$. A comparison is also drawn between experimentally deduced glucose diffusion coefficients with diffusion coefficient values calculated from Stokes-Einstein's equation as well as from Wilke-Chang's correlation. While Stokes-Einstein's equation gives a fair estimation based on solvent viscosity and temperature but in practice, empirical corrections are necessary to obtain more accurate estimations of liquid diffusivity. The most commonly used method based on empirical corrections is Wilke-Chang's correlation. The focus of this work is not to determine the influence of temperature on the diffusion coefficient. Hence, only two different temperatures were used in the experiments in this work.

As stated earlier, before the start of the diffusion experiments, the diffusion cell was calibrated using ethanol in order to deduce the cell constant, β . By measuring the concentration in both compartments at different times, the cell constant, β , was calculated by fitting the experimental data to Eq. (3.11). β was found to be 61197.92 m^{-2} .

Table 3.1 summarizes the results from the concentration measurements and it is apparent that the glucose diffusion coefficients in CCM are significantly reduced at a given temperature. This is due to the higher dynamic viscosity of CCM compared to water which is evident from Table 3.1. This may also be due to the presence of other molecules in CCM hindering glucose diffusion; however, we believe that this is a minor effect as the glucose is a small molecule. It is also clear that the diffusion coefficient increases from 27°C to 37°C for both CCM and water (Table 3.1). This is due to a decrease in viscosity at a higher temperature. This is also due to the increased kinetic energy of the glucose molecules at higher temperatures.

Table 3.1: Self-diffusivities of glucose in CCM and water

	Temperature (°C)	Average dynamic viscosity (kg/m/s)	Experimentally Determined	Stokes-Einstein's Equation	Wilke-Chang's Equation	From literature		Deviation between values calculated from Eq. 3.11 and Eq. 3.12 (%)
			(Eq. 3.11)	(Eq. 3.12)	(Eq. 3.13)	D (m²/s)		
			D (m²/s)			Values	Reference	
CCM	27 ± 1	0.001306489	5.67 ± 0.74 x 10 ⁻¹⁰	4.61 x 10 ⁻¹⁰	Not calculated due to lack of data	NA	NA	23.0
	37 ± 1	0.001100855	6.16 ± 1.25 x 10 ⁻¹⁰	5.65 x 10 ⁻¹⁰	Not calculated due to lack of data	5.90 x 10 ⁻¹⁰	Provin et al. (2008)	9.0
Water	27 ± 1	0.000865269	6.98 ± 0.60 x 10 ⁻¹⁰	6.96 x 10 ⁻¹⁰	7.92 x 10 ⁻¹⁰	5.40 x 10 ⁻¹⁰	Kleinstreuer and Agarwal (1986)	0.3
	37 ± 1	0.000649516	9.58 ± 0.13 x 10 ⁻¹⁰	9.58 x 10 ⁻¹⁰	1.09 x 10 ⁻⁹	9.00 x 10 ⁻¹⁰	Buchwald (2011)	0.0

In Table 3.1, a comparison is also drawn between glucose diffusivities deduced experimentally, diffusion coefficients derived from Stokes-Einstein's equation as well as from Wilke-Chang's correlation and values reported in literature. The glucose diffusion coefficient in CCM at 37°C calculated from the Stokes-Einstein's equation is found to be $5.65 \times 10^{-10} \text{ m}^2/\text{s}$. This is consistent with the results of Provin et al. (2008), who have also estimated glucose diffusivity in CCM for the application of designing 3D scaffolds for high-density cell attachment using the same equation at the same temperature. Their result was found to be $5.90 \times 10^{-10} \text{ m}^2/\text{s}$. In addition, Buchwald (2011) has quoted a value of $9 \times 10^{-10} \text{ m}^2/\text{s}$ for the glucose diffusivity in water at 37°C for the study of glucose-induced insulin secretion model. The value obtained by Buchwald is very similar to what has been deduced experimentally in the current study, which is $9.58 \times 10^{-10} \text{ m}^2/\text{s}$.

The percentage deviation values calculated in Table 3.1 are based between the experimentally determined values and values calculated from the Stokes-Einstein's equation.

The Stokes-Einstein's equation is defined in this work as (Einstein, 1905):

$$D = \frac{k_B T}{6\pi\eta r} \quad (3.12)$$

where k_B is Boltzmann's constant with a value of $1.3807 \times 10^{-23} \text{ J/K}$, T is the working temperature in K, η is the liquid dynamic viscosity in kg/m/s and r is the Stokes radius of glucose with a value of $3.65 \times 10^{-10} \text{ m}$ (Bouchoux et al., 2005). The liquid dynamic viscosity at different temperature is determined in-house using a U-tube viscometer (Poulten, Selfe & Lee Ltd, Essex, UK) (Kim et al., 2002), which are provided in Table 3.1. The experiments provided values of kinematic viscosity, which were converted to dynamic viscosity for the purpose of this work. The experiments for the measurements of the fluid viscosity were performed at two operating temperatures, i.e., 27 and $37 \pm 1^\circ\text{C}$ for both CCM and water.

The Wilke and Chang correlation is given as (Wilke and Chang, 1955):

$$D = 7.4 \times 10^{-8} \frac{(\phi M)^{1/2} T}{\eta V^{0.6}} \quad (3.13)$$

where ϕ is the association factor for water (2.26), M is the relative molecular mass of solvent in g/mol, T is the working temperature in K, η is the liquid dynamic viscosity in cP and V is the glucose molar volume at its normal boiling point in

cm³/mol. Wilke-Chang correlation is used to calculate the glucose diffusion coefficient in water only due to an unknown association factor for CCM.

3.4 Chapter summary

A diffusion cell has been designed and constructed to determine the self-diffusion of glucose in CCM and water. The cell was calibrated prior to conducting the diffusion experiments to determine the cell constant, β , which is essential for the determination of the glucose self-diffusion coefficient in CCM and water. All diffusion experiments for both 27 and $37 \pm 1^\circ\text{C}$ were repeated three times. The results show the diffusion coefficients of glucose in CCM are significantly reduced at a given temperature due to the larger dynamic viscosity of CCM compared to the ones in water. This may also be due to the multi-component interactions present in CCM and what we obtained is therefore a lumped effect from a number of inter-related phenomena.

CHAPTER 4

GLUCOSE DIFFUSIVITY OF TISSUE ENGINEERING MEMBRANES AND SCAFFOLDS

Chapter overview

There has been an increasing interest in the concept of growing artificial tissues in bioreactors which use numerous membranes and scaffolds to support the cellular processes such as cell growth and nutrient uptake. While these approaches are promising and may be considered to be successful in some circumstances, there is a general lack of quantitative information on the glucose (nutrient) diffusivity of these materials. In addressing this issue we have carried out a series of well-defined laboratory experiments to measure the glucose diffusion coefficient across a number of tissue engineering membranes and scaffolds saturated with water and cell culture medium (CCM). For this purpose, a diffusion cell was constructed and five different membranes and scaffolds with varying pore size and shapes were employed, which include cellulose nitrate membrane, polyvinylidene fluoride membrane, poly(L-lactide) scaffold, poly(caprolactone) scaffold and collagen scaffold. Pore size distribution, porosity and tortuosity of these materials were then determined and correlated to the glucose diffusivity values. As expected, we found that the diffusion coefficient increases with increasing pore size of the materials. These relationships are non-linear and may be non-monotonic in nature as they depend on a number of factors such as the basic building blocks of the materials which are non-periodic and heterogeneous in nature and vary within the same material, or from one material to another. We observed that glucose diffusivities in the materials saturated with CCM are significantly reduced at a given temperature which is contrary to what have been generally assumed in the previous studies on glucose transport processes. Therefore, a conclusion can be drawn that the presence of extra components and difference in fluid properties of CCM compared to water have a significant effect on the glucose diffusion coefficient in the tissue engineering membranes and scaffolds.

4.1 Introduction

The concept of growing cells outside the human body and their survival has been proven to work dated back almost a century ago when Wilhelm Roux, a German zoologist, had successfully cultured chick neural crest in warm saline water for over a period of few days (Hamburger, 1997). This is supported by Alexis Carrel, a Nobel Prize winner in 1912, whose work showed that not only it is possible to grow tissues including connective and heart tissues *in vitro* but also maintain their characteristics for over a long period of time (Carrel, 1912). Tissue engineering has emerged now to be a valuable tool as a solution to overcome health problems such as tissue damage, degeneration and failure.

Engineered bone (Kimelman-Bleich et al., 2011; Grayson et al., 2010), cartilage (Schulz et al., 2008), tendon (Abousleiman et al., 2009; Omae et al., 2012) and blood vessel tissues (L'Heureux et al., 2007) have been successfully cultured both *in vitro* and *in vivo* (Kimelman-Bleich et al., 2011; Omae et al., 2012; L'Heureux et al., 2007). But studies have shown that culturing functional tissues *in vitro* is more complex than *in vivo* due to the need for a controlled environment during cell cultivation (Li et al., 2013). Hence, a bioreactor system is essential. To date, there have been several types of bioreactors designed to culture and grow 3D tissues, such as spinner flasks (Page et al., 2013), rotating vessels (Nishi et al., 2013; Chao and Das, 2015), perfusion systems (Baptista et al., 2013), magnetic force bioreactors (Bock et al., 2010), compression or strain bioreactors (Abousleiman et al., 2009; Wartella and Wayne, 2009), combined bioreactors which may couple perfusion with compression (Liu et al., 2012) such as rotating compression bioreactors (Wu et al., 2013) and, another perfusion bioreactor, namely, hollow fibre membrane bioreactors (Ye et al., 2006; Abdullah et al., 2009; Napoli et al., 2011, 2014; Chapman et al., 2012). Even though these bioreactors give hopes to tissue engineering approaches, they may not be able to prolong the cell culture environments (Li et al., 2013). One of the reasons for this is limited nutrient diffusion through scaffolding matrix and membrane. To achieve the desired rate of mass transfer and allow the development of novel membranes and scaffold, a good understanding of the quantitative relationship between their properties and nutrient transport behaviour is essential (Chao and Das, 2015). A good understanding of the mass transfer behaviour in these

materials is also necessary as these materials may be used to calibrate and develop biosensors, e.g., for monitoring glucose level (Boss et al., 2012; Wang et al., 2013).

One of the important components of most tissue engineering bioreactors is the scaffold/membrane matrix which acts as a support for cells to grow into new tissues before being implanted into the host tissue. Some of the general characteristics of the support materials are that they must be porous for ease of nutrient diffusion and waste product removal (Florczyk et al., 2013; Guan et al., 2013; Deans et al., 2012), biocompatible (Stamatialis et al., 2008), the material must possess comparable mechanical properties to that of *in vivo* tissues (Karageorgiou and Kaplan, 2005; Karande et al., 2004), allow cell seeding, and others. Some examples of these support materials for tissue engineering purposes are summarised in Table 4.1.

Table 4.1: Some examples of commonly used support porous materials and their characteristics

Material	Fabrication technique	Pore size (μm)	Porosity (%)	Reference
Poly(lactic-co-glycolic acid)(PLGA) scaffold	Fiber knitting	NA	NA	Ouyang et al. (2003); Sequeira et al. (2012)
Poly(caprolactone) (PCL) scaffold	Salt leaching and thermal induced phase separation	NA	93.6 ± 0.6	Zhang et al. (2013)
Hydroxyapatite (HA) scaffold	Imaging techniques and stereo lithography	250	40	Chu et al. (2002); Kim et al. (2007)
Poly(L-lactide)/ β -tricalcium phosphate (PLLA/ β -TCP) scaffold	Solvent self-proliferating/model compressing/particulate leaching	100-250	57	Xiong et al. (2002); Kang et al. (2009)
Collagen-glycosaminoglycan (GAG) scaffold	Lyophilisation technique	96	99.5	O'Brien et al. (2005); Keogh et al. (2010)
Poly(lactic-co-glycolic acid)(PLGA) membrane	Dry/wet- and wet-spinning	0.2-1.0	NA	Ellis and Chaudhuri (2007)
Poly(lactic-co-glycolic acid)(PLGA)/polyvinyl alcohol	Wet-spinning	0.54 ± 0.11 (PLGA)	46	Meneghello et al.

(PVA) membrane		0.67 ± 0.15 (1.25 % PVA-	67	(2009)
		0.89 ± 0.16 μm (2.5% PVA-	76	
		1.1 ± 0.1 μm (5 %	77	
Poly (lactide-co-glycolide)(P _{DL} LGA) membrane	Wet-spinning phase-inversion	0.16 ± 0.006	NA	Morgan et al. (2007)
Nanoporous polyethylene membrane	Stereolithography using a biocompatible medical-grade resin (proform)	0.01649	28.9 ± 4.93	Boss et al. (2012); Boss et al. (2011)
Polypropylene microporous membrane	Melt-extrusion/cold-stretch	0.10	45-50	Yu et al. (2008)
Titania nanotubular membrane	NA	0.125	60-70	Paulose et al. (2008)

Tissue growth and survival are undoubtedly complex, involving an immense variety of processes from intracellular transduction pathways to tissue-level mechanics (O'Dea et al., 2013). Cell differentiation, survival and proliferation of tissue-engineered constructs are highly dependent on the availability of nutrients. Therefore, the diffusion as well as the distribution and availability of the relevant solutes, e.g., nutrients, must be fully grasped as they are important for tissue formation, growth and survival (Liu et al., 2013). Glucose and oxygen are critical molecules in these regards as shown in both experimental and modelling studies (e.g., Mauck et al., 2003a; Ye et al., 2006). In contrast to oxygen which has been extensively studied over the years (Malda et al., 2004a, 2004b; Kellner et al., 2002; Guaccio et al., 2008; Ellis et al., 2001), there is limited knowledge available on the diffusion coefficients of other nutrients or metabolites especially glucose and lactic acid in porous membrane and scaffold within cell culture media (CCM) (Liu et al., 2013). Most diffusion coefficient data are for cases where these materials are saturated with water at ambient conditions. However, the cell/tissue culture experiments are typically conducted at 37-38°C and the materials are imbibed with cell culture medium (CCM).

The diffusivities of glucose in aqueous solutions were measured some sixty years ago (Longworth, 1952). More extensive measurements of glucose diffusion coefficients in different fluid and porous media have been studied as well, such as water (Dionne et al., 1996), poly-ether-sulphone and poly-sulphone (Curcio et al., 2005), polyvinyl alcohol (Phanthong and Somasundrum, 2003), calcium alginate (Chai et al., 2004), collagen gel (Shaw and Schy, 1981), agarose gel (Weng et al., 2005) and hemodialysis films and hollow fibers for blood purification processes (Klein et al., 1977). However, there is little or no published information that discuss specifically the glucose diffusivity across membranes or scaffolds that are used for cell/tissue engineering. Lactic acid is beyond the scope of this study and will not be covered here.

While a number of techniques have been studied and developed to study the diffusion of small molecules such as light scattering (Bica et al., 2001), nuclear magnetic resonance microscopy (NMR) (Kwak and Lafleur, 2003; George et al., 2004), fluorescence spectroscopy (Ye et al., 2003; McCain et al., 2004), fourier transform infrared microscopy (FTIR) (Sahlin and Peppas, 1996; Peppas and

Wright, 1996), electrochemical techniques (Zhang et al., 2002; Cleary et al., 2003) and fluorescence recovery after photobleaching (FRAP) (Pluen et al., 1999), these often require sophisticated and indirect methods for the concentration measurements of the molecule diffusing across the membrane. These may not allow the diffusion process to be monitored continuously (Lu et al., 2013). Furthermore, the suitability of these techniques to study the materials investigated in the present study may not match with the materials' properties. For instance, the light transmission from and to the solute molecules in the gel-like scaffolds to capture its speed is not possible for used in the present study due to the membranes/scaffolds investigated are generally not transparent. We propose in this study the use of a simple diffusion cell that is easy to use and allows us to monitor the diffusion process continuously over time.

The interest in the determination of diffusion coefficients in membranes particularly in chemical and biotechnological applications can be found in many applications of membranes, e.g., water treatments, drug delivery and tissue engineering (Choi et al., 2013; Bai et al., 2012; Jeon et al., 2012; Parizek et al., 2012; Peter et al., 2010). Despite a number of literature works, it does seem that the mass transfer behaviour in terms of dependence of diffusion on membrane morphology is still not fully understood (Wang and Ma, 2012). Molecular diffusion is dependent on the membrane morphology and the fluid that saturates it may have an effect on the diffusivity values (Cussler, 2009). Diffusional boundary layers that are created at the porous material-liquid interfaces may offer different resistances to diffusion as the fluid and materials change (Chan et al., 2012). The temperature of the system also plays important roles in determining the molecular diffusion. For example, the temperature affects both the solubility and diffusion coefficient of a molecule in a fluid and the porous material (Chen et al., 2013). The temperature also impacts the interactions among the multi-components that make up the fluid (e.g., a cell culture media) which may affect the diffusion coefficient of the molecule particularly if the molecular size is big (Abdullah and Das, 2007). What we obtain for the measurements of the diffusion coefficient of a molecule is therefore a lumped effect from a number of inter-related phenomena.

It is therefore the purpose of our work to quantify the relationship between diffusion coefficient and membrane morphology by engaging typical membrane and scaffold materials for tissue engineering in diffusion experiments and relating the diffusivity

values to the quantitative information of the pore morphology of the materials. We acknowledge that some papers have discussed the dependence of the diffusion coefficient on temperature, for example, that by Yui et al. (2013) which discusses the change in diffusion coefficient of some solutes in water as temperature changes. Cai et al. (2012) reported the diffusion of glucose in membranes at 20°C and 37°C in deionized water and in NaCl solution. Umecky et al. (2013) also reported the influence of temperature on the values of the diffusion coefficient of amino acids in water. However, none of these papers really relate to the specific tissue engineering membranes, fluids (i.e., cell culture media) or combination of these two as they are normally used in tissue engineering.

In this chapter, we have adopted a two-compartment diffusion cell technique to investigate the glucose transport properties of typical tissue engineering membranes and scaffolds within CCM and water. This includes the relationship between the morphology of membranes and scaffolds and its effect on glucose diffusivities. In addition, tortuosity and porosity as well as the diffusion coefficient of glucose in free media have been determined.

Please note that although the materials chosen for this work are designed for tissue engineering purposes, they are not seeded with any biological cells yet (see chapter 5) in the experiments. This is because this chapter is aimed at quantifying simple passive diffusion of glucose through the materials. As mentioned earlier, the diffusivity values are needed for a number of practical scenarios, e.g., modelling of mass transport in tissue engineering bioreactors, choosing the materials for tissue engineering bioreactors and biosensors, and any others. If indeed the membranes and scaffolds are seeded with biological cells (e.g., stem or epithelial cells; adherent or suspended cells), the mass transfer rate may be different due to their presence. The effective passive diffusion in this case may be different depending on a number of factors, e.g., density of cells in the materials, glucose uptake rate by the cells and any other factors. We consider this to be a ‘derived’ property and not discussed in this chapter.

4.2 Materials and methods

4.2.1 Membranes

Two types of membranes were used in this study: cellulose nitrate (CN) and polyvinylidene fluoride (PVDF). The CN and PVDF membranes were purchased from Fisher Scientific UK Ltd (Loughborough, UK) and Millipore UK Ltd (Watford, UK), respectively. Table 4.2 shows the main characteristics of these membranes. Prior to conducting all experiments, the membranes were soaked in deionised water for a day in order to remove any remaining preservative on the membrane surface. We define that water fully imbibes into the membrane during this time period and, that there is no significant swelling and, hence, changes in the pore morphology of the membrane after this period. Table 4.3 shows the thicknesses of these membranes as measured using a surface profiling (non-contact mode) instrument (Talysurf CLI 2000, Taylor Hobson Ltd, Leicester, UK). The differences between the thicknesses at different time intervals are defined as due to the swelling of the membrane because of imbibition. The measurements were only done for water. As evident from the table, there is no significant change in the thickness of the membrane and, hence, swelling.

4.2.2 Scaffolds

Poly(caprolactone) (PCL), poly(L-lactide) (PLLA) and collagen scaffolds were used in this study. PCL was purchased from the Electrospinning Company Ltd (Didcot, UK) while PLLA was a kind gift from the same company. Collagen was purchased from Matricel GmbH (Herzogenrath, Germany). Table 4.2 shows the main characteristics of these scaffold materials. Before their use, all scaffolds were treated as follows. PCL was treated with 15% ethanol (Fisher Scientific UK Ltd, Loughborough, UK) for 30 min to aid in wetting the material and to remove any trapped air, before being soaked and washed with deionised water, replacing the water twice in 30 min in order to remove any trace of ethanol. The same treatment was applied to PLLA except that a 70% ethanol solution (Fisher Scientific UK Ltd, Loughborough, UK) was used. Collagen scaffold was pre-soaked in deionised water for 30 min before used in experiments. A different treatment was used in this case as the collagen scaffold is hydrophilic while both PCL and PLLA are hydrophobic in nature. Similar to the membranes, we define that there is no significant swelling and,

hence, changes in the pore morphology of the scaffold after this period. Table 4.3 shows the thicknesses of these scaffold materials. Similar to the membranes, it is deduced that there is no significant swelling based on the results depicted in the table.

4.2.3 Other materials

The cell culture medium (CCM) used was Dulbecco's Modified Eagle Medium (DMEM) (Life Technologies Ltd, Paisley, UK). The glucose was of analytical grade powder D-glucose-anhydrous (Fisher Scientific UK Ltd, Loughborough, UK) of molecular weight 180.16 g/mol.

Table 4.2: Summary of the commercial membrane and scaffold properties

Material		Thickness (µm) based on Manufacturers' information	Manufacturers' pore size (µm)	Min pore size (µm)	Mean pore size (µm)	Max pore size (µm)	Source
Membrane	PVDF	125	0.1	0.08	0.32 ± 0.29	1.65	Merck Millipore (Watford, UK)
	CN	122.5	0.45	0.21	0.6 ± 0.30	2.09	Whatman International Ltd (Maidstone, UK)
Scaffold	PLLA	50	12-18	4.04	13.67 ± 4.25	25.87	The Electrospinning Company Ltd (Didcot, UK)
	PCL	50	20-30	5.8	21.69 ± 6.85	44.84	The Electrospinning Company Ltd (Didcot, UK)
	Collagen	1500	80	12.55	75.15 ± 5.21	175.18	Matricel GmbH (Herzogenrath, Germany)

Table 4.3: Material thicknesses as measured a surface profiling instrument (Talysurf CLI 2000, Taylor Hobson Ltd, Leicester, UK), and their respective swelling percentage. Please note that the average thicknesses we have measured vary slightly from the values of average thickness that the manufactures provide for the same samples (Table 4.2)

Material	Average thickness of dry sample (1)	Average thickness of wet sample after soaking in water for 24 hours (2), which represent the samples at the beginning of diffusion experiment	Average thickness of wet sample after soaking in water for 48 hours (3), which represent the samples at the end of diffusion experiments	Swelling between dry sample (1) and wet sample (2)	Swelling between wet sample (2) and wet sample (3)
	(μm)	(μm)	(μm)	(%)	(%)
PVDF membrane	98.38	98.61	101.23	0.23	2.66
CN membrane	124.22	125.54	129.79	1.06	3.39
PLLA scaffold	32.04	33.58	34.11	4.81	1.58
PCL scaffold	37.79	38.85	40.89	2.80	5.25
Collagen scaffold	1659.37	1699.9	1715.3	2.44	0.91

4.2.4 Determination of pore size distribution of the membrane and scaffold materials

Measurement of pore size is done manually using the software ImageJ (Wayne Rasband, National Institute of Mental Health, USA). The analysis of the pore size distribution of the sample materials also used scanning electron microscopy (SEM) images where it enables visual images of membrane/scaffold's morphology and can be used directly in ImageJ software. Although these images refer to the surface morphology of the membranes and scaffolds investigated, they represent the sample morphology well as the samples have a fairly homogeneous (narrow range) of pore size distribution. The SEM images were uploaded on to the software and lines were drawn for every pore after setting the scale to track the measurements. The minimum, maximum and average of pore size are shown in Table 4.2. On the other hand, the pore size distributions for the selected materials are shown in Figure 4.3.

4.2.5 Evaluation of the porosity (ε) and tortuosity (τ) of the membrane and scaffold materials

Besides the pore size distribution, the porosity values of the materials were determined as they effect the solute diffusion through the materials. The porosity values depend on the size and distributions of the pores in the materials. Further, they are required to find out the tortuosity of each membrane/scaffold material in this study.

Porosity is defined as the ratio of voids volume to total volume:

$$\varepsilon = 1 - \frac{V_m}{V_t} \quad (4.1)$$

where, v_m is solid volume and v_t is total volume of sample.

Porosity can be determined either using indirect or direct approaches. Apparent densities estimation, pycnometric methods and mercury porosimetry are direct approaches while computerised analysis of scanning electron microscopy images and air-liquid displacement techniques are indirect approaches (Palacio et al., 1999). In this study, we opted for a direct approach, which is a pycnometric method. By measuring the masses and fitting the experimental data into the equation below, porosity is evaluated.

$$\varepsilon = 1 - \frac{m_1 + m_2 - m_3}{V_t \rho_w} \quad (4.2)$$

where m_1 is the mass of dry sample, m_2 is the mass of pycnometer levelled with water, m_3 is the mass of pycnometer levelled with water together with sample contained inside and ρ_w is the water density which is 0.9970 g/cm^3 at room temperature.

The dry membranes and scaffolds were each weighed separately before soaking them wet in the pycnometer. Assuming the porous materials were soaked completely and effectively in water, the masses of these wet samples were measured together with the water-levelled pycnometer, giving m_3 . The experimental data were then fitted into Eq. (4.2) above giving porosity of the materials investigated.

Tortuosity, on the other hand, considers the increase in distance of a diffusing molecule due to pore bending and curves. Tortuous channels hinder the movement of molecules which gives resistance to mass transfer. This hindrance is included and defined by the tortuosity factor which takes into account the fluid transport system as well as the pore connectivity. A relatively straight channel gives a tortuosity value of unity while porous materials give a tortuosity value greater than unity, but typically between 2 and 3 (Martin, 1993).

Nuclear magnetic resonance (NMR) based measurements, mercury intrusion porosimetry, image analysis (Wu et al., 2006) and determination of the ratio of diffusion coefficient in free media to the diffusion coefficient in the porous network (Barrande et al., 2007) are some example methods used to evaluate the tortuosity. The latter is used in this study where the effective diffusion coefficient (D_e) is derived from diffusivity measurements with the diffusion cell; porosity (ε) is derived from the aforementioned method and the diffusion coefficient in free media (D) is calculated from Eq. (3.11). Hence, tortuosity (τ) is derived from the following relationship:

$$D_e = D \frac{\varepsilon}{\tau} \quad (4.3)$$

It must be noted that different types of diffusivities are used in the above equation where D_e leads to transport diffusivity by fitting experimental measurements into Eq. (4.6) while D represent self-diffusivities calculated from Eq. (3.11).

4.2.6 Measurement of glucose diffusion coefficient

4.2.6.1 Diffusion cell for measurement of glucose diffusion coefficient

Two rectangular diffusion cells, which are similar to those described by Chenu and Roberson (1996), were made to measure the diffusion coefficient of glucose across the membranes and scaffolds in both CCM and water. Both cells consisted of two acrylic chambers with identical volumes. The chambers were called donor and receptor phase, respectively. A larger cell was used to determine the diffusion of glucose across the membranes and scaffolds in water while the smaller cell was used with CCM to help reduce the amount of CCM consumed per experiment. The diffusion cells were assembled by tightly screwing the half chambers into the rubber gaskets, with the membrane/scaffold fixed in between (Figure 4.1). The rubber gaskets were embodied to prevent leakage between the half chambers.

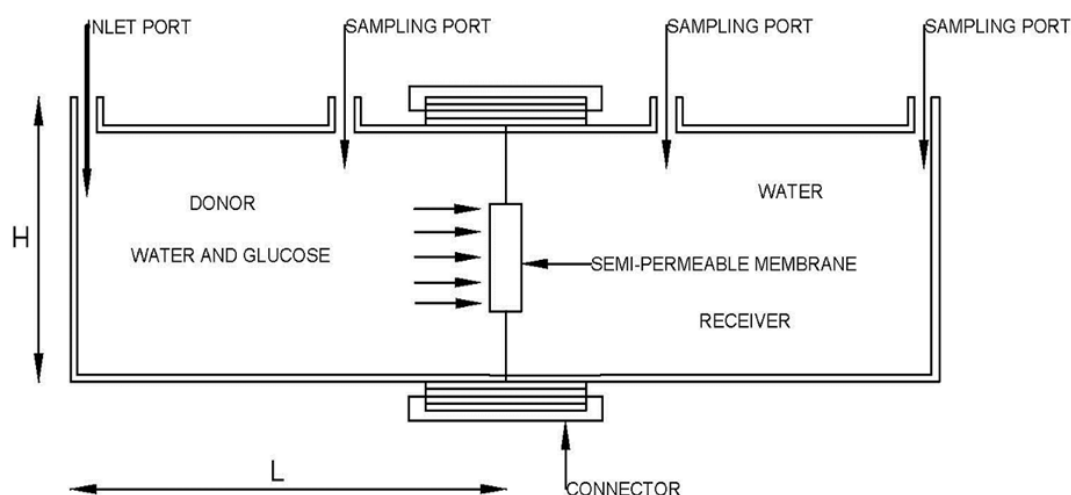


Figure 4.1: Schematic drawing of a diffusion cell

The larger cell has a volume of 207.5 ml per chamber with an internal geometry of length 100 mm x height 45 mm x width 50 mm. The smaller cell has a volume of 41 ml per chamber with an internal geometry of length 20 mm x height 45 mm x width 45 mm. Each half chamber was filled with either CCM or water. The donor phase also contained glucose solution. The glucose powder was pre-mixed in a beaker with either CCM or water prior to the start of the experiment. Both solutions of pure CCM/water (receptor phase) and glucose mixed with CCM/water (donor phase) were allowed to equilibrate at either 27 or 37°C in the heated water bath for 60 min

before the apparatus was assembled. The whole apparatus was placed in a thermostated water bath at either 27 or $37 \pm 1^\circ\text{C}$.

The corresponding diffusion coefficients were calculated according to Fick's first law. Fick's first law describes the diffusion of small uncharged molecules well. It is given by (e.g., Crank, 1975)

$$J = -D \frac{\partial c}{\partial z} \quad (4.4)$$

where J is the mass flux describing the mass transfer through an area per unit time, D is the diffusion coefficient of the solute molecule; c is the concentration of the diffusing solute molecule while z is the diffusion length. Obstruction effects as a result from diffusion across membranes and scaffolds must be considered with certain porosity and partition coefficient. These properties are included in the effective diffusion coefficient of the material (Gutenwik et al., 2004) defined by

$$J = -D_e \frac{\partial c}{\partial z} \quad (4.5)$$

Assuming that there was no change in volume, Eq. (4.5) was transformed into Eq. (4.6) and that the glucose diffusion across membranes and scaffolds in CCM was calculated as given below:

$$V_d \frac{\partial c_d}{\partial t} = -D_e A \frac{c_d - c_r}{l} \quad (4.6)$$

where l was the membrane/scaffold thickness, A the membrane/scaffold area, D_e the effective diffusion coefficient of the material and V_d the donor volume. By measuring the concentration in both chambers at different times, a diffusion coefficient was calculated by fitting Eq. (4.6) to the experimental data.

4.2.6.2 Measurements of glucose diffusivities of the samples saturated in water

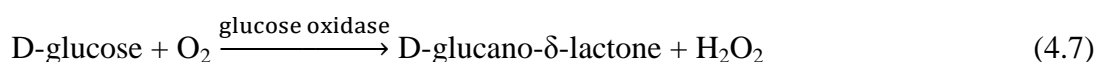
A UV spectrophotometer (UV Mini 1240, Shimadzu, Japan) was used to monitor the change in glucose concentration over time. Each chamber (Figure 4.1) was filled with 207.5 ml of deionized water as this is the amount that is required to fill the chamber completely. The donor phase also contained 2 mg/ml of glucose solution. Samples of 2.5 ml were taken using a plastic syringe from both the donor and receptor phase at intervals of 1 h until equilibrium was established. The samples were placed in a glass cuvette and analysed by the UV spectrophotometer at a wavelength of 190 nm. Immediately after being analysed, the samples were poured

back into the donor and receptor phase, respectively, to keep the volume constant. All experiments were conducted in duplicate.

4.2.6.3 Measurements of glucose diffusivities of the samples saturated in CCM

An issue was encountered while investigating the diffusion of glucose in CCM. The photometric elution curve showed significant noise at around 190 nm suggesting that the presence of other molecules in CCM might interfere and obscure the concentration measurements. To resolve this issue, a glucose analyser was used instead. To resolve this issues and to measure the diffusion of glucose in CCM, an YSI glucose analyser (YSI 2300 STAT PLUS, YSI UK Ltd, Hampshire, UK) was used. The outstanding performance of YSI glucose analyser has been known for more than two decades (Lindh et al., 1982; Clarke et al., 1987; Burrin and Alberti, 1990). It has been well accepted as a device for measuring glucose concentration due to its ease of use, quick analysing time (1 min) and small sample size (25 µl). This instrument is based on enzymatic reaction. The system consists of two membrane layers, an enzyme layer and a platinum electrode. The first layer which houses porous polycarbonate minimises the glucose diffusion into the enzyme layer to avoid the reaction from becoming enzyme-limited while the third layer which contains cellulose acetate only allows small molecules such as hydrogen peroxide to pass through and finally reaches the platinum electrode where it is oxidised to produce electrons.

Immobilized enzyme reaction:



Anode reaction:



Each half chamber was filled with 41 ml of CCM. The donor phase also contained 8 mg/ml of glucose solution. The diffusion of glucose was monitored by withdrawing samples using a plastic syringe from both the chambers, at intervals of 1 h for a period of 8-9 h. The samples were placed in a glass cuvette and 25 µl were aspirated by the sipper for glucose concentration determination. The volume loss for each chamber remains consistent for every sample, thus the issue of keeping the volume constant can be ignored. All diffusion experiments were conducted in duplicate.

4.2.7 Determination of glucose diffusion coefficient in liquid

Diffusion coefficient of glucose in liquid media is an important factor to evaluate tortuosity. In this work, Eq. (3.11) is used to evaluate this parameter for both water and CCM (see section 3.2.3.1).

Stokes-Einstein's equation is also considered in this chapter to compare with liquid diffusion coefficient values reported in previous papers (see Table 4.7).

$$D = \frac{k_B T}{6\pi\eta r} \quad (4.9)$$

where k_B is Boltzmann's constant with a value of 1.3807×10^{-23} J/K, T is the working temperature in K, η is the liquid dynamic viscosity in kg/m/s and r is the Stokes radius of glucose with a value of 3.65×10^{-10} m (Bouchoux et al., 2005). The liquid dynamic viscosity is determined in-house using a U-tube viscometer (Poulten, Selfe & Lee Ltd, Essex, UK) (Kim et al., 2002), which are provided in Table 4.4. This gave kinematic viscosity, which were converted to dynamic viscosity. The experiments for the measurements of the fluid viscosity were performed at two operating temperatures, i.e., 27 and $37 \pm 1^\circ\text{C}$ for both water and CCM.

Table 4.4: Dynamic viscosities of liquids at different temperatures (determined in-house using a U-tube viscometer)

Liquid	Temperature ($^\circ\text{C}$)	Average dynamic viscosity (kg/m/s)
Water	27 ± 1	0.000865269
	37 ± 1	0.000649516
CCM	27 ± 1	0.001306489
	37 ± 1	0.001100855

4.3 Results and discussions

To investigate the relationship between diffusion and membrane morphology, the microstructures of all the materials were investigated using a scanning electron microscopy (SEM) as discussed in the next section. The diffusion of glucose across membranes and scaffolds saturated in water and CCM was monitored. The results show that the diffusion coefficient is higher at a larger pore size, indicating least resistance of glucose molecules diffusing through the channel. Porosity and tortuosity were also determined to develop a correlation between diffusion and membrane morphology with porosity and tortuosity.

4.3.1 Material characterization

SEM was utilized to observe the morphology of membranes and scaffolds used in this work. The dry samples were placed on a sample stand and coated with carbon. The high voltage SEM (Cambridge Stereoscan 360 SEM) was used to view the surface morphology of the investigated membranes and scaffolds. Figure 4.2 presents typical SEM images of PVDF membrane, CN membrane, PCL scaffold, PLLA scaffold and collagen scaffold. The photographs show the distribution of pores and channels within the material where Figure 4.2a and 4.2b show the pore distribution of the membranes. Please note that Figures 4.2a and 4.2b have different scale bars. Figure 4.2c-4.2e show the distribution of channels and that collagen scaffold has relatively straight orientation and larger pores and this attributes to the diffusivity value presented in Table 4.6.

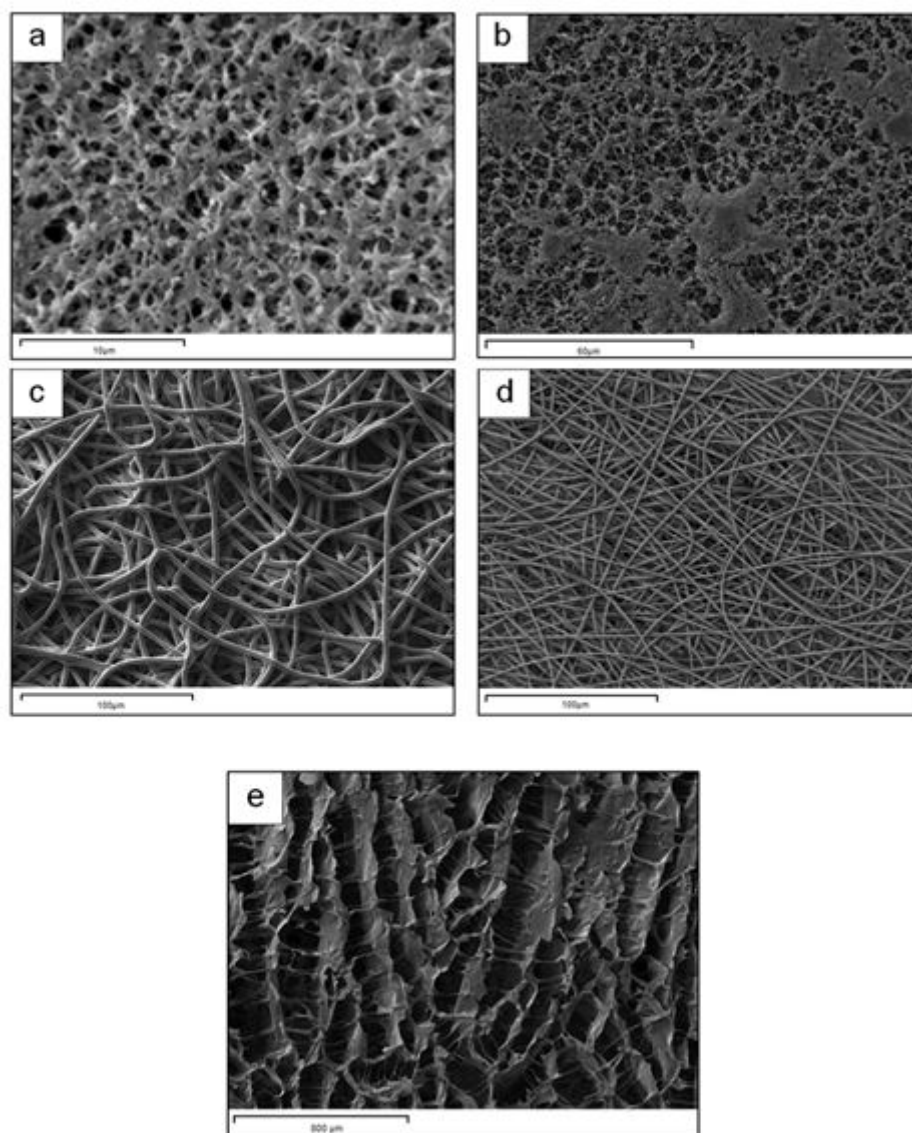


Figure 4.2: SEM micrographs showing surface morphology of the selected sample materials: (a) PVDF membrane, (b) Cellulose Nitrate membrane, (c) PCL scaffold, (d) PLLA scaffold and (e) Collagen scaffold

Pore size distribution across the surface of the material was also investigated (Figure 4.3) using the software ImageJ. It is done manually as described in section 4.2.4 and the procedure is reproducible. Most results are in good agreement with the manufacturer's size rating except for PVDF membrane. PVDF gave a higher mean pore size than the rating and can be ignored.

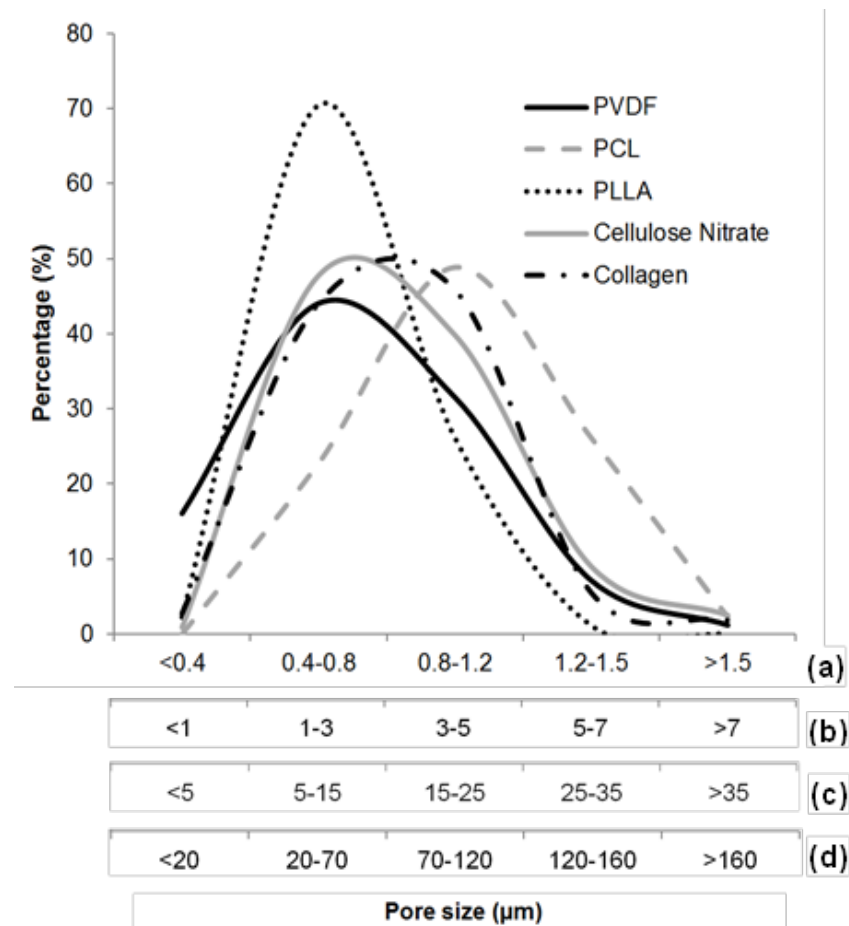


Figure 4.3: Average pore size distribution of membrane/scaffold as determined by us; x-axis scales are referred as follows: (a) Cellulose Nitrate membrane, (b) PVDF membrane, (c) PCL and PLLA scaffolds and (d) Collagen scaffold. The pore sizes have been manually obtained using ImageJ

4.3.2 Atomic force microscopy (AFM) observation for surface roughness

Atomic force microscopy is a characterisation method and presents high possibilities of application in both the field of microscopy observation and characterisation of various surfaces (Ochoa et al., 2001). The difference between AFM and SEM is that AFM can be used to determine 3D surface topography/roughness while SEM is used to determine pore size, both of which have been reported to affect the diffusion process. Figure 4.4 shows the 3D AFM images of cellulose nitrate (CN) membrane and PVDF membrane at a scan area of 10 μm using an atomic force microscope model Topometrix Explorer (Veeco Explorer AFM, Santa Barbara, USA) with a high resonant frequency (HRF) silicon probe and tapping mode as the imaging mode. The nodules are seen as bright high peaks.

The results for roughness parameters R_a and R_{rms} are presented in Table 4.5. R_a is the average surface roughness while R_{rms} is the root mean squared values. The average surface roughness values and the root mean squared values were estimated by the AFM software using the following expressions (Henke et al., 2002):

$$R_a = \frac{1}{N} \sum_{i=1}^N |z_i| \quad (4.10)$$

$$R_{rms} = \sqrt{\frac{1}{N} \sum_{i=1}^N z_i^2} \quad (4.11)$$

where N is the number of points sampled on the surface and z_i is the surface height variation of the point ($\pm z$) from the mean surface level.

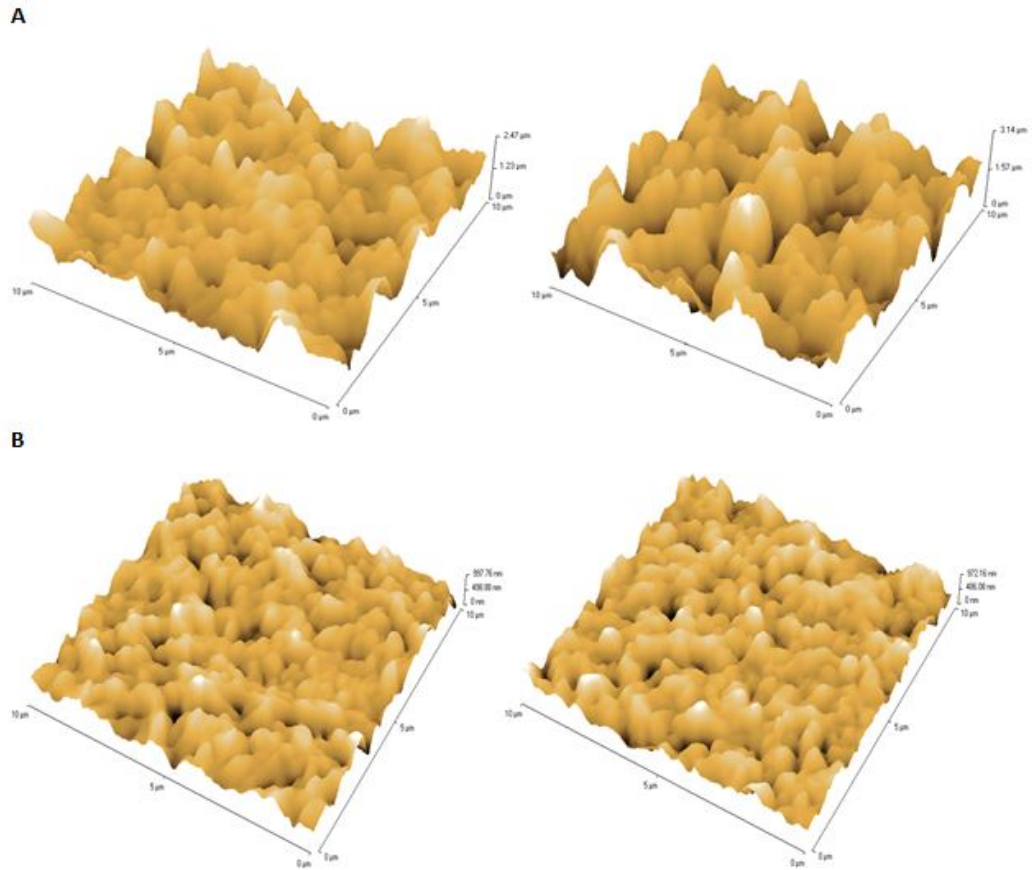


Figure 4.4: AFM topographic images of (A) CN and (B) PVDF membranes

When the surface consists of deep depressions and high peaks, high roughness parameters are expected (Idris et al., 2007). It was also observed from other study that less tightly packed nodules created a rough surface indicated by the high roughness parameter values (Idris et al., 2007). The change in the roughness parameters is proportional to the change in the pore size (Bessieres et al., 1996). The

values in Table 4.5 clearly shows that PVDF membrane with a smaller pore size than cellulose nitrate membrane has lower surface roughness values and the 3D AFM image also shows that PVDF membrane has lower peaks as compared to cellulose nitrate membrane.

Comparison between Figure 4.4A and Figure 4.4B indicates that the nodules are slightly merged and much lower peaks observed. In theory, this means that the roughness parameter decreases and it agrees well with the values presented in Table 4.5. It has been shown in other studies (Goodyer and Bunge, 2012; Idris et al., 2007) that high surface roughness on membranes indicates increased flux as well as decreased diffusion path length. A decrease in diffusion path length may imply less tortuous pores/channels, increasing the ease of diffusion and this is reflected in the diffusion coefficient values obtained in Table 4.6 where cellulose nitrate membrane has a higher average diffusion coefficient value than that of PVDF membrane. The surface topography of the scaffolds is not included due to their high height ranges on small scanned areas which are built for the atomic force microscope used in this study.

Table 4.5: Roughness parameters of Cellulose Nitrate and Polyvinylidene Fluoride (PVDF) membranes

Membrane	R_a (nm)	R_{rms} (nm)
PVDF	164.3	208.6
	144.9	181.2
Cellulose Nitrate	286.2	367.2
	440.9	548.8

4.3.3 Glucose diffusion analysis

The basis for engaging different pore size and shapes tissue engineering membranes and scaffolds is to study if the varying morphological porous structures of the materials engaged have an effect on the diffusion of glucose. Typical curves for the temporal change in glucose concentration for both donor and receptor phases are shown in Figure 4.5. All other membranes show similar pattern as depicted in Figure 4.5. It can be clearly seen that this measurement gives a smooth concentration change. Table 4.6 summarizes the results from all these measurements. As expected,

the effective diffusion coefficient is higher for a material with larger pore size. Figure 4.2e highlights the morphology of collagen scaffold that enables a relatively low resistance to diffusion of glucose molecules through the scaffold. The image clearly shows relatively straight channels and larger pores in comparison to other scaffolds/membranes, thus providing less hindrance to glucose molecules diffusing through the path length. All other membranes/scaffolds' compositions are much more intertwined, thus providing more resistance to glucose diffusion through the materials (Figure 4.2a-4.2d). This is reflected in the diffusion coefficient values shown in Table 4.6 where PVDF membrane with the smallest pore size of $0.1\ \mu\text{m}$ has the smallest glucose diffusivity while collagen scaffold with $80\ \mu\text{m}$ pore size has the largest glucose diffusivity. They show that the corresponding diffusion coefficient increases with increasing pore size of the material. This is true independent of the media used. This effect can be explained with the fact that the pore radius increases. However it must be noted that apart from pore size, other microscopic properties such as porosity and tortuosity also have an effect on diffusion. It is also apparent that the results for both water and CCM saturated membranes/scaffolds are significantly different. The glucose diffusion coefficients of membranes and scaffolds saturated with CCM are significantly reduced at a given temperature. This shows that other molecules present in CCM have significant influence with respect to diffusion.

It is worth pointing out that the diffusion coefficient for the materials increases from 27°C to 37°C . This is apparent for both water and CCM saturated membranes/scaffolds. This is due to a decrease in viscosity at a higher temperature. This is also due to the increased kinetic energy of the glucose molecules at higher temperatures and the results can be seen in Table 4.6. However, it must be noted that the focus of this work is not to determine the influence of the temperature on the diffusion coefficient. Hence there were only two different temperatures used in the experiments in this work.

The diffusion coefficient in free media (liquid) calculated from Stokes-Einstein's equation is comparable to what have been reported in literature, as shown in Table 4.7. As expected, glucose diffusion through membrane/scaffold is smaller than in the liquid which is reflected in the values shown in Table 4.6 except for collagen scaffolds both at 27°C and 37°C . This may be due to the homogeneous and

relatively parallel pore structure as can be seen from the surface morphology of the collagen scaffold in Figure 4.2e. Although glucose was still able to diffuse through the membrane/scaffold, the diffusion coefficient is reduced compared to its value in free media. This may be due to several reasons. The diffusion length for glucose increases due to impermeable segments of the membrane; this is an obstruction or tortuosity effect (Westrin and Axelsson, 1991). The amount of water/CCM available for diffusion is also reduced to a fraction of the total volume due to the microstructure of the material. Hence, a much lowered value compared to the diffusivity of glucose in free media.

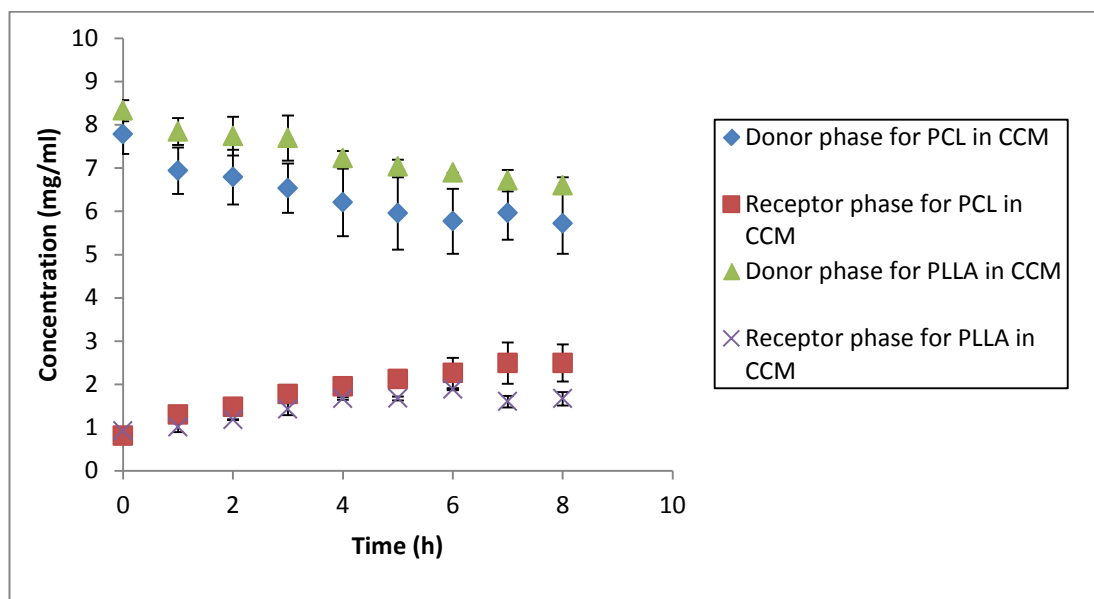


Figure 4.5: Diffusion cell experiment with 8 mg/ml glucose for both PCL and PLLA scaffolds saturated in CCM at 37°C

Table 4.6: Effective diffusion coefficients with standard deviations for glucose across membranes/scaffolds saturated in water and CCM

Material		Manufacturers' pore size (μm)	Effective diffusion coefficient (m^2/s)			
			Water at 27°C	Water at 37°C	CCM at 27°C	CCM at 37°C
Membrane	PVDF	0.1	$1.20 \pm 0.38 \times 10^{-10}$	$1.87 \pm 0.17 \times 10^{-10}$	$7.28 \pm 3.37 \times 10^{-11}$	$7.68 \pm 2.78 \times 10^{-11}$
	CN	0.45	$1.87 \pm 0.50 \times 10^{-10}$	$1.95 \pm 0.28 \times 10^{-10}$	$7.63 \pm 0.17 \times 10^{-11}$	$8.91 \pm 0.80 \times 10^{-11}$
Scaffold	PLLA	12-18	$2.08 \pm 0.20 \times 10^{-10}$	$2.57 \pm 0.92 \times 10^{-10}$	$1.36 \pm 0.45 \times 10^{-10}$	$1.39 \pm 0.28 \times 10^{-10}$
	PCL	20-30	$3.52 \pm 2.35 \times 10^{-10}$	$4.13 \pm 1.75 \times 10^{-10}$	$1.64 \pm 1.33 \times 10^{-10}$	$1.78 \pm 0.50 \times 10^{-10}$
	Collagen	80	$9.59 \pm 3.64 \times 10^{-9}$	$1.07 \pm 0.47 \times 10^{-8}$	$3.56 \pm 0.84 \times 10^{-9}$	$3.71 \pm 2.78 \times 10^{-9}$

Table 4.7: Comparison of the diffusion coefficient values for liquid only calculated from Stokes-Einstein's equation and found in previous papers as well as experimentally determined diffusion coefficient values

	Experimentally determined (Eq. 3.11)	Calculated from Stokes-Einstein's equation (Eq. 4.9)	Values reported in previous papers
Diffusion coefficient in water at 27°C (m ² /s)	$6.98 \pm 0.60 \times 10^{-10}$	6.96×10^{-10}	5.4×10^{-10} (Kleinstreuer and Agarwal, 1986)
Diffusion coefficient in water at 37°C (m ² /s)	$9.58 \pm 0.13 \times 10^{-10}$	9.58×10^{-10}	9.0×10^{-10} (Buchwald, 2011)
Diffusion coefficient in CCM at 27°C (m ² /s)	$5.67 \pm 0.74 \times 10^{-10}$	4.61×10^{-10}	NA
Diffusion coefficient in CCM at 37°C (m ² /s)	$6.16 \pm 1.25 \times 10^{-10}$	5.65×10^{-10}	5.9×10^{-10} (Provin et al., 2008)

Many papers have been published on the diffusion coefficients of glucose across various membranes and scaffolds at different temperatures. Papenburg et al. (2007) reported a value of 1.04×10^{-10} m²/s of glucose diffusion coefficient across PLLA scaffold saturated with water at 4°C while Shanbhag et al. (2005) obtained the glucose diffusion coefficient across inverted colloidal crystal (ICC) scaffold saturated in water at 25°C to be 2.7×10^{-10} m²/s. In other studies conducted by Wang et al. (2009) and Boss et al. (2012) at 37°C using hydroxypropyl chitosan (HPCTS) crosslinked with gelatin (GEL) and chondroitin sulphate (CS) scaffold and asymmetric alumina membrane, both saturated in water, glucose diffusion coefficient values were found to be 1.16×10^{-10} m²/s and 1.39×10^{-10} m²/s, respectively. These reported values are within the range of experimentally-deduced diffusion coefficients found in the present study (Table 4.6).

4.3.4 Relationship between porosity (ε) and tortuosity (τ)

As stated earlier, tortuous channels which are part of the pores of the membranes and scaffolds hinder the diffusion of the molecules (namely, glucose in this case) through the materials. The tortuosity of the molecule represents the average path length resulting from all resistances to diffusion over which the molecule travels during the diffusion through the material. The fluid that saturates the pores should hinder the molecular diffusion in different ways. Furthermore, as the resistance to diffusion changes due to change in temperature, the tortuosity values should also change.

The porosity is a macroscopic property of the material that represents the amount of void spaces in the material and pore size distribution although in reality it may be difficult to determine the subtle differences in the effects of these on the porosity values. Nevertheless, in an attempt to understand how the diffusional paths of the molecules change with the pore structures of the materials, we attempt to correlate the tortuosity values to porosity of the materials at different temperatures and for different fluids. In traditional literature of flow and transport in porous media, many such relationships can be found. Some of these relationships are reported for idealised porous material as shown in Table 4.9. It is visible from the image (Figure 4.2) that PCL scaffold benefits from larger pores and less tortuous channels which give a lower tortuosity value compared to other membranes/scaffolds. This is depicted in Table 4.8 where PCL scaffold gives a tortuosity value of 2.8 and consequently a higher diffusion coefficient (Table 4.6) in comparison to other materials. PVDF membrane, with the smallest pore size, gives the largest tortuosity value of 5.6 (Table 4.8) and the lowest diffusion coefficient value (Table 4.6). One can also observe from Table 4.8 that the tortuosities vary with temperature and this is consistent with what have been found in several studies before (e.g., Gao et al., 2014; Sadighi et al., 2013; Sharma and Chellam, 2005).

Figure 4.6 shows the plot of porosity-tortuosity relations between experimental and empirical results. As expected, both results are not comparable as the approaches in equation were based on a specific idealised model of a porous medium (Sun et al., 2013) while the experimental results were collated from different membranes and scaffolds of different pore size and microstructure.

Table 4.8: Experimentally-calculated porosity and tortuosity for all materials

Material		Manufacturers' pore size (μm)	Porosity (%)	Tortuosity (-)			
				Water at 27°C	Water at 37°C	CCM at 27°C	CCM at 37°C
Membrane	PVDF	0.1	69	4.0	3.5	5.4	5.6
	CN	0.45	64	2.4	3.1	4.8	4.4
Scaffold	PLLA	12-18	80	2.7	3.0	3.3	3.5
	PCL	20-30	80	1.6	1.9	2.8	2.8
	Collagen	80	72	NA	NA	NA	NA

Table 4.9: Porosity-tortuosity relations for ideal porous materials saturated with water

Equation number	Relation	Reference
4.12	$\tau = 1 - 0.41 \ln \varepsilon$	Comiti and Renaud (1989)
4.13	$\tau = 1 - 0.49 \ln \varepsilon$	Mauret and Renaud (1997); Barrande et al. (2007)
4.14	$\tau = 1/\varepsilon^{0.33}$	Bear (1972); Dullien (1975)
4.15	$\tau = 1 + 0.8 (1 - \varepsilon)$	Koponen et al. (1996)

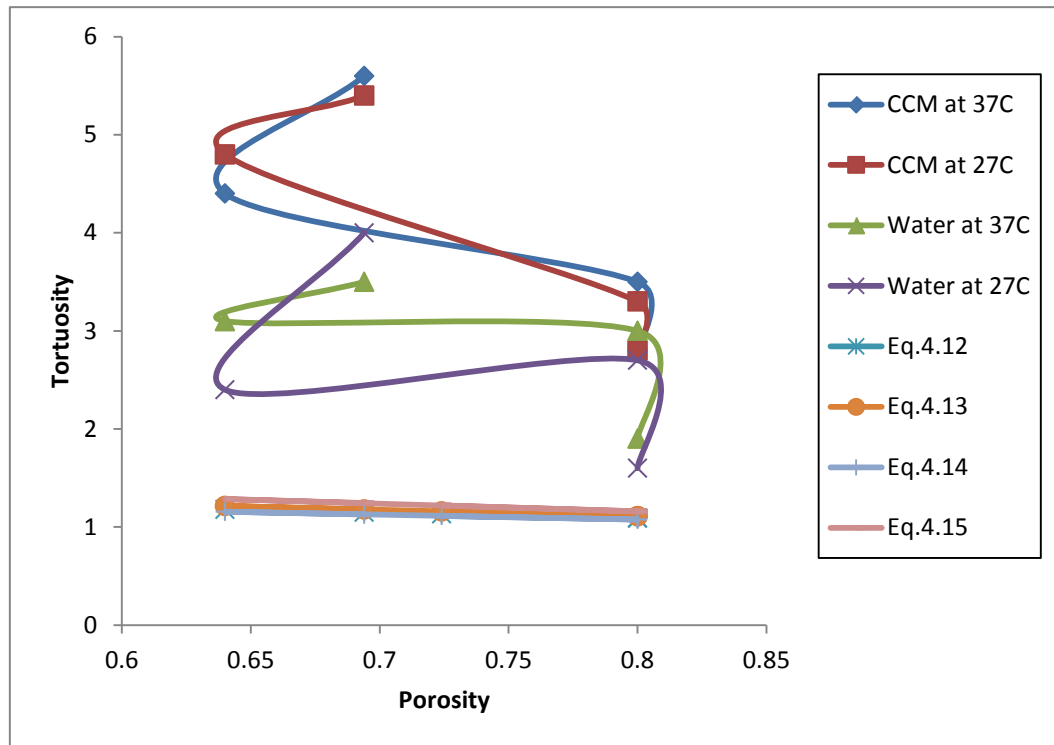


Figure 4.6: Comparison of porosity-tortuosity relations for all materials which are determined from the experiments in this work and four models of ideal porous material. The equations for the relationship between tortuosity and porosity for ideal porous media saturated with water (Eq. 4.12 – Eq. 4.15) are shown in Table 4.9

4.4 Chapter summary

A diffusion cell has been constructed to measure the diffusion coefficient of glucose across varying pore size and shapes tissue engineering membranes and scaffolds which are saturated with water and CCM. The rationale behind selecting different porous structure of membranes and scaffolds in this study was to observe how the different morphological porous structure of the materials investigated might have an effect on the glucose diffusion. The results showed the glucose diffusion coefficients for materials saturated with CCM are significantly reduced at a given temperature. This may be due to the multi-components that make up CCM and what we obtained is therefore a lumped effect from a number of inter-related phenomena. A similar trend was observed for both diffusion in water and CCM where a higher diffusion coefficient was evident with larger pores due to increased pore size. SEM enabled visual images of materials investigated including the morphology, porosity, pore size and tortuosity. Both porosity and tortuosity were evaluated in this study and

based on our results, a low tortuosity value was found for the PCL scaffold used in this study and this is true independent of the media used. The low tortuosity value coupled with a higher diffusion rate compared to other materials were due to less hindrance to mass transfer and less tortuous channels. Varying the glucose concentration for diffusivity measurements and determining the mass transfer rate with the presence of biological cells (e.g., stem or epithelial cells; adherent or suspended cells) in the scaffolds will be valuable for future work.

CHAPTER 5

GLUCOSE DIFFUSIVITY IN CELL-SEEDED TISSUE ENGINEERING SCAFFOLDS

Chapter overview

One of the keys to producing artificial tissues lies on sufficient nutrient diffusion, especially glucose, into the cells, tissues and/or scaffolds. Studies have shown the importance of understanding nutrient diffusion within tissue engineering scaffolds. In order to further understand this behaviour, we have attempted a series of well-defined diffusion experiments to determine the effective glucose diffusion coefficient through the pores of scaffolds where cells are grown. For this purpose, a diffusion cell was constructed and three commercialised scaffolds were employed, which include poly(caprolactone), poly(L-lactide) and collagen. The results of the experiments indicate the effect of cell growth has on the effective glucose diffusivity. We observed that the cell growth changed the morphological structure of the cultured scaffolds reducing the effective pore space in the scaffold and inevitably reduced the effective glucose diffusivity. Therefore, a conclusion can be drawn that the presence of cells over time during cell culture reduces the mobility of glucose. The results of this study should be possible to use to predict the glucose concentration profiles in thick engineered tissues.

5.1 Introduction

The main goal of tissue engineering (TE) field is to design, construct, regenerate and repair damaged tissues in the human body (Ahn et al., 2014). For TE to be a forefront approach, it needs a support system that mimics native extracellular matrices (ECM). Native ECM exhibits a biologically induced stable environment which should promote cell and tissue growth as well as providing mechanical support (Daniele et al., 2014). ECM typically contains glycoproteins, proteoglycans and functional proteins and it has a 3-dimensional (3D) structure (Kang et al., 2006). Many TE scaffolds have emerged to mimic ECM, and they have been shown to play

a crucial role in the successful reconstruction of diseased tissues. These scaffolds must be porous, biocompatible and non-toxic, and they provide mechanical support to the cells. Another important characteristic of the TE scaffolds is that they must have interconnected porous network for easy access of nutrients into the cells and removal of metabolic wastes such as lactate from the cells (Ahn et al., 2014). As the amount of interconnected pores varies in different TE scaffolds, the nutrient diffusivity in these scaffolds may also vary as discussed recently by Suhaimi et al. (2015b).

The presence of a natural capillary network of blood vessels plays an important role in supplying both the nutrients and oxygen to the cells and tissues in humans. However, *in vitro* conditions pose a major setback due to the absence of these blood vessels. Many studies have suggested the use of a bioreactor system to facilitate the growth of artificial tissues (Bock et al., 2010; Page et al., 2013; Chao and Das, 2015), e.g., hollow fibre membrane bioreactors (HFMBs) (Ye et al., 2006; Abdullah et al., 2009; Chapman et al., 2012). HFMBs have been proven to be a promising alternative to growing artificial bone tissues where studies have reported the potential of successful growth of 3D tissue constructs of clinically relevant size (Das, 2007; Ye et al., 2007; Chesnick et al., 2007; Ellis and Chaudhuri, 2007; Bettahalli et al., 2011).

In general, the solutes for cell growth (e.g., nutrients and oxygen) are transported in the scaffold in a bioreactor and into the cells by diffusion process. The morphological structure of the scaffolds (e.g., pore size and shape distribution, average porosity, tortuosity, and any other) has a significant effect on the solute transport processes (Wu et al., 2010; Park et al., 2014). For example, increasing the cell mass grown in scaffolds has been shown to affect the diffusivity of oxygen by Kang et al. (2011) who reported a decrease in oxygen diffusivity with increasing tissue formation within a TE scaffold.

In principle, the presence of cells should have affected the solute diffusivity in scaffolds due to the possibility of the cells exerting significant contractile forces on the scaffolds which is also dependent on the cell and scaffold type. For example, fibroblasts and mesenchymal stem cells were shown to exert contractile forces on collagenous scaffolds, as reported by Brown et al. (2002) and Awad et al. (2000), while Leddy et al. (2004) reported the effects of changes in scaffold material leading

to decreased diffusivity as a result of contractile forces exerted on the scaffold by cells.

In contrast to oxygen diffusivity which has been reported in a number of studies (Bettinger et al., 2006; Kang et al., 2011; Cheema et al., 2012; Fiedler et al., 2014), there is limited study on the nutrient diffusivity especially glucose within cell-seeded TE scaffolds. In addressing this issue, we report the glucose diffusivity of TE scaffolds seeded with human osteoblast cells in cell culture media (CCM) at 37°C. The scaffolds employed in this study have been used in our previous work (Suhaimi et al., 2015b). However, these materials, at the time, were not seeded with any biological cells as the previous work aimed only at quantifying passive diffusion of glucose through the materials, i.e., the relationship between glucose diffusion with different amount of connected pores and pore morphology in different TE scaffolds. In contrast to this study (Suhaimi et al., 2015b), the goal of the present study is to quantify the diffusive properties of cell-seeded scaffolds and compare with our previous results of non-seeded TE scaffolds. 37°C is chosen as the typical optimal temperature for cell culture or tissue engineering experiments. It is shown how the glucose diffusivity would change with morphological changes of the scaffolds and cell culture time. Specifically, the glucose diffusion coefficient is shown decrease with increasing cell mass grown on the surface and inside the scaffolds.

5.2 Materials and methods

5.2.1 Materials

Human osteoblast HOSTE85 cell line (European Collection of Cell Culture (ECACC), UK) was donated by the Centre for Biological Engineering, Loughborough University. It was derived from a 13 year old female Caucasian from USA. Dulbecco's modified eagle medium (DMEM), 10% foetal bovine serum (FBS) and 2% non-essential amino acids (NEAA) were purchased from Fisher Scientific UK Ltd. (Loughborough, UK). Poly(caprolactone) (PCL) and poly(L-lactide) (PLLA) scaffolds were purchased from the Electrospinning Company Ltd. (Didcot, UK). Collagen scaffold was purchased from Matricel GmbH (Herzogenrath, Germany). TE scaffolds should be biodegradable for successful tissue formation *in vivo*; however, PCL, PLLA and collagen scaffolds were stable

for culturing periods of up to three weeks. This shows that they have a long time of degradation in comparison to the culturing periods and diffusion experiments and hence, we define that any biodegradation has no effect on the diffusivity. Table 5.1 shows the main characteristics of the scaffold materials. Initial porosity of the materials (i.e., before cells were seeded) was evaluated by a pycnometric method, as described in Suhaimi et al. (2015b). Analytical grade powder D-glucose-anhydrous was purchased from Fisher Scientific UK Ltd. (Loughborough, UK) which has a molecular weight of 180.16 g/mol.

Table 5.1: Summary of the commercial scaffold properties

Scaffold	Thickness (μm) based on Manufacturers' information	Manufacturers' pore size (μm)	Porosity (%)	Min pore size (μm)	Mean pore size (μm)	Max pore size (μm)	Source
Poly(L-lactide) (PLLA)	50	12-18	80	4.04	13.67 ± 4.25	25.87	The Electrospinning Company Ltd. (Didcot, UK)
Poly(caprolactone) (PCL)	50	20-30	80	5.8	21.69 ± 6.85	44.84	The Electrospinning Company Ltd. (Didcot, UK)
Collagen	1500	80	72	12.55	75.15 ± 5.21	175.18	Matricel GmbH (Herzogenrath, Germany)

5.2.2 Pore size distribution determination and morphological structure of scaffolds

Pore structures and distribution as well as the morphological structure of the scaffold materials were observed by a scanning electron microscopy (Hitachi TM3030 SEM, Tokyo, Japan). The cell culture medium was removed and the scaffold specimens were washed with phosphate buffered saline (PBS) (Fisher Scientific UK Ltd., Loughborough, UK) to discard any remaining DMEM. The scaffolds were then left to dry inside a class II biological safety cabinet (Microflow Class II BSC, ABS1200CLS2-MK2, Bioquell, Andover, UK) before the SEM analysis. The dry specimens were coated with carbon for 120s by a sputter coater (Edwards S150). The images were taken at a voltage of 5 keV.

The minimum, mean and maximum pore sizes of the scaffolds (Table 5.1) were determined using the ImageJ version 1.48 software (Wayne Rasband, National Institute of Mental Health, USA) where the SEM images were uploaded. Briefly, lines were drawn between the pores and measurements were tracked and recorded by the software (Suhaimi et al., 2015b).

5.2.3 Scaffold preparation

Prior to cell seeding, both PCL and PLLA scaffolds were pre-wetted in 20% ethanol (Fisher Scientific UK Ltd., Loughborough, UK) for 30 min followed by washing with DMEM twice in another 30 min. Collagen scaffolds were highly purified and could therefore be seeded in the dry state without previous washing with DMEM. This procedure was carried out after sterilizing the class II biological safety cabinet by exposure to ultraviolet (UV) light for 30 min.

5.2.4 Cell culture and seeding

The HOSTE85 human osteoblast cells were cultured in DMEM supplemented with 10% FBS and 2% NEAA at 37°C and 5% CO₂ – 95% air in a humidified incubator (HERAcell 150, Fisher Scientific UK Ltd., Loughborough, UK). The medium was changed every 2 days and the HOSTE85 cells were detached using 0.25% trypsin – 0.1% EDTA (Fisher Scientific UK Ltd., Loughborough, UK) followed by re-suspending in the supplemented DMEM. After pre-wetting with 20% ethanol and washing both the PCL and PLLA scaffolds twice with DMEM, 1 ml of the

HOSTE85 cell suspension containing 1.2×10^5 cells and 1.5×10^5 cells was seeded onto both the PCL and PLLA scaffolds in a 16-well plate, respectively. As for collagen scaffolds, 1 ml of the HOSTE85 cell suspension containing 6×10^5 cells was seeded onto collagen in the dry state, also in a 16-well plate. The cell suspension was also added into an empty well (no scaffold) of the 16-well plate as control. After seeding, the collagen scaffolds were incubated at 37°C for 2 hr before adding additional medium. All seeding plates were maintained at 37°C in the humidified incubator and the medium was changed every 2 days. The doubling time of HOSTE85 cells is found to be 1.49 days (Figure 5.1).

After 1, 2 and 3 weeks post seeding, the culture medium was removed and both the control and wells containing scaffold specimens were washed out with PBS solution to discard any remaining medium. The scaffolds were then removed for SEM analysis. Trypsin-EDTA solution was used to detach cells followed by re-suspending in the supplemented DMEM. The mixture solution was centrifuged for 5 min followed by re-suspending in DMEM for cell count using a haemocytometer.

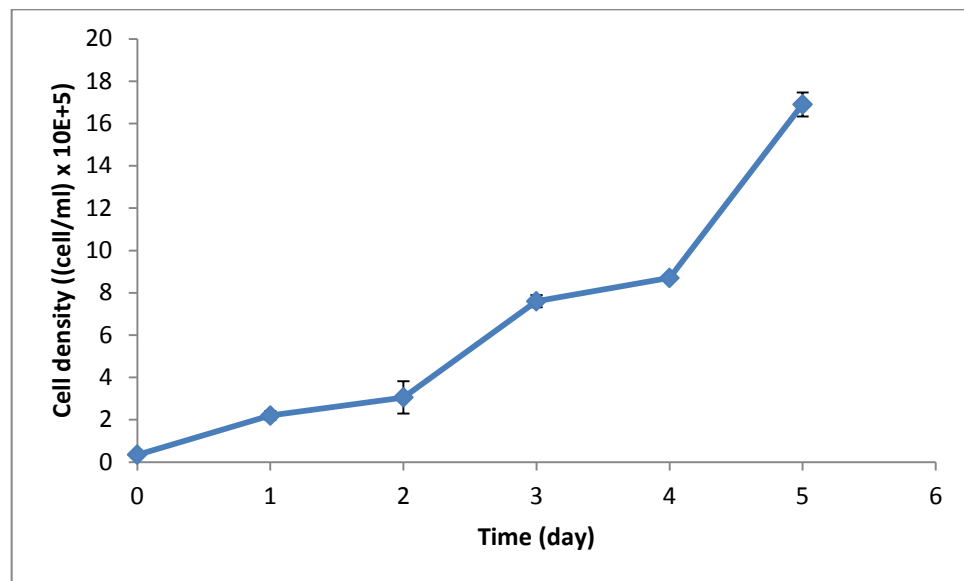


Figure 5.1: The cell growth curve for HOSTE85 as a function of time where the doubling time of HOSTE85 cells is 1.49 days. The cells were cultured for 5 days and cell number was calculated on each day using a haemocytometer where trypan blue was added into the cell suspension to differentiate between live and dead cells

5.2.5 Glucose diffusivity measurement

A diffusion cell was constructed to measure the glucose diffusivity within the seeded scaffolds in CCM. The design and the operation principle of the diffusion cell were described in detail in another paper (Suhaimi et al., 2015b). Briefly, the cell consisted of two acrylic chambers, namely, donor and receptor chamber. Both chambers held equal volumes of 41 ml per chamber with an internal geometry of length 20 mm x height 45 mm x width 45 mm. The seeded scaffold was fixed in between the chambers (Figure 5.2). The donor chamber was filled with 8 mg/ml of glucose solution dissolved in CCM while the receptor chamber contained pure CCM. The glucose powder was dissolved without further purification in a beaker containing pure CCM before the start of the diffusion experiment. Both solutions of pure CCM and glucose solution containing CCM were placed inside a heated water bath at 37°C for 1 hr for the purpose of equilibrating to the experimental temperature. The whole apparatus was placed in the water bath at 37°C.

The change in the glucose concentration was measured using the same method described by Suhaimi et al. (2015b). Briefly, the diffusion of glucose was monitored using an YSI glucose analyser (YSI 2300 STAT PLUS, YSI UK Ltd, Hampshire, UK). The samples were taken simultaneously from both chambers using a plastic syringe. The samples were then placed inside a glass cuvette where 25 µl were aspirated by the sipper of the glucose analyser. After the measurements were recorded, the samples were poured back into the diffusion cell to keep the volume constant. The measurements were taken at an hourly interval until equilibrium was achieved.

The diffusion study was conducted at the time points of 1, 2 and 3 weeks post seeding for both PLLA and collagen scaffolds while 1 and 2 weeks post seeding for PCL scaffold. After 1, 2 and 3 weeks post seeding, scaffold specimens were removed from the well plate and placed in between the chambers of the diffusion cell for diffusion experiments. All experiments were conducted in duplicate.

The corresponding diffusivities were calculated according to Fick's first law which was modified to include the effective diffusivity by Gutenwik et al. (2004) defined by:

$$J = -D_e \frac{\partial C}{\partial z} \quad (5.1)$$

Assuming that there was no change in volume in the diffusion cell, Eq. (5.1) was translated into Eq. (5.2) as given below:

$$V_d \frac{\partial c_d}{\partial t} = -D_e A \frac{c_d - c_r}{l} \quad (5.2)$$

where l was the scaffold thickness, A was the area of the scaffold, D_e was the effective diffusivity of glucose in the seeded scaffold and V_d was the donor volume. The effective diffusivity was determined by fitting the experimental data into Eq. (5.2) as described in Suhaimi et al. (2015b).

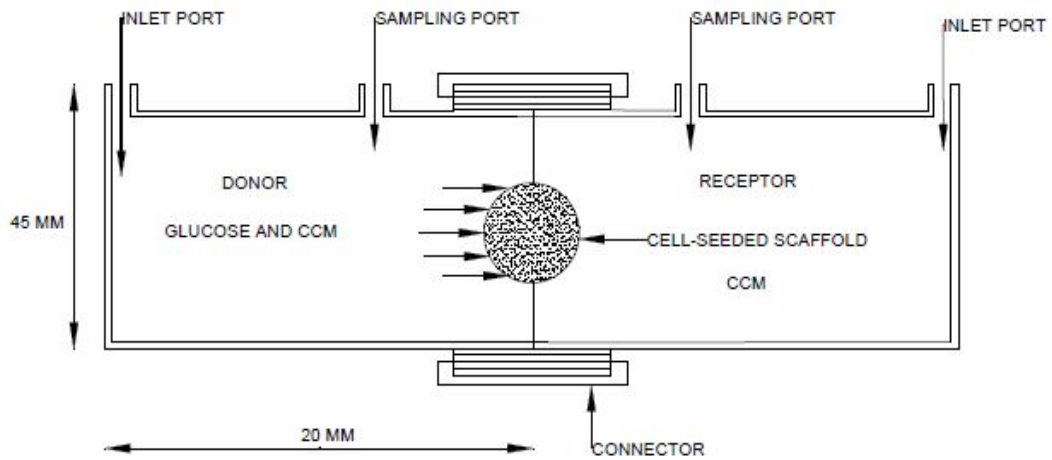


Figure 5.2: Schematic drawing of a diffusion cell to measure the glucose diffusivity across the seeded scaffolds saturated in cell culture medium at 37°C (dimensions of the cell are shown in the figure)

5.3 Results and discussions

5.3.1 Cell proliferation on scaffolds

To confirm the morphological changes of the cell-seeded scaffolds at various cell culture time intervals the materials were viewed for surface morphology and cross-sections using SEM. Figure 5.3 illustrates some typical micrographs of osteoblasts seeded on the surface of collagen, PLLA and PCL scaffolds after 1, 2 and 3 weeks of culture as well as the blank scaffolds (no cells). A clear comparison is depicted on the morphological change between blank scaffolds and seeded scaffolds. The cells have gradually covered the surface and have almost filled all of the pores by week 3. Figure 5.4 illustrates the cross-sectional view of the fibres of the scaffold where cells

have migrated. It is observed that more cells are attached on the surface rather than in between the fibres of the scaffold. Figure 5.5 presents the number of seeded cells on all scaffolds at 1, 2 and 3 weeks of culture time which shows similar pattern as the cell growth kinetics curve (Figure 5.1). The method for counting the seeded cells is described in section 5.2.4.

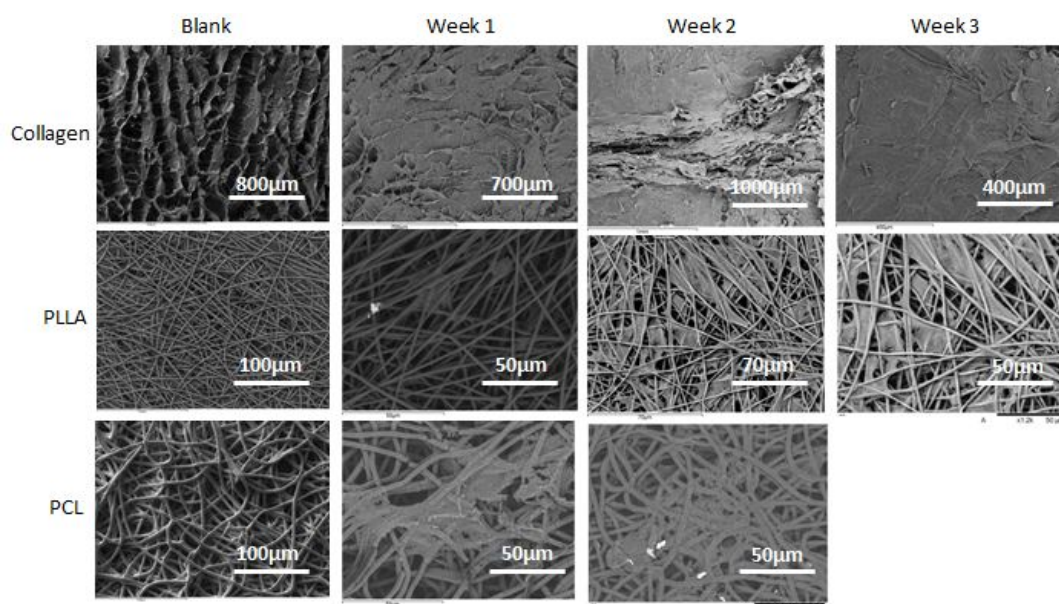


Figure 5.3: SEM micrographs showing morphological changes on the surface of collagen, PLLA and PCL scaffolds from no cells attached (blank scaffold) to cells cultured on week 1, week 2 and week 3

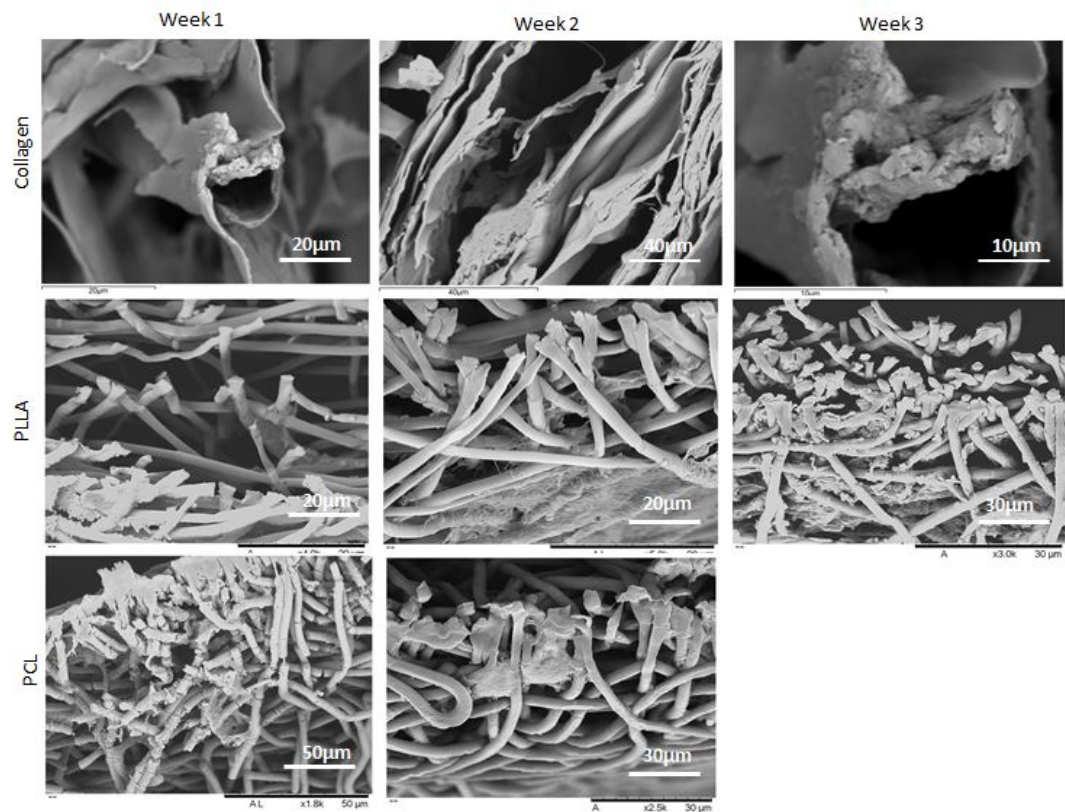


Figure 5.4: SEM images showing the cross-sectional cell distribution in collagen, PLLA and PCL scaffolds where cells have migrated into on the time points of week 1, week 2 and week 3 of culture period

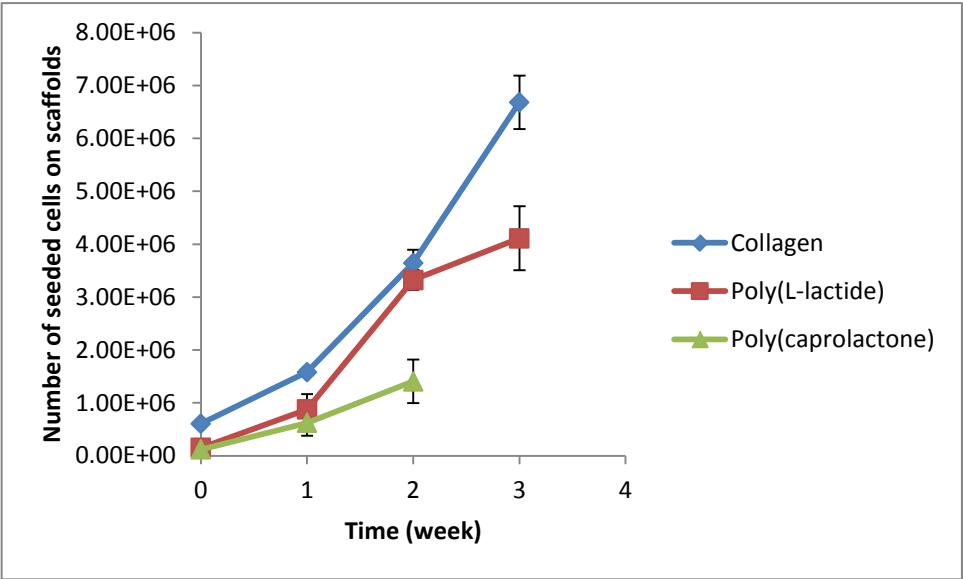


Figure 5.5: The approximate number of cells grown on collagen, PLLA and PCL scaffolds at culture time periods of week 1, week 2 and week 3. The difference between cell number contained inside the control well and cell number contained inside the wells that initially were present with scaffold specimens, represents the number of cells that have grown on the scaffolds

5.3.2 Glucose diffusion analysis

The method for measuring the glucose diffusivity is described in section 5.2.5. Typical curves for the temporal change in glucose concentration for both donor and receptor chambers are shown in Figure 5.6 which depict the changes in the two chambers during the diffusion experiment for collagen scaffold. Both PLLA and PCL scaffolds show similar patterns as collagen scaffold and are not shown in the figure. The diffusion coefficients of the cultured scaffolds are calculated by fitting the experimental data into Eq. (5.2) and the diffusivity values are listed in Table 5.2. As shown, the effective diffusion coefficient decreases as cells fill up the pores of the scaffold (Figure 5.7A, 5.7B and 5.7C). This is attributed to the change in the pore volume available for diffusion. Table 5.2 also shows the percentage difference between scaffolds with no cells and cultured scaffolds.

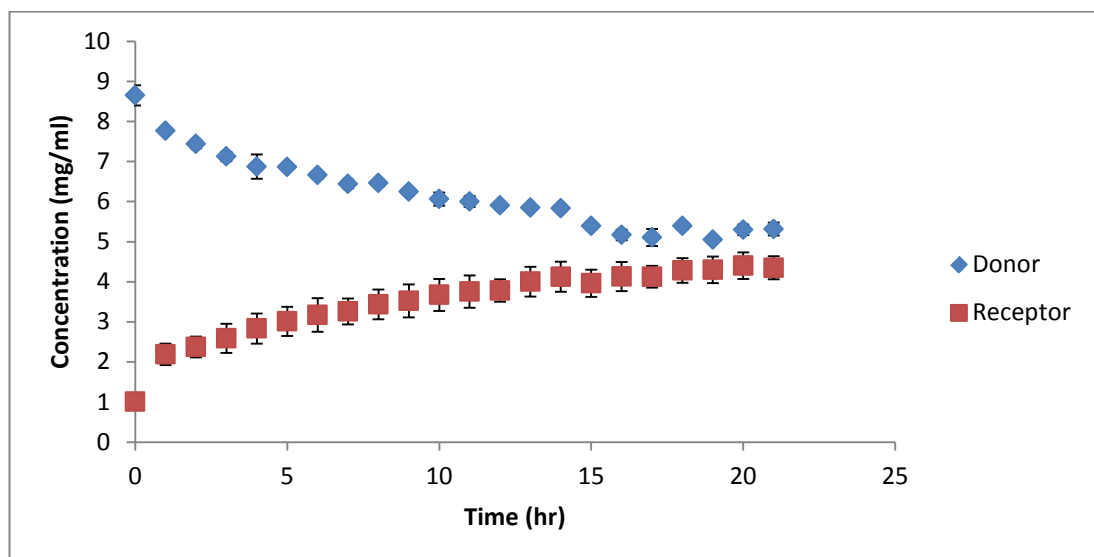
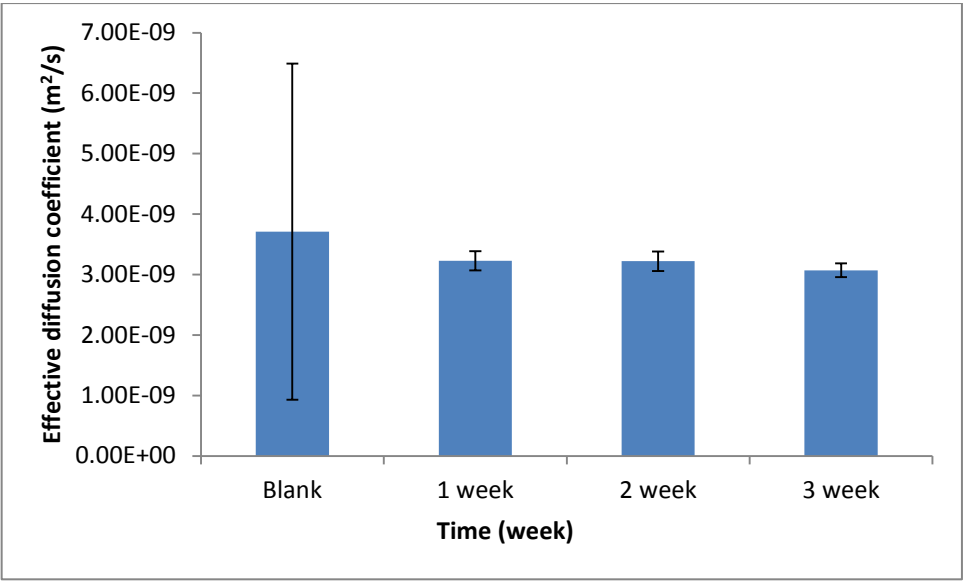
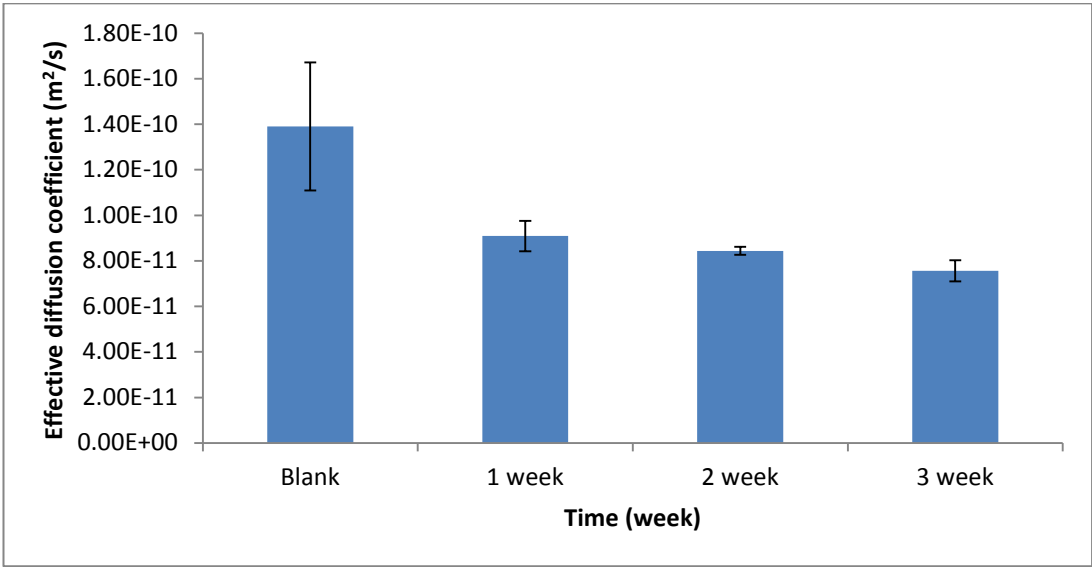


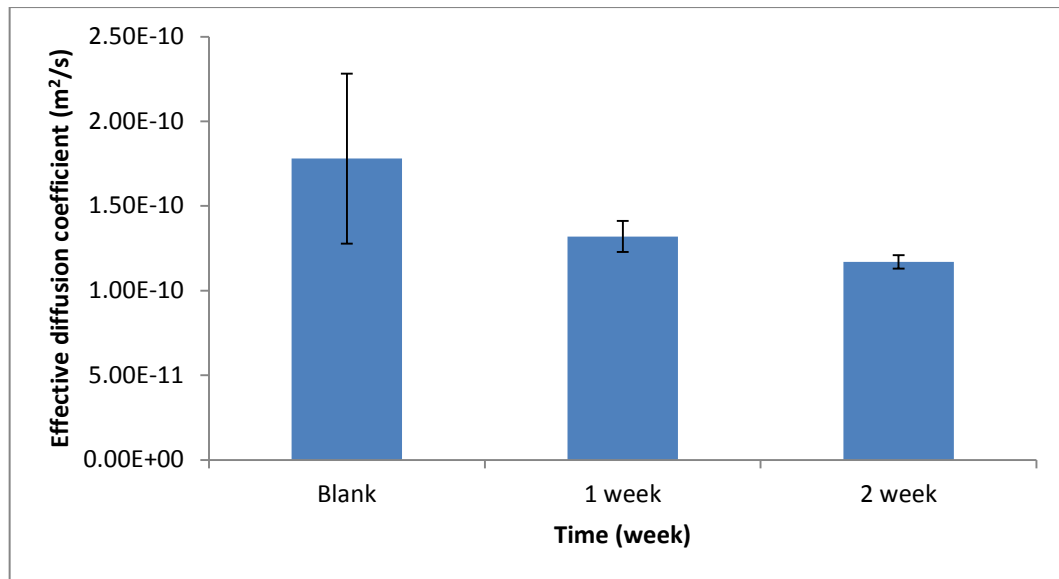
Figure 5.6: Diffusion cell experiment with 8 mg/ml glucose for cultured collagen scaffold saturated in CCM at 37°C. Both PLLA and PCL scaffolds show similar patterns as collagen scaffold and are not shown in the figure



(A)



(B)



(C)

Figure 5.7: Effective diffusion coefficient of glucose in different TE scaffolds at different culture time: (A) collagen scaffold, (B) PLLA scaffold and (C) PCL scaffold

There is an obvious decrease in the values of effective diffusivity between scaffolds with no cells attached (blank) and cultured scaffolds on week 1. However, we did not observe significant difference in the effective diffusion coefficients of the cultured scaffolds between weeks 1, 2 and 3 which are likely due to a slower proliferation rate of osteoblast cells. To further quantify the relationship between the effective diffusion coefficient and number of cells grown on and inside the scaffold, a graph of the effective diffusivity against cell number was plotted as shown in Figure 5.8 for PLLA scaffold. This figure shows a decrease in the effective diffusion coefficient values as cell number increases. Both collagen and PCL scaffolds follow similar trends and are not shown in the figure. Diffusion is generally defined by a random motion of molecules from a higher concentration to a lower concentration. In this case, glucose molecules have diffused from the donor chamber into the receptor chamber through the connected pores of the scaffold. In our previous work (Suhaimi et al., 2015b), we have identified that the effective diffusion coefficient is higher for a material with a larger pore size. In the present work, the results show that the effective diffusion coefficient is still higher in the collagen scaffold (properties described in Table 5.1) compared to PCL and PLLA even though cells have grown and changed the morphological structure of the collagen, followed by

PCL and finally PLLA. The decreasing trend of the glucose diffusivity in the cultured scaffolds follows the notion of ‘higher diffusivity for a larger pore size’. As the cells gradually cover the surface and almost all of the pores of the scaffold starting from week 1 to week 3, the effective diffusion coefficient of glucose seems to decrease monotonically with the cell number. The SEM images have also shown the morphological change of the cultured scaffold due to growth of cells (Figures 5.3 and 5.4) and consequently the significant decrease of the effective diffusivity which is evident from Table 5.2 and Figure 5.7A-5.7C. An interesting point to note here is that gravity may affect cell growth and behaviour, however, gravity was constant during the course of this work. Hence, we define that gravity has the same effect on cell growth and fluid flow and therefore no effect on the results of this work.

Table 5.2: Effective diffusion coefficients with standard deviations for glucose across blank and cultured scaffolds saturated in CCM

Scaffold	Manufacturers' pore size (µm)	Effective diffusion coefficient (m ² /s)				Difference between values calculated from blank and cultured scaffolds (week 1) (%)
		Blank (Suhaimi et al. (2015b))	Week 1	Week 2	Week 3	
Collagen	80	$3.71 \pm 2.78 \times 10^{-9}$	$3.23 \pm 0.16 \times 10^{-9}$	$3.22 \pm 0.16 \times 10^{-9}$	$3.07 \pm 0.11 \times 10^{-9}$	12.9
PLLA	12-18	$1.39 \pm 0.28 \times 10^{-10}$	$9.09 \pm 0.67 \times 10^{-11}$	$8.44 \pm 0.17 \times 10^{-11}$	$7.56 \pm 0.46 \times 10^{-11}$	34.6
PCL	20-30	$1.78 \pm 0.50 \times 10^{-10}$	$1.32 \pm 0.10 \times 10^{-10}$	$1.17 \pm 0.04 \times 10^{-10}$	NA	25.8

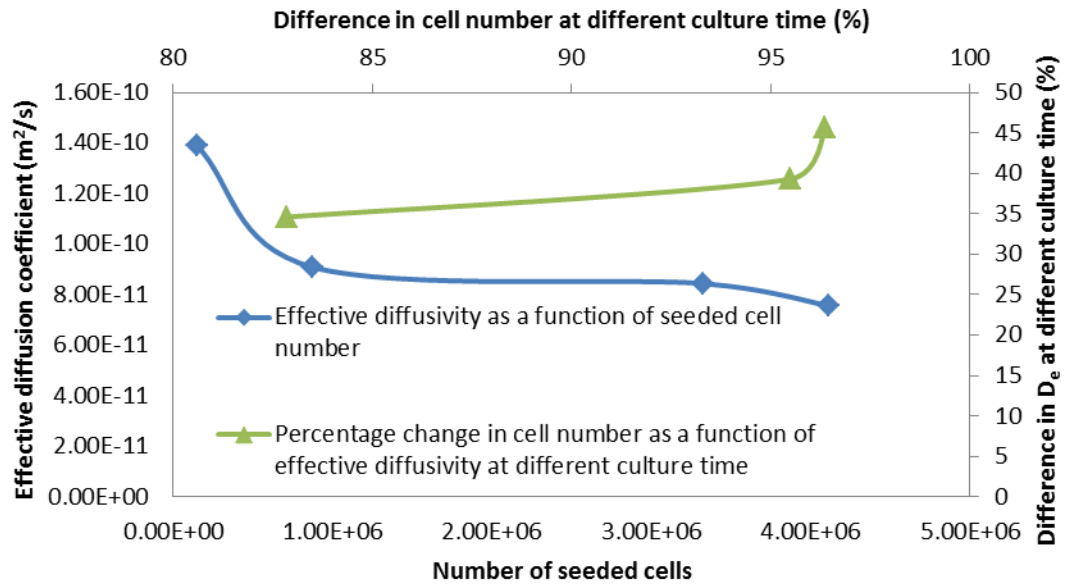


Figure 5.8: The relationship between effective diffusivity and seeded cell number for PLLA scaffold. The percentage difference for both cell number and effective diffusivity at different culture time were calculated at the time points of 1, 2 and 3 weeks of culture time with reference to initial time (at 0 week)

5.4 Chapter summary

A diffusion cell has been constructed to carry out glucose diffusion experiments through cell-seeded scaffolds saturated in CCM at 37°C. The results show that cell growth changes the morphological structure of the scaffold which affects the effective diffusion coefficient of glucose. The pore volume for glucose diffusion has been reduced and it is concluded that increasing cell mass grown on and inside the scaffold decreases the mobility of glucose. Further investigation on cell proliferation rate by DNA quantification is necessary to further understand the relationship between effective diffusion coefficient and culture time.

CHAPTER 6

GLUCOSE TRANSPORT IN HOLLOW FIBRE MEMBRANE BIOREACTOR FOR TISSUE ENGINEERING: MATHEMATICAL MODELLING USING EXPERIMENTAL MEASUREMENTS OF GLUCOSE DIFFUSIVITY

Chapter overview

Hollow fibre membrane bioreactors (HFMBs) have been shown to overcome the diffusion limitation of nutrients (e.g., glucose) from the hollow fibres (lumens) to the porous regions of a scaffold (extra capillary space). However, direct monitoring of glucose diffusion inside the HFMBs is almost impossible due to their small size; thus, various computational modelling frameworks have been developed in the past. These models have defined that the glucose diffusivity in the cell culture medium used in the HFMBs as similar to the diffusivity in water. Similarly, other assumptions have been made which do not represent the nutrient transport processes in the HFMB accurately. In addressing these issues, a mathematical model is presented in this chapter, where we employ experimentally deduced effective glucose diffusivities of tissue engineering membranes and scaffolds with and without cells, along with glucose diffusivity in cell culture medium. The governing equations are non-dimensionalised and solved analytically using MATLAB. The results demonstrate the roles of various dimensionless numbers (e.g., Péclet and Damköhler numbers) and non-dimensional groups of variables on determining the glucose concentration especially in the scaffold region. The result of this study is expected to help optimize designs of HFMB as well as carry out more accurate scaling analyses.

6.1 Introduction

Bone grafting is a surgical procedure to move bone tissues from one site to another on a body which has been considered a standard criterion to treat bone defects as early as 1912 (Donati et al., 2007). Despite its popularity and well-established procedures, bone grafting is not always successful. The outcome of bone graft is associated with donor site pain, size and blood type match as well as immune system rejections (Norimoto et al., 2014; Khademi et al., 2014). Advances in bone tissue engineering have created alternatives to bone grafting, however, it still presents certain limitations. Creating a thick bone tissue mass *in vitro* is still restricted to diffusion limitation due to the absence of a natural vascular network. For an *in vitro* culture, diffusion governs the transport of solutes (e.g., nutrients and oxygen) present in a cell culture medium into a scaffold. However, the diffusion of nutrients is only typically limited to a few hundred microns (Mohebbi-Kalhari and Hadjizadeh, 2010; Zhao and Harrison, 2015), thereby, producing thinner tissues.

To overcome this restriction, perfusion bioreactors have been developed over the years (Zhao and Ma, 2005; Grayson et al., 2011; Liu et al., 2012; Viateau et al., 2014). An example of a perfusion bioreactor is hollow fibre membrane bioreactors (HFMBs) (Ye et al., 2006; Abdullah et al., 2009; Chapman et al., 2012). In a perfusive culture environment, an artificial network that resembles a blood vessel *in vivo* carries the medium containing nutrients and oxygen via convection and diffusion processes over a large area of scaffold. This enables a thicker bone tissue mass to be produced *in vitro*.

The presence of hollow fibres inside HFMBs allows a relatively high flow rate to be maintained as it serves as a barrier between the culture medium and cells as well as reducing the risk of cell damage. Furthermore, the HFMBs contain a scaffolding material where cells are cultured, attached and supported into a matrix and finally forming into a functional bone tissue (Mohebbi-Kalhari et al., 2012). They also allow high cell expansion densities due to a large surface area to volume ratio (Diban and Stamatialis, 2014). However, one major downturn of the HFMBs is direct sampling of nutrient concentration (e.g., glucose) during tissue formation is almost impossible (Chesnick et al., 2007) as cells are cultured in the porous scaffold, making it difficult to obtain a representative sample of the total population of cells. Therefore, various numerical modelling frameworks have been developed to

generate the glucose concentration profiles inside the HFMBs. However, to our best knowledge, none of these models employed experimentally deduced glucose diffusivities in cell-free and cell-seeded tissue engineering (TE) membranes and scaffolds imbibed with the culture medium. In other words, most of the existing models found in the literature are based on the assumption that the glucose diffusivities in the culture medium are similar to the ones in water. We have reported in our previous work (Suhaimi et al., 2015b) a decrease in glucose diffusivity for materials saturated with the culture medium.

The main objective of the present work is therefore to simulate the glucose transport inside HFMBs using the measured glucose diffusivity in cell-free and cell-seeded TE membranes and scaffolds obtained from experimental measurements. In contrast to the previous models (Ye et al., 2006; Abdullah and Das, 2007; Mohebbi-Kalhari et al., 2012; Khademi et al., 2014), the approach adopted in this work involves use of non-dimensionless forms of equations as it allows one to carry out an analysis of HFMB in terms of various dimensionless groups of variables (e.g., dimensionless HFMB radius) and numbers (e.g., Reynolds and Damköhler numbers). The materials employed in the present model and the diffusivity measurements are described in detail in our previous works (Suhaimi et al., 2015a, 2015b, 2015c). In addition, the influences of changing dimensionless groups of parameters have on the glucose concentration profiles to increase the scale of the HFMB are analysed. It is anticipated that a more accurate analysis would be possible in future works.

6.2 Mathematical model development

To predict the glucose concentration profiles within the HFMB, a mathematical model based on the Krogh cylinder model (Hewitt et al., 2008) is used in this work. The Krogh cylinder model defines that the HFMB consists of numerous identical hollow fibres. Figure 6.1 shows an example of a single hollow fibre which comprises of three main sections mainly the extracapillary space (ECS) which can be referred as scaffold, membrane and lumen. In the figure, R_1 refers to the fibre lumen radius while R_2 illustrates R_1 and the thickness of the membrane wall. R_3 represents R_2 and the ECS thickness while L refers to the fibre length. As for A_1 , A_2 and A_3 , they refer to the lumen, membrane wall and half of the ECS, respectively.

The transport of a solute in the fibre lumen region is governed by advection and diffusion, but the advective process dominates the diffusive process. In the membrane region, solute transport is governed by diffusion only. In the scaffold region, the solute transport is governed by reaction and diffusion processes; however, reaction process dominates the diffusive transport (Ye et al., 2006; Das, 2007; Abdullah et al., 2009).

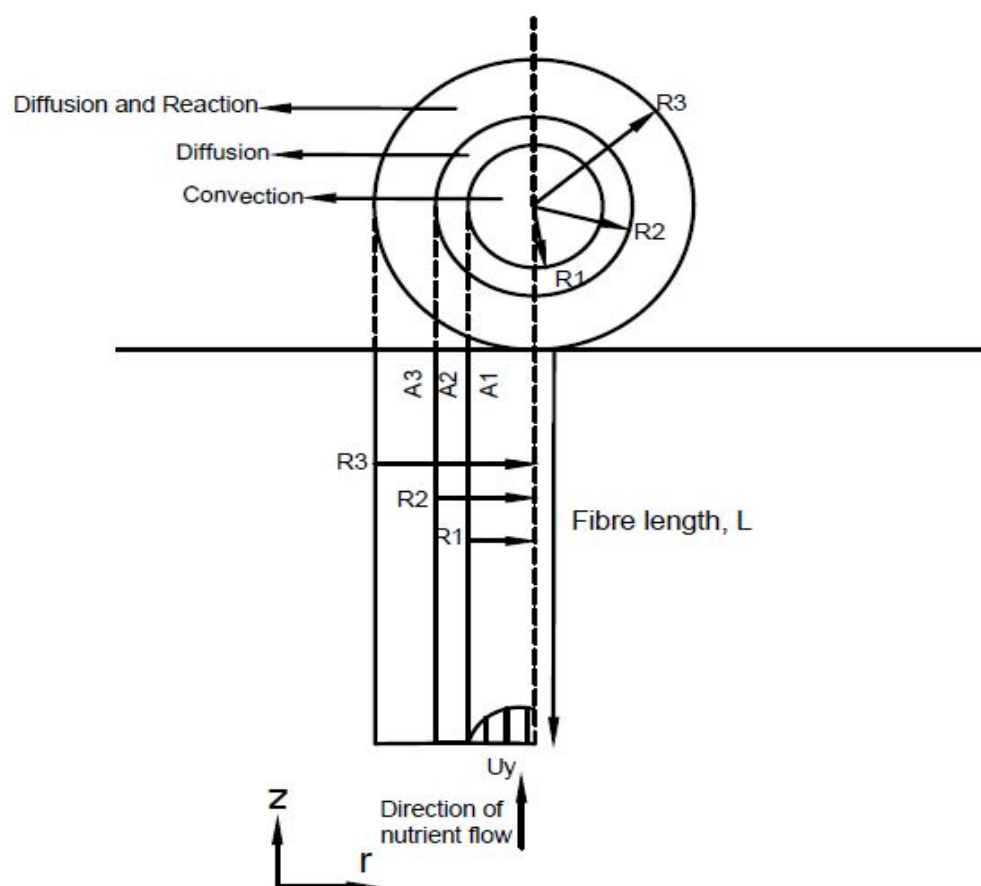


Figure 6.1: Schematic diagram of a single hollow fibre showing the lumen, membrane and scaffold

Under perfusive culture conditions, the culture medium which is saturated with glucose is delivered into the porous region of both the membrane and scaffold from the lumen where cells are cultured and supported to form tissue-like structures. The effective diffusivity values of glucose used in the present model as well as the diffusivity of glucose in cell culture medium (CCM) are taken from the experimental measurements previously reported by Suhaimi et al. (2015a, 2015b, 2015c). All simulations are done based on the dimensions found in Tables 6.1 and 6.2. Table 6.2

summarizes the dimensionless parameters and their respective values based on the data presented in Table 6.1.

Table 6.1: Values of dimensional parameter used in the present model

Parameters	Values	Units	References
Fibre inner radius (a)	1.0×10^{-4}	m	Abdullah et al. (2006)
Fibre membrane (PVDF) thickness (m)	1.25×10^{-4}	m	Suhaimi et al. (2015b)
Fibre length (l)	3.0×10^{-2}	m	Abdullah et al. (2006)
Krogh cylinder radius (A)	3.2×10^{-4}	m	Abdullah et al. (2006)
Average axial flow velocity (U_0)	0.745×10^{-2}	m/s	Abdullah et al. (2006)
CCM kinematic viscosity (ν)	7.48×10^{-7}	m ² /s	Suhaimi et al. (2015a)
Temperature	37	°C	Suhaimi et al. (2015b)
Diffusivity of glucose in lumen (D_l)	6.16×10^{-10}	m ² /s	Suhaimi et al. (2015a)
Diffusivity of glucose in polyvinylidene fluoride membrane ($D_{m,PVDF}$)	7.68×10^{-11}	m ² /s	Suhaimi et al. (2015b)
Diffusivity of glucose in poly(L-lactide) scaffold ($D_{s,PLLA}$)	1.39×10^{-10}	m ² /s	Suhaimi et al. (2015b)
Diffusivity of glucose in cell-seeded poly(L-lactide) scaffold ($D_{s,PLLA}^{cell}$)	9.09×10^{-11}	m ² /s	Suhaimi et al. (2015c)
Glucose inlet concentration (C_0)	5.55	mol/m ³	Abdullah et al. (2006)
Cell seeding density (n)	2.0×10^{12}	cells/m ³	Abdullah et al. (2006)
Glucose uptake rate per cell (k_0)	3.83×10^{-16}	mol cell ⁻¹ s ⁻¹	Abdullah et al. (2006)

Glucose consumption rate coefficient ($nk_1 = nk_0/C_0$)	1.38×10^{-4}	s^{-1}	NA
Glucose degradation rate in the water/acidic environment	$\sim 10^{-5}-10^{-4}$	s^{-1}	Mosier et al. (2002)

6.2.1 Glucose transport equations

The cell growth inside the HFMB is dependent upon several factors, such as growth solutes (e.g., glucose and oxygen), pH level and shear stress (Hossain et al., 2015). For the purpose of this work, we define glucose as our main specie employed in the present model. It is also defined that there are interactions among different solutes in the cell culture medium such as those discussed by Abdullah and Das (2007). These authors have earlier demonstrated that the interactions among the solutes have little effects on the mass transport in HFMB.

The flow of glucose in the lumen region ($0 < r < a$) is continuous and governed by convection. The glucose diffusivity in this region is denoted by D_l and for this model, we define the Reynolds number ($Re = \frac{U_0 a}{\nu}$) (Acheson DJ, 1990) to be low (Table 6.2). We define that the culture medium containing glucose is incompressible, Newtonian and has Poiseuille laminar flow. The transport of glucose in the membrane ($a < r < a + m$) and scaffold regions ($a + m < r < A$) is governed by diffusion and denoted by D_m and D_s , respectively.

In consistent with Hewitt et al. (2008), we define continuity of concentration, c , and normal diffusive flux, $-D \frac{\partial c}{\partial r}$, at each interface between media. The cell seeding density, n , is taken to be constant for the whole of the scaffold area and the glucose uptake rate per cell is proportional to the glucose concentration (first-order kinetics) or constant (zeroth-order kinetics). For the case of first-order cell kinetics, the governing equations are given as follows.

Convection-diffusion equation (CDE):

$$2U_0(1 - r^2) \frac{\partial c}{\partial z} = D_l \left(\frac{1}{r} \frac{\partial}{\partial r} \left(r \frac{\partial c}{\partial r} \right) + \frac{\partial^2 c}{\partial z^2} \right), \quad 0 < r < a \quad (6.1)$$

Diffusion equation (DE):

$$D_m \left(\frac{1}{r} \frac{\partial}{\partial r} \left(r \frac{\partial c}{\partial r} \right) + \frac{\partial^2 c}{\partial z^2} \right) = 0, \quad (a < r < a + m) \quad (6.2)$$

Reaction-diffusion equation (RDE):

$$D_s \left(\frac{1}{r} \frac{\partial}{\partial r} \left(r \frac{\partial c}{\partial r} \right) + \frac{\partial^2 c}{\partial z^2} \right) = k_1 n c, \quad (a + m < r < A) \quad (6.3)$$

for $0 < z < L$. The glucose concentration at the lumen inlet is denoted by C_0 and by taking into account the concentration continuity and diffusive fluxes at interfaces between the media, the boundary and continuity conditions based on the glucose concentration at the lumen outlet are defined by:

$$c = C_0 \quad \text{at } z = 0, 0 < r < a \quad (6.4)$$

$$\frac{\partial c}{\partial z} = 0 \quad \text{at } z = 0, a < r < A \quad (6.5)$$

$$\frac{\partial c}{\partial z} = 0 \quad \text{at } z = l, 0 < r < A \quad (6.6)$$

$$\frac{\partial c}{\partial r} = 0 \quad \text{at } r = 0 \quad (6.7)$$

$$D_l \frac{\partial c}{\partial r} \Big|_{a-} = D_m \frac{\partial c}{\partial r} \Big|_{a+} \quad c|_{a-} = c|_{a+} \quad \text{at } r = a \quad (6.8)$$

$$D_m \frac{\partial c}{\partial r} \Big|_{(a+m)-} = D_s \frac{\partial c}{\partial r} \Big|_{(a+m)+} \quad c|_{(a+m)-} = c|_{(a+m)+} \quad \text{at } r = a + m \quad (6.9)$$

$$\frac{\partial c}{\partial r} = 0 \quad \text{at } r = A \quad (6.10)$$

where $c|_{a-}$ represents the glucose concentration limit near the lumen-membrane boundary ($r = a$) with respect to lumen ($r < a$) and $c|_{a+}$ represents the glucose concentration limit near the lumen-membrane boundary with respect to membrane ($r > a$).

6.2.2 Non-dimensionalisation

We now proceed to non-dimensionalise the glucose transport equations (Eq. (6.1) – Eq. (6.3)) as defined by:

$$Pe(1 - r^2) \frac{\partial c}{\partial z} = \frac{1}{r} \frac{\partial}{\partial r} \left(r \frac{\partial c}{\partial r} \right) + \epsilon^2 \frac{\partial^2 c}{\partial z^2}, \quad 0 < r < 1 \quad (6.11)$$

$$\frac{1}{r} \frac{\partial}{\partial r} \left(r \frac{\partial c}{\partial r} \right) + \epsilon^2 \frac{\partial^2 c}{\partial z^2} = 0, \quad 1 < r < 1 + \delta \quad (6.12)$$

$$\frac{1}{r} \frac{\partial}{\partial r} \left(r \frac{\partial c}{\partial r} \right) + \epsilon^2 \frac{\partial^2 c}{\partial z^2} = Da c \quad 1 + \delta < r < R \quad (6.13)$$

with their respective boundary and continuity conditions:

$$c = 1 \quad \text{at } z = 0, 0 < r < 1 \quad (6.14)$$

$$\frac{\partial c}{\partial z} = 0 \quad \text{at } z = 0, 1 < r < R \quad (6.15)$$

$$\frac{\partial c}{\partial z} = 0 \quad \text{at } z = 1, 0 < r < R \quad (6.16)$$

$$\frac{\partial c}{\partial r} = 0 \quad \text{at } r = 0 \quad (6.17)$$

$$\left. \frac{\partial c}{\partial r} \right|_{1-} = D_m^* \left. \frac{\partial c}{\partial r} \right|_{1+} \quad c|_- = c|_+ \quad \text{at } r = 1 \quad (6.18)$$

$$D_m^* \left. \frac{\partial c}{\partial r} \right|_{(1+\delta)-} = D_s^* \left. \frac{\partial c}{\partial r} \right|_{(1+\delta)+} \quad c|_{(1+\delta)-} = c|_{(1+\delta)+} \quad \text{at } r = 1 + \delta \quad (6.19)$$

$$\frac{\partial c}{\partial r} = 0 \quad \text{at } r = R \quad (6.20)$$

where ϵ , δ , R , D_m^* , D_s^* , Pe and Da are the fibre lumen aspect ratio, dimensionless membrane thickness, dimensionless Krogh cylinder radius, normalized membrane diffusivity, normalized scaffold diffusivity, Péclet number and Damköhler number, respectively, and given as follows:

$$\epsilon = \frac{a}{l}$$

$$\delta = \frac{m}{a}$$

$$R = \frac{A}{a}$$

$$D_m^* = \frac{D_m}{D_l}$$

$$D_s^* = \frac{D_s}{D_l}$$

$$Pe = \frac{2U_0 l a^2}{D_l l^2}$$

$$Da = \frac{k_1 n a^2}{D_s} \quad (6.21)$$

Figure 6.2 shows the non-dimensionless glucose transport equations together with the boundary and continuity conditions for lumen, membrane and scaffold regions.

$$\begin{array}{c}
 r = R \text{-----} \frac{\partial c}{\partial r} = 0 \\
 \text{Scaffold} \quad \frac{1}{r} \frac{\partial}{\partial r} \left(r \frac{\partial c}{\partial r} \right) = Da c \\
 c(0, r) = 1 \quad r = 1 + \delta \text{-----} D_m^* \frac{\partial c}{\partial r} \Big|_{1+\delta-} = D_s^* \frac{\partial c}{\partial r} \Big|_{1+\delta+} \\
 \text{Membrane} \quad \frac{1}{r} \frac{\partial}{\partial r} \left(r \frac{\partial c}{\partial r} \right) = 0 \\
 r = 1 \text{-----} \frac{\partial c}{\partial r} \Big|_{1-} = D_m^* \frac{\partial c}{\partial r} \Big|_{1+} \\
 \text{Lumen} \quad Pe(1-r^2) \frac{\partial c}{\partial z} = \frac{1}{r} \frac{\partial}{\partial r} \left(r \frac{\partial c}{\partial r} \right) \\
 r = 0 \text{-----} \frac{\partial c}{\partial r} = 0 \\
 z = 0 \qquad \qquad \qquad z = 1
 \end{array}$$

Figure 6.2: A representation of the Krogh cylinder problem with the relevant governing equations and boundary/interfacial conditions for first-order cell kinetics

Table 6.2: Values of non-dimensional parameter used in the present model

Parameters	Values	Symbols
Fibre lumen aspect ratio	3.33×10^{-3}	ϵ
Dimensionless membrane thickness	1.25	δ
Dimensionless Krogh cylinder radius	3.2	R
Normalized membrane (PVDF) diffusivity	0.125	D_m^*

Normalized scaffold (PLLA) diffusivity	0.226	D_s^*
Péclet number	8.06	Pe
Damköhler number	9.93×10^{-3}	Da
Reynolds number	0.996	Re

6.2.3 Numerical procedure

The governing non-dimensional transport equations (Eq. (6.11) – Eq. (6.13)) are solved using the commercial MATrix LABoratory (MATLAB) software. These transport equations are subjected to the various boundary and continuity conditions presented in section 6.2.2. The derivatives of the boundary conditions are replaced with r before solving the resulting transport differential equations using MATLAB.

The differential equations of the lumen region are solved first before the differential equations of the membrane and scaffold regions are solved. The boundary conditions in the lumen region after the derivatives have been replaced by r , are shown below:

$$c = 1 \quad \text{at } z = 0 \quad (6.22)$$

$$\frac{\partial c}{\partial r} = 0 \quad \text{at } r = 0 \quad (6.23)$$

$$\frac{\partial c}{\partial r} = -\lambda c \quad \text{at } r = 1 \quad (6.24)$$

where λ (Eq. (6.27)) is an effective mass transfer coefficient solved using a Bessel function in Mathematical Problem-solving and programming Environment (MAPLE). λc defines the transport of glucose at the lumen-membrane boundary ($r = 1$) where the components of λ present the effect of membrane and scaffold properties have on the glucose transport and consequently the downstream concentration of the lumen region. Once the concentration has been solved for lumen, the concentrations in the membrane and scaffold are given by Eq. (6.25) and Eq. (6.26), respectively.

$$c = c|_{1-} + \frac{1}{D_m^*} \frac{\partial c}{\partial r} \Big|_{1-} \log r \quad (6.25)$$

$$c = \left(c|_{1-} + \frac{\log(1+\delta)}{D_m^*} \frac{\partial c}{\partial r} \Big|_{1-} \right) \times$$

$$\left(\frac{K_0(rDa^{1/2})I_0'(RDa^{1/2}) - K_0'(RDa^{1/2})I_0(rDa^{1/2})}{K_0((1+\delta)Da^{1/2})I_0'(RDa^{1/2}) - K_0'(RDa^{1/2})I_0((1+\delta)Da^{1/2})} \right) \quad (6.26)$$

where $K_0(rDa^{1/2})$ and $I_0(rDa^{1/2})$ are modified Bessel functions. The numerical solutions generate glucose concentration profiles based on the data presented in Table 6.2 by changing the dimensionless groups specific to the values presented in Table 6.1.

$$\lambda = \frac{D_s^* D_m^* (1+\delta) Da^{1/2} k}{\log(1+\delta) D_s^* (1+\delta) Da^{1/2} k - D_m^*}$$

$$k = \frac{K_0'((1+\delta)Da^{1/2})I_0'(RDa^{1/2}) - K_0'(RDa^{1/2})I_0'((1+\delta)Da^{1/2})}{K_0((1+\delta)Da^{1/2})I_0'(RDa^{1/2}) - K_0'(RDa^{1/2})I_0((1+\delta)Da^{1/2})} \quad (6.27)$$

6.3 Results and discussions

Experimental results from our previous works (Suhaimi et al., 2015a, 2015b, 2015c) are employed in the present model to validate the numerical procedure. The model is then used to observe the influences of changing the dimensionless groups of parameters have on the glucose concentration profiles in general. In particular, we are keen to observe the difference in the minimal concentration of the glucose inside the HFMB when varying the dimensionless variables. The minimal concentration inside the HFMB is defined near the outlet of the bioreactor ($z = 1, r = R$). We also define the dimensionless concentration at the inlet to be 1. In the present model, we fix the dimensionless membrane thickness (δ), normalized membrane (D_m^*) and scaffold diffusivities (D_s^*) and vary the dimensionless Krogh cylinder radius (R), Péclet (Pe) and Damköhler (Da) numbers to enable us to observe the effect of changing one dimensionless group of variables while holding the other pairs fixed.

6.3.1 Effect of fibre spacing on glucose concentration

As mentioned earlier, the present model is based on the Krogh cylinder model and it is defined that HFMB consists of numerous identical hollow fibres. Varying the dimensionless Krogh cylinder radius (R) physically means varying the spacing of fibres. This effect is studied due to its potential in limiting the glucose concentration which is essential for cell growth in the scaffold region. Figure 6.3 represents the glucose concentration profile of a PVDF-PLLA (without cell) membrane-scaffold system imbibed in the culture medium at 37°C. Figure 6.4 indicates how the

minimum glucose concentration (c) varies when R changes from 2.5 to 3.2 and 5 for fixed Pe and Da . It is expected that the lowest minimum concentration will occur at the largest value of R and it is shown clearly in the simulated results. The minimum glucose concentration decreases from 0.99 to 0.95 and finally to 0.82 (with reference to 1) with increasing dimensionless Krogh radius (R) values of 2.5, 3.2 and 5, respectively (Figure 6.4). This is due to an increase of diffusion distance from the inlet ($c = 1$) towards the outlet of the bioreactor. The glucose concentration profiles for PVDF-cell-seeded PLLA system with varying R values follow similar trends as the system without cell; however, there is a noticeable decrease of the minimal concentration as shown in Figures 6.5 and 6.6. This can be attributed to a lower diffusivity value of cell-seeded scaffold in comparison to a blank (without cell) scaffold (Table 6.1).

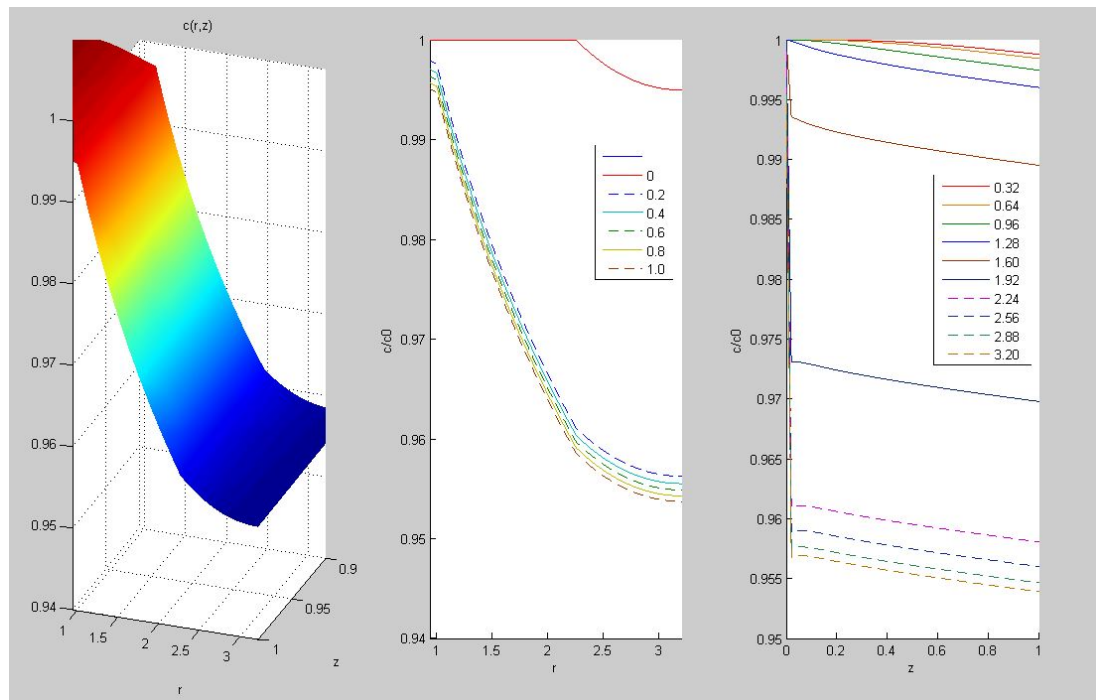


Figure 6.3: Glucose concentration profile for PVDF-PLLA (without cell) system at 37°C

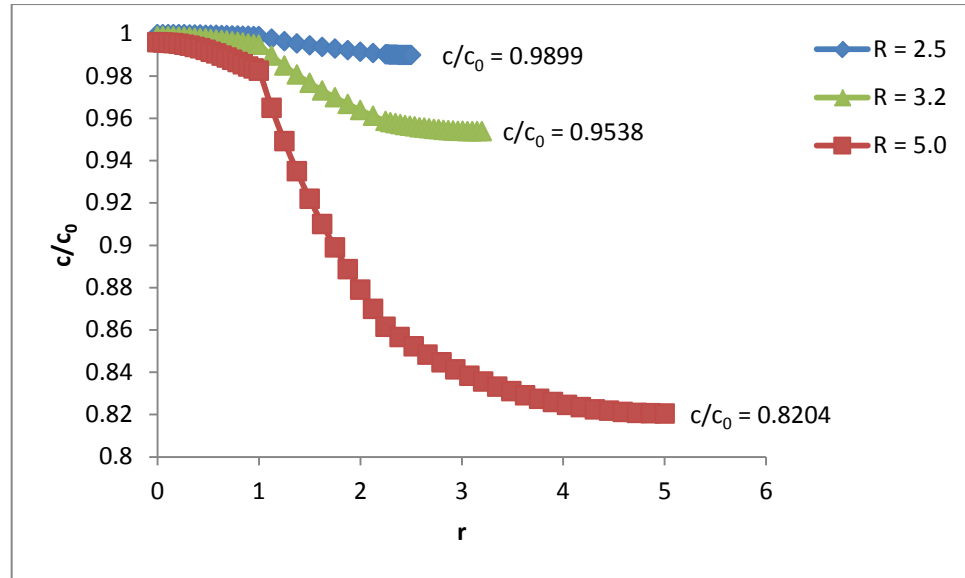


Figure 6.4: Glucose concentration profile for PVDF-PLLA (without cell) system at 37°C for $R = 2.5, 3.2$ and 5 at $z = 1$

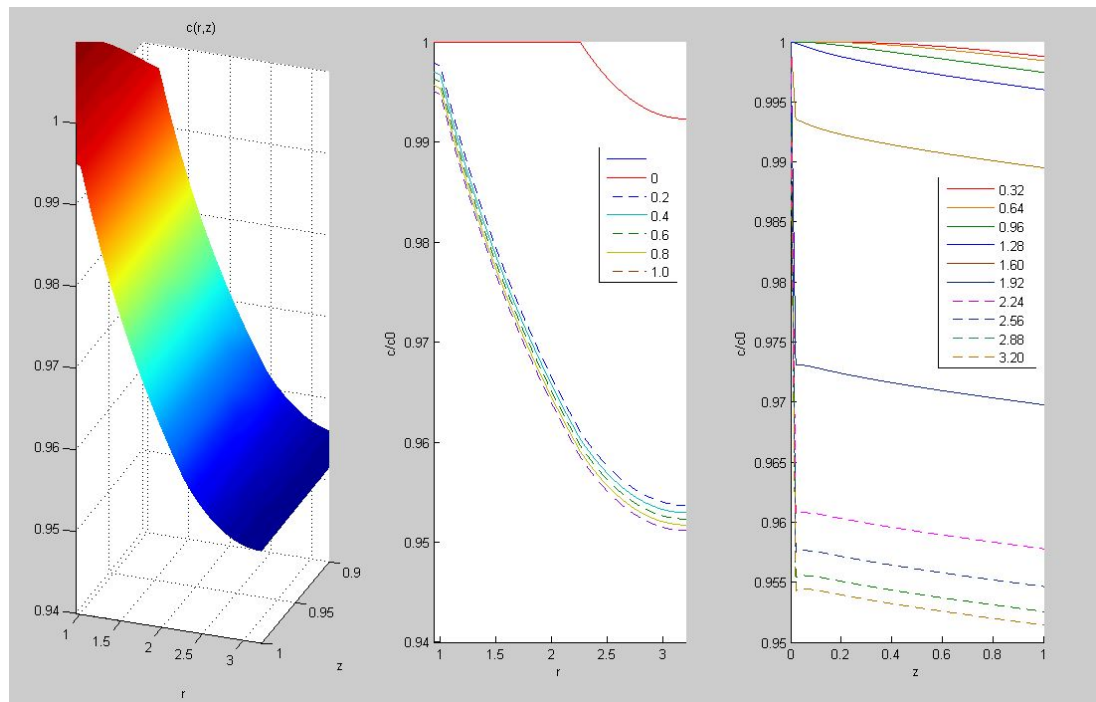


Figure 6.5: Glucose concentration profile for PVDF-cell-seeded PLLA system at 37°C

The simulated results for all other combinations of membrane-scaffold systems (e.g., PVDF-PCL, CN-Collagen and CN-PLLA) with and without cell indicate similar trends as shown in Figure 6.3 – Figure 6.6 and are not included here.

It is evident from the simulated results that the spacing of fibres affects the glucose concentration especially towards the outlet of the bioreactor. Therefore, fibre

spacing should be considered as one of the major design parameters in developing a larger bioreactor scale for producing 3D bone tissues.

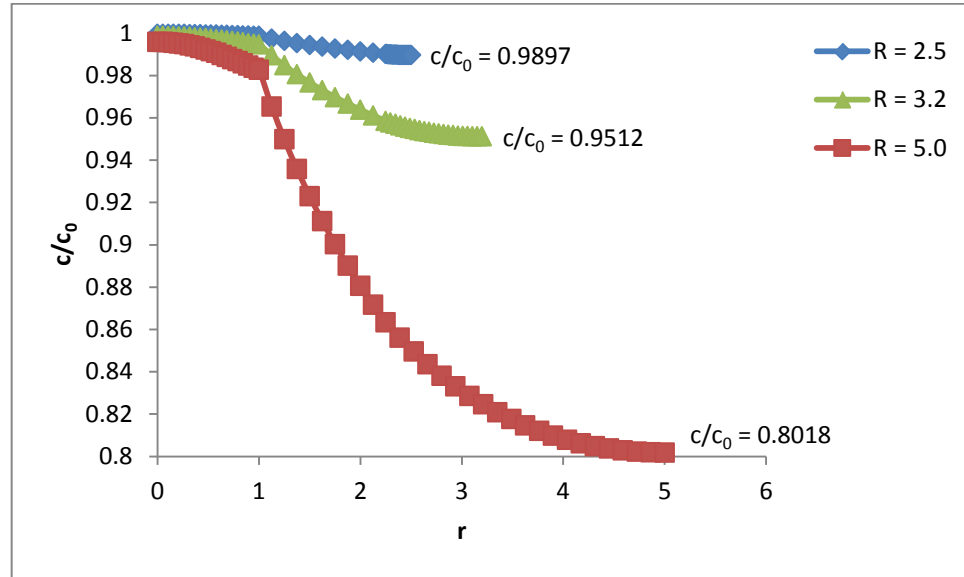


Figure 6.6: Glucose concentration profile for PVDF-cell-seeded PLLA system at 37°C for $R = 2.5, 3.2$ and 5 at $z = 1$

6.3.2 Effect of bioreactor length on glucose concentration

As the glucose transport in lumen region of HFMB is governed by Péclet number, varying this dimensionless number corresponds to varying the length of the bioreactor, or vice versa, provided all other factors remain the same. It is seen in Figure 6.7 that the minimal glucose concentration decreases by increasing the length of the bioreactor from $c = 0.96$ to $c = 0.95$ and $c = 0.94$ (with reference to 1) for $Pe = 20$, $Pe = 8.06$ and $Pe = 1$, respectively. Similar to the fibre spacing, this can be attributed to the increase in diffusion distance of glucose due to the increase of the bioreactor length. Furthermore, increasing Pe number implies that convective mass transfer in the lumen is increased. Therefore, at steady state, we observe the trend as shown in Figure 6.7. Figure 6.8 indicates a noticeable decrease for PVDF-cell-seeded PLLA system which is due to a lower effective diffusivity value of the cell-seeded PLLA scaffold (Table 6.1). The simulated results for all other combinations of membrane-scaffold systems (e.g., PVDF-PCL, CN-Collagen and CN-PLLA) with and without cell indicate similar trends as shown in Figures 6.7 and 6.8 and are not included here. From the results shown, it is evident that the bioreactor length should

also be considered when one wants to develop a larger bioreactor scale, especially for a long-term culture process within the scaffold region.

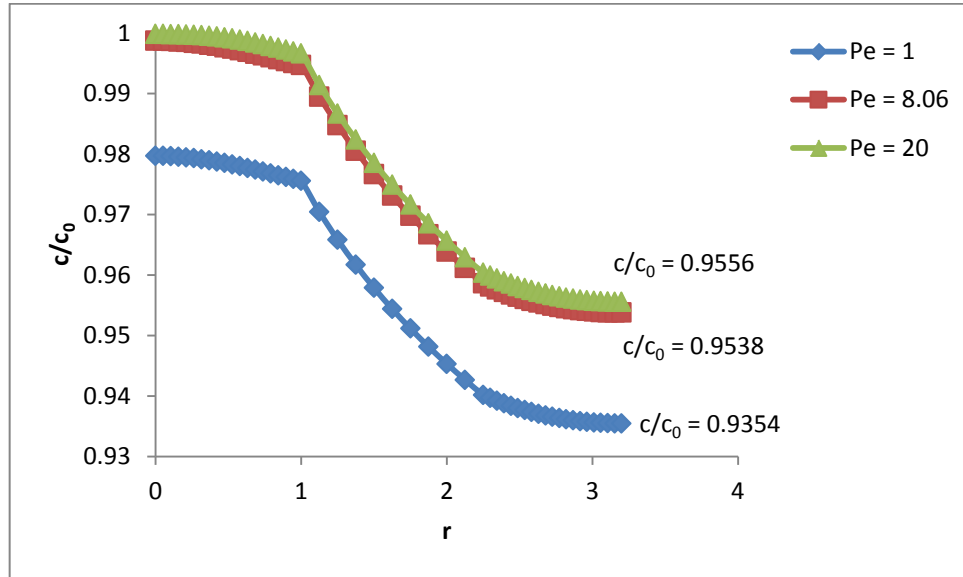


Figure 6.7: Glucose concentration profile for PVDF-PLLA (without cell) system at 37°C for $Pe = 1, 8.06$ and 20 at $z = 1$

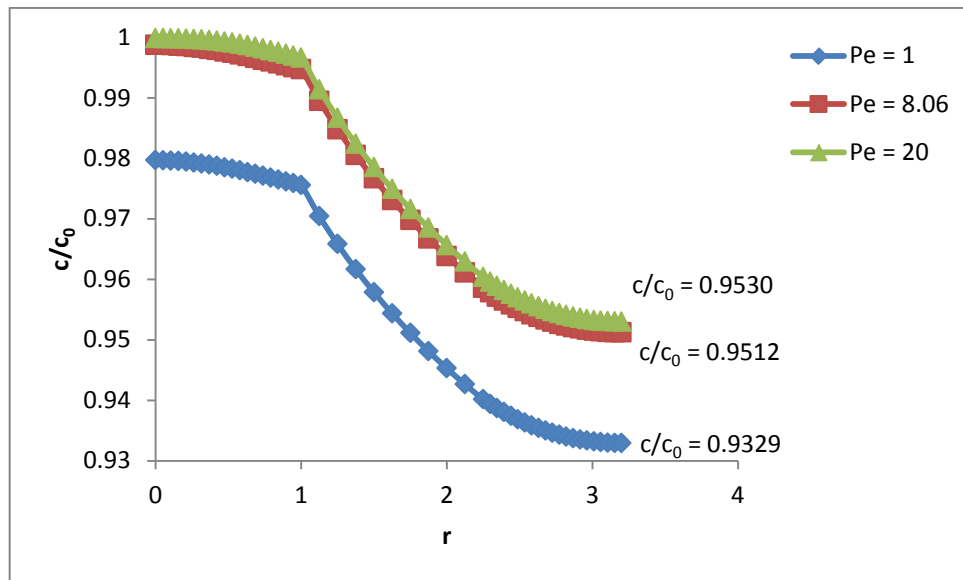


Figure 6.8: Glucose concentration profile for PVDF-cell-seeded PLLA system at 37°C for $Pe = 1, 8.06$ and 20 at $z = 1$

6.3.3 Effect of cell density on glucose concentration

Damköhler number describes the nutrient transport in the scaffold region where cells are grown and supported. The change in Da may correspond to change in the density of cells located within the scaffold. By increasing the cell density, the glucose uptake rate is also increased; hence the minimal glucose concentration near the bioreactor outlet ($z = 1$) is the lowest at the highest cell density, as shown in Figure 6.9. As the cell density increases which corresponds to an increase in Da , the minimal glucose concentration near the outlet decreases from $c = 0.93$ to 0.39 (Figure 6.9). The first-order cell kinetics depicts a similar trend and is not included here. In consistent with fibre spacing and bioreactor length, the glucose concentration profiles of PVDF-cell-seeded PLLA system also show a decrease in the glucose concentration near the outlet. All other combinations of membrane-scaffold system with and without cell also indicate a similar trend as in Figure 6.9 and are not included here.

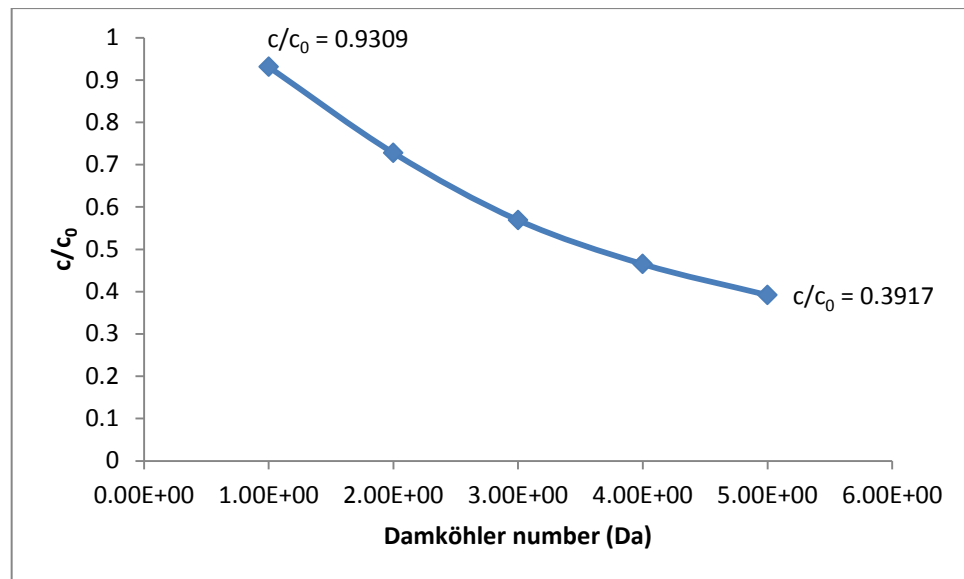


Figure 6.9: Glucose concentration profile for PVDF-cell-seeded PLLA system at 37°C for change in cell density within the scaffold at $z = 1$ for zeroth-order cell kinetics

In addition, the effect of varying the average flow velocity at the inlet of the bioreactor is also analysed. As the velocity increases, both Pe and Re also increase and Pe indicates a lower value at a higher fibre length of 4×10^{-2} m (Figure 6.10). Figure 6.11 shows the glucose concentration profile at different radial positions

within the scaffold region, where the concentration is believed to be the lowest, with respect to both Pe and Re . As expected, the glucose concentration is found to be the lowest at $r = 3.2$ which is the Krogh cylinder radius (R) near the bioreactor outlet, followed by at $r = 2.88$ and finally at $r = 2.24$. This confirms that the glucose diffusion within the scaffold area is the main limitation of glucose transport from the lumen into the cell inside the HFMB.

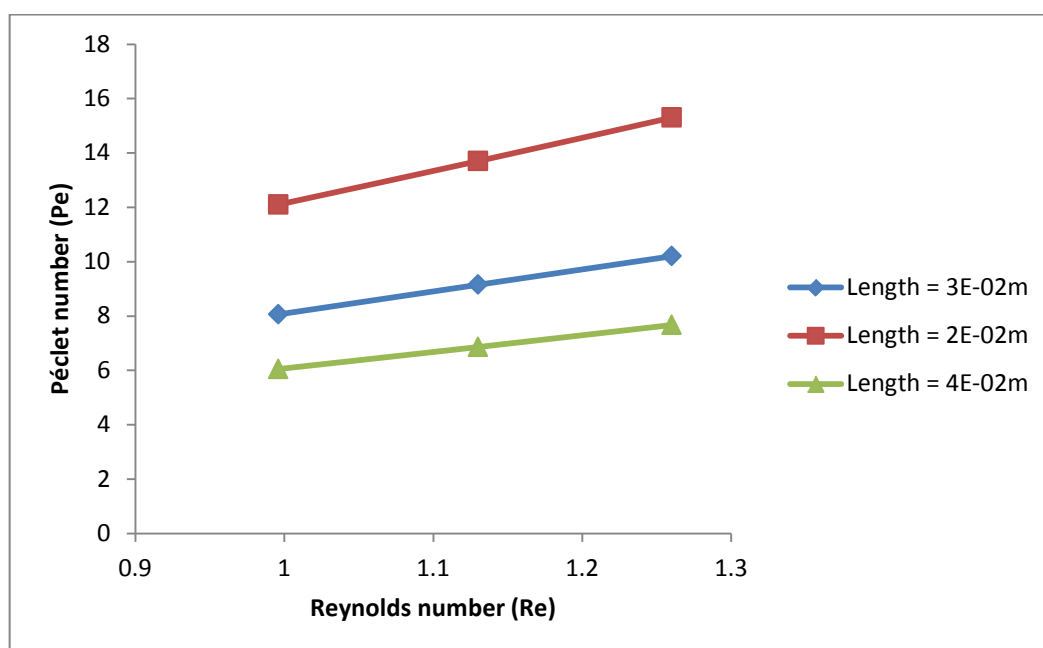


Figure 6.10: Reynolds and Péclet numbers effects on changing the average flow velocity at different fibre length

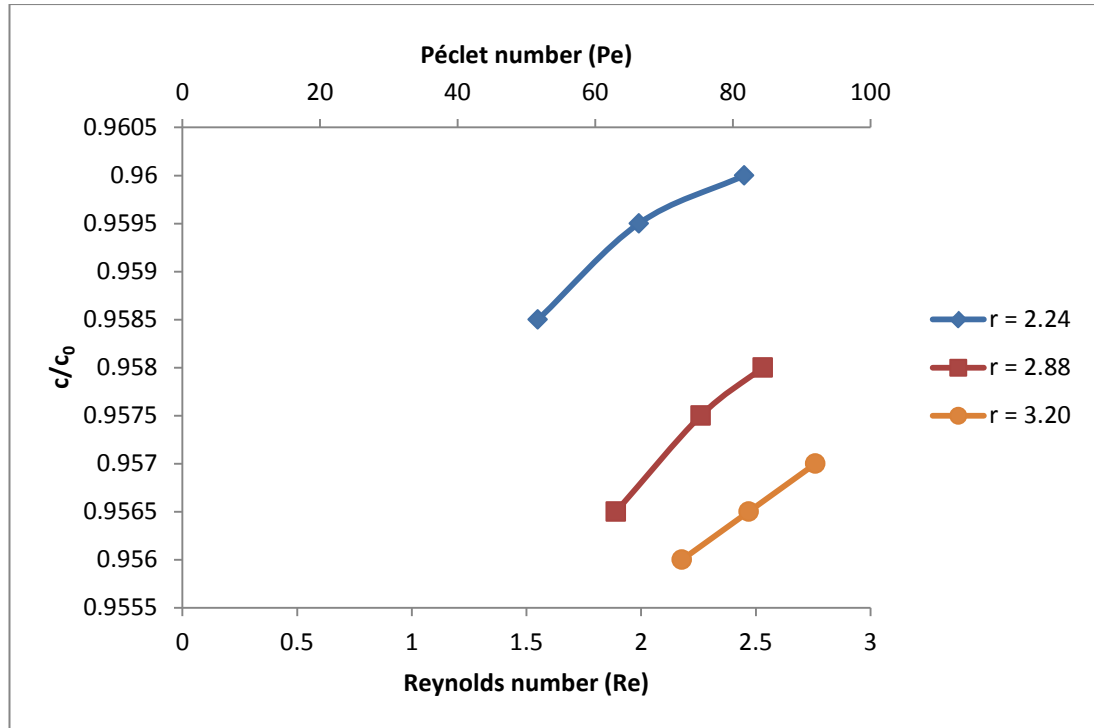


Figure 6.11: The glucose concentration within the scaffold region at different radial position in terms of two dimensionless numbers, Re and Pe

6.4 Chapter summary

We report a modelling framework based on the Krogh cylinder model for the purpose of modelling glucose transport in HFMB. The non-dimensional transport equations together with the boundary and continuity conditions are solved using MATLAB. We vary in this work a number of dimensionless groups of variables. The results show that increasing the fibre spacing, bioreactor length and the cell density varies the minimal glucose concentration near the bioreactor outlet ($z = 1$). It is concluded that these parameters should be considered when developing a large scale bioreactor for producing 3D bone tissues. While TE scaffolds did not degrade during the course of our experiments which indicates they have a long degradation time, it is worth noting for future work as the biodegradation could affect the effective diffusivity of these materials.

CHAPTER 7

CONCLUSIONS AND FUTURE WORK

7.1 Conclusions

This PhD research proposes the use of experimental measurements of glucose diffusivity to model the glucose transport in hollow fibre membrane bioreactor (HFMB) for tissue engineering purposes. Experimental work that consists majorly of diffusion experiment has been carried out to investigate the relationship between diffusion and membrane and scaffold morphology. The experimental measurements are fed into a mathematical model to observe the glucose concentration profile inside the HFMB in an effort to further improve the design and operation of such bioreactors. The key conclusions from this research are as follows:

- 1) While many studies in the literature assumed a similar value for the glucose diffusivity in both water and cell culture media (CCM), we hypothesize the difference in the composition and hydrodynamic properties of both media should give different respective diffusivities. The results shown have proven the hypothesis to be correct.
- 2) The glucose diffusivity in CCM has been found to be significantly reduced than the one in water due to CCM having a larger dynamic viscosity than water. Another reason may be due to the presence of extra components and therefore the difference in fluid properties of CCM.
- 3) Although the result from this research does not exclusively apply to all other biological media/cultures since the variation in composition of media may imply a different diffusivity value, it does highlight the danger of assuming glucose diffusivity in CCM as equal to that in water.
- 4) Similar to the self-diffusivity of glucose in CCM, the effective diffusivity for tissue engineering (TE) materials imbibed in CCM has also been found to be significantly smaller than those in water which is contrary to what have been generally assumed in the previous studies. This further proves that the presence

of extra components is a contributing factor to a difference in the effective diffusivity value.

- 5) Five TE membranes and scaffolds of varying pore size and shapes were engaged in this research for the purpose of quantifying the relationship between diffusion and morphological porous structures and the results shown that the effective diffusivity increases correspondingly with the pore size. Furthermore, the relationship between porosity and tortuosity is found to be non-linear as it depends on a number of factors such as the basic building blocks of the materials.
- 6) Osteoblasts grown on and inside the scaffolds change the morphology of the materials such as reducing the effective pore space of the scaffolds which in turn reduces the glucose mobility. In other words, the effective glucose diffusivity between cell-free and cell-seeded scaffolds presents a significant difference. In addition, the effective glucose diffusivity decreases monotonically with the cell number.
- 7) A mathematical model based on the Krogh cylinder assumption has been employed to facilitate the glucose concentration profiles inside HFMB, especially at the region where the concentration is believed to be the lowest. Results show that the concentration at the point of interest (scaffold region) varies depending on the change of dimensionless groups of variables and numbers.
- 8) The simulated results will help to effectively design and optimise the operation of HFMB especially with the use of real values of glucose diffusivities for producing 3D bone tissues.

7.2 Future work

There are several suggestions that can be done in the future as outlined below:

- 1) Lactic acid is an example of a metabolic waste product produced by cells. As similar to the vascular system *in vivo*, we should mimic the system in such a way that the diffusion of lactate acid within the scaffold is also monitored. In this way, it may complete the biochemical communication and especially useful in developing a mathematical model that can simulate real situations.

- 2) The development of an online glucose monitoring system that can measure the glucose concentration inside CCM without having the risk of contaminating the sample. As CCM is quite sensitive to the surrounding environment, it would be beneficial for the online monitoring system to be developed and it is particularly useful for monitoring glucose concentration in cell-seeded scaffolds since cells are highly sensitive in nature.
- 3) The effect of membrane fouling should be considered in future especially in experiments saturated with CCM as it can affect the diffusivity value.
- 4) Cell proliferation rate by DNA quantification should also be investigated to further understand the quantitative relationship between effective diffusivity and cell proliferation. The insignificant difference in the effective diffusivity between culture periods of 3 weeks may be due to a slower rate of proliferation after a certain period.
- 5) Samples of different sections of cell-seeded scaffolds should be taken and frozen in liquid nitrogen to observe in between the cell layer to further investigate the possibility of cell death, damaged layers and healthy layers by cell staining using calcium. This is one way to characterize pockets of cell death which may affect the diffusivity value.
- 6) Although TE scaffolds did not degrade during the course of our experiments, biodegradation studies should be carried out in the future, particularly if the cells have the potential to produce extracellular matrix proteins and in turn would affect the diffusivity value of the scaffold.
- 7) The pH of culture medium should be regularly checked so as to maintain pH stability for successful cell cultivation. A slight disturbance such as opening of an incubator door even for only 30 sec may have negative consequences for cell growth. The use of 1% penicillin/streptomycin as an antibiotic in cell culture is also suggested to safe guard against bacterial contamination and especially useful in shared labs.
- 8) The mathematical model assumed a uniform distribution of cells inside HFMB where in reality, the cell number will vary due to cell multiplication and death. Therefore, more data on cell kinetics studies should be investigated to further understand the concentration variation on cell distribution inside HFMB.

Future research will contribute in further understanding the nutrient and possibly waste product transport processes in tissue engineering materials and hopefully will help in the advancement of regenerative medical therapy.

REFERENCES

- Abdullah NS, Das DB (2007) Modelling nutrient transport in hollow fibre membrane bioreactor for growing bone tissue with consideration of multi-component interactions, *Chemical Engineering Science*, Vol. 62, Issue 21, 5821-5839
- Abdullah NS, Das DB, Ye H, Cui ZF (2006) 3-D bone tissue growth in hollow fibre membrane bioreactor: implications of various process parameters on tissue nutrition, *International Journal of Artificial Organs*, Vol. 9, Issue 29, 841-851
- Abdullah NS, Jones DR, Das DB (2009) Nutrient transport in bioreactors for bone tissue growth: why do hollow fibre membrane bioreactors work?, *Chemical Engineering Science*, Vol. 64, Issue 1, 109-125
- Abousleiman RI, Reyes Y, McFetridge P, Sikavitsas V (2009) Tendon tissue engineering using cell-seeded umbilical veins cultured in a mechanical stimulator, *Tissue Engineering Part A*, Vol. 15, Issue 4, 787-795
- Acheson DJ, *Elementary fluid dynamics*, Oxford, 1990
- Adams FV, Dlamini DS, Nxumalo EN, Krause RWM, Hoek EMV, Mamba BB (2013) Solute transport and structural properties of polysulfone/ β -cyclodextrin polyurethane mixed-matrix membranes, *Journal of Membrane Science*, Vol.429, 58-65
- Agrawal CM, Ray RB (2001) Biodegradable polymeric scaffolds for musculoskeletal tissue engineering, *Journal of Biomedical Materials Research*, Vol. 55, Issue 2, 141-150
- Ahn G, Kim Y, Lee SW, Jeong YJ, Son H, Lee D (2014) Effect of heterogeneous multi-layered gelatin scaffolds on the diffusion characteristics and cellular activities of preosteoblasts, *Macromolecular Research*, Vol. 22, Issue 1, 99-107
- Amini AR, Laurencin CT, Nukavarapu SP (2012) Bone tissue engineering: recent advances and challenges, *Critical Review Biomedical Engineering*, Vol. 40, Issue 5, 363-408

- Andersson AP, Oste RE (1994) Diffusivity data of an artificial food system, *Journal of Food Engineering*, Vol.23, Issue 4, 631-639
- Andersson M, Axelsson A, Zacchi G (1997) Diffusion of glucose and insulin in a swelling *N*-isopropylacrylamide gel, *International Journal of Pharmaceutics*, Vol.157, 199-208
- Archie GE (1942) The electrical resistivity log as an aid in determining some reservoir characteristics, *Petroleum Technology*, Vol.1, 55-62
- Awad HA, Butler DL, Harris MT, Ibrahim RE, Wu Y, Young RG, Kadiyala S, Boivin GP (2000) *In vitro* characterization of mesenchymal stem cell-seeded collagen scaffolds for tendon repair: effects of initial seeding density on contraction kinetics, *Journal of Biomedical Materials Research Part A*, Vol. 51, Issue 2, 233-240
- Bai H, Liu Z, Sun DD (2012) A hierarchically structured and multifunctional membrane for water treatment, *Applied Catalysis B: Environmental*, Vol. 111-112, 571-577
- Baptista RP, Fluri DA, Zandstra PW (2013) High density continuous production of murine pluripotent cells in an acoustic perfused bioreactor at different oxygen concentrations, *Biotechnology and Bioengineering*, Vol. 110, Issue 2, 648-655
- Barrande M, Bouchet R, Denoyel R (2007) Tortuosity of porous particles, *Analytical Chemistry*, Vol. 79, Issue 23, 9115-9121
- Bashkatov AN, Genina EA, Sinichkin YP, Kochubey VI, Lakodina NA, Tuchin VV (2003) Glucose and mannitol diffusion in human dura mater, *Biophysical Journal*, Vol.85, Issue 5, 3310-3318
- Bear J (1972) *Dynamics of fluids in porous media*, American Elsevier, New York
- Bechhold H, Schlesinger M, Silbereisen K (1931) Porenweite von ultrafiltern, *Kolloid-Zeitschrift*, Vol.55, Issue 2, 172-198
- Beeckman JW (1990) Mathematical description of heterogeneous materials, *Chemical Engineering Science*, Vol.45, Issue 8, 2603-2610
- Bessieres A, Meireles A, Coratger M, Beauvillain R, Sanchez V (1996), Investigations of surface properties of polymeric membranes by near field microscopy, *Journal of Membrane Science*, Vol. 109, Issue 2, 271-284

- Bettahalli NMS, Groen N, Steg H, Unadkat H, de Boer J, van Blitterswijk CA, Wessling M, Stamatialis D (2014) Development of multilayer constructs for tissue engineering, *Journal of Tissue Engineering and Regenerative Medicine*, Vol. 8, 106-119
- Bettahalli NMS, Steg H, Wessling M, Stamatialis D (2011) Development of poly(L-lactic acid) hollow fiber membranes for artificial vasculature in tissue engineering scaffolds, *Journal of Membrane Science*, Vol. 371, 117-126
- Bettahalli NMS, Vicente J, Moroni L, Higuera GA, van Blitterswijk CA, Wessling M, Stamatialis DF (2011) Integration of hollow fiber membranes improves nutrient supply in three-dimensional tissue constructs, *Acta Biomaterialia*, Vol. 7, Issue 9, 3312-3324
- Bettinger CJ, Weinberg EJ, Kulig KM, Vacanti JP, Wang Y, Borenstein JT, Langer R (2006) Three-dimensional microfluidic tissue-engineering scaffolds using a flexible biodegradable polymer, *Advanced Materials*, Vol. 18, Issue 2, 165-169
- Bhatia SK (1985) Directional autocorrelation and the diffusional tortuosity of capillary porous media, *Journal of Catalysis*, Vol.93, 192-196
- Bica CID, Borsali R, Geisslet E, Rochas C (2001) Dynamics of cellulose whiskers in agarose gels 1: polarized dynamic light scattering, *Macromolecules*, Vol. 34, Issue 15, 5275-5279
- Binnig G, Quate CF, Gerber CH (1986) Atomic force microscope, *Physical Review Letters*, Vol.56, Issue 9, 930-933
- Bock N, Riminucci A, Dionigi C, Russo A, Tampieri A, Landi E, Goranov VA, Marcacci M, Dediu V (2010) A novel route in bone tissue engineering: Magnetic biomimetic scaffolds, *Acta Biomaterialia*, Vol. 6, Issue 3, 786-796
- Boss C, Meurville E, Sallese JM, Ryser P (2011) A viscosity-dependent affinity sensor for continuous monitoring of glucose in biological fluids, *Biosensors and Bioelectronics*, Vol. 30, Issue 1, 223-228
- Boss C, Meurville E, Sallese JM, Ryser P (2012) Size-selective diffusion in nanoporous alumina membranes for a glucose affinity sensor, *Journal of Membrane Science*, Vol.401-402, 217-221

- Bouchoux A, Balmann HRD, Lutin F (2005) Nanofiltration of glucose and sodium lactate solutions variations of retention between single- and mixed-solute solutions, *Journal of Membrane Science*, Vol. 258, Issues 1-2, 123-132
- Boudreau BP (1996) The diffusive tortuosity of fine-grained unlithified sediments, *Geochimica et Cosmochimica Acta*, Vol.60, Issue 16, 3139-3142
- Breer J, de Groot K, Schonert H (2014) Diffusion in the diaphragm cell: continuous monitoring of the concentrations and determination of the differential diffusion coefficient, *Journal of Solution Chemistry*, Vol.43, Issue 1, 71-82
- Brown RA, Sethi KK, Gwanmesia I, Raemdonck D, Eastwood M, Mudera V (2002) Enhanced fibroblast contraction of 3D collagen lattices and integrin expression by TGF- β 1 and - β 3: mechanoregulatory growth factors?, *Experimental Cell Research*, Vol. 274, 310-322
- Brun M, Lallemand A, Quinson JF, Eyraud C (1977) A new method for the simultaneous determination of the size and the shape of pores: the thermoporometry, *Thermochimica Acta*, Vol.21, 59-88
- Buchwald P (2011) A local glucose-and oxygen concentration-based insulin secretion model for pancreatic islets, *Theoretical Biology and Medical Modelling*, Vol.8, Issue 20, 1-25
- Burrin JM, Alberti KGMM (1990) What is blood glucose: Can it be measured?, *Diabetic Medicine*, Vol. 7, Issue 3, 199-206
- Buzier R, Charriau A, Corona D, Lenain JF, Fondaneche P, Joussein E, Poulier G, Lissalde S, Mazzella N, Guibaud G (2014) DGT-labile As, Cd, Cu and Ni monitoring in freshwater: toward a framework for interpretation of *in situ* deployment, *Environmental Pollution*, Vol.192, 52-58
- Cai T, Li M, Neoh KG, Kang ET (2012) Preparation of stimuli responsive polycaprolactone membranes of controllable porous morphology *via* combined atom transfer radical polymerization, ring-opening polymerization and thiol-yne click chemistry, *Journal of Materials Chemistry*, Vol. 22, 16248-16258
- Carrel A (1912) On the permanent life of tissues outside of the organism, *The Journal of Experimental Medicine*, Vol. 15, Issue 5, 516-528

- Chai Y, Mei LH, Lin DQ, Yao SJ (2004) Diffusion coefficients in intrahollow calcium alginate microcapsules, *Journal of Chemical & Engineering Data*, Vol. 49, Issue 3, 475-478
- Chan C, Zamel N, Li X, Shen J (2012) Experimental measurement of effective diffusion coefficient of gas diffusion layer/microporous layer in PEM fuel cells, *Electrochimica Acta*, Vol. 65, 13-21
- Chance B, Liu H, Kitai T, Zhang Y (1995) Effects of solutes on optical properties of biological materials: models, cells, and tissues, *Analytical Biochemistry*, Vol. 227, 351-362
- Chao TC, Das DB (2015) Numerical simulation of coupled cell motion and nutrient transport in NASA's rotating bioreactor, *Chemical Engineering Journal*, Vol. 259, 961-971
- Chapman LAC, Waters SL, Shipley RJ, Byrne HM, Whiteley JP, Ellis MJ (2012) Modelling fluid and nutrient transport to determine the influence of cell seeding on the growth of cell aggregates on a permeable membrane, *European Cells and Materials*, Vol. 23, Issue 4, 99
- Chaudhuri JB, Davidson MG, Ellis MJ, Jones MD, Wu XJ (2008) Fabrication of honeycomb-structured poly (DL-lactide) and poly[(DL-lactide)-co-glycolide] films and their use as scaffolds for osteoblast-like cell culture, *Macromolecular Symposia*, Vol. 272, 52-57
- Cheema U, Rong Z, Kirresh O, MacRobert AJ, Vadgama P, Brown RA (2012) Oxygen diffusion through collagen scaffolds at defined densities: implications for cell survival in tissue models, *Journal of Tissue Engineering and Regenerative Medicine*, Vol. 6, Issue 1, 77-84
- Chen J, Liu T, Yuan WK, Zhao L (2013) Solubility and diffusivity of CO₂ in polypropylene/micro-calcium carbonate composites, *The Journal of Supercritical Fluids*, Vol. 77, 33-43
- Chen JS, Clunie JC, Baird JK, Rosenberger F (1992) Diaphragm diffusion cell: a closed form solution to the transport equation and its application to the determination of the concentration dependence of the HCl:H₂O interdiffusion coefficient, *Physics and Chemistry of Liquids: An International Journal*, Vol. 24, Issue 4, 261-272, DOI: 10.1080/00319109208027278

- Chenu C, Roberson EB (1996) Diffusion of glucose in microbial extracellular polysaccharide as affected by water potential, *Soil Biology and Biochemistry*, Vol. 28, Issue 7, 877-884
- Chesnick IE, Avallone F, Leapman RD, Landis WJ, Eidelman N, Potter K (2007) Evaluation of bioreactor-cultivated bone by magnetic resonance microscopy and FTIR microspectroscopy, *Bone*, Vol. 40, Issue 4, 904-912
- Chin WYW, Annur MSM, Tan BC, Khalid N (2014) Evaluation of a laboratory scale conventional shake flask and a bioreactor on cell growth and regeneration of banana cell suspension cultures, *Scientia Horticulturae*, Vol. 172, 39-46
- Choi YK, Park SM, Lee S, Khang DY, Choi DC, Lee CH (2013) Characterization and theoretical analysis of isoporous cycloaliphatic polyurethane membrane for water treatment, *Desalination and Water Treatment*, 1-7
- Choy EM, Evans DF, Cussler EL (1973) A selective membrane for transporting sodium ion against its concentration gradient, *Journal of the American Chemical Society*, Vol.96, Issue 22, 7085-7090
- Chu TMG, Orton DG, Hollister SJ, Feinberg SE, Halloran JW (2002) Mechanical and *in vivo* performance of hydroxyapatite implants with controlled architectures, *Biomaterials*, Vol. 23, Issue 5, 1283-1293
- Churchouse SJ, Battersby CM, Mullen WH, Vadgama PM (1986) Needle enzyme electrodes for biological studies, *Biosensors*, Vol.2, 325-342
- Clark AR, Stokes YM, Thompson JG (2011) Estimation of glucose uptake by ovarian follicular cells, *Annals of Biomedical Engineering*, Vol. 39, 2654-2667
- Clarke WL, Cox D, Gonder-Frederick LA, Carter W, Pohl SL (1987) Evaluating clinical accuracy of systems for self-monitoring of blood glucose, *Diabetes Care*, Vol. 10, 622-628
- Cleary J, Bromberg LE, Magner E (2003) Diffusion and release of solutes in pluronic-g-poly(acrylic acid) hydrogels, *Langmuir*, Vol. 9, Issue 22, 9162-9172
- Comiti J, Renaud M (1989) A new model for determining mean structure parameters of fixed beds from pressure drop measurements: application to beds packed with parallelepipedal particles, *Chemical Engineering Science*, Vol. 44, Issue 7, 1539-1545

- Couch NP, Wilson RE, Hager EB, Murray JE (1966) Transplantation of cadaver kidneys: experience with 21 cases, *Surgery*, Vol. 59, Issue 2, 183-188
- Crank J (1975) *The Mathematics of diffusion*, Oxford University Press, Oxford
- Crock CA, Rogensues AR, Shan W, Tarabara VV (2013) Polymer nanocomposites with graphene-based hierarchical fillers as materials for multifunctional water treatment membranes, *Water Research*, Vol.47, Issue 12, 3984-3996
- Curcio E, De Bartolo L, Barbieri G, Rende M, Giorno L, Morelli S, Drioli E (2005) Diffusive and convective transport through hollow fiber membranes for liver cell culture, *Journal of Biotechnology*, Vol. 117, Issue 3, 309-321
- Cussler EL, *Diffusion: mass transfer in fluid systems*, second edition, Cambridge, 1997
- Daniele MA, Adams AA, Naciri J, North SH, Ligler FS (2014) Interpenetrating networks based on gelatin methacrylamide and PEG formed using concurrent thiol click chemistries for hydrogel tissue engineering scaffolds, *Biomaterials*, Vol. 35, Issue 6, 1845-1856
- Daraei P, Madaeni SS, Ghaemi N, Khadivi MA, Astinchap B, Moradian R (2013) Enhancing antifouling capability of PES membrane via mixing with various types of polymer modified multi-walled carbon nanotube, *Journal of Membrane Science*, Vol.444, 184-191
- Das DB (2007) Multiscale simulation of nutrient transport in hollow fibre membrane bioreactor for growing bone tissue: sub-cellular scale and beyond, *Chemical Engineering Science*, Vol. 62, Issue 13, 3627-3639
- Das DB, Jones DR (2006) Multiscale modeling of nutrient transport in bioreactors for growing 3-D bone tissues: subcellular to laboratory scale, *Cytotherapy*, Vol. 8, Issue 2, 34
- Deans TL, Singh A, Gibson M, Elisseeff JH (2012) Regulating synthetic gene networks in 3D materials, *Proceedings of the National Academy of Sciences of the United States of America*, Vol. 109, Issue 38, 15217-15222
- DeFriend KA, Wiesner MR, Barron AR (2003) Alumina and aluminate ultrafiltration membranes derived from alumina nanoparticles, *Journal of Membrane Science*, Vol.224, Issue 1-2, 11-28

- De Napoli IE, Scaglione S, Giannoni P, Quarto R, Catapano G (2011) Mesenchymal stem cell culture in convection-enhanced hollow fibre membrane bioreactors for bone tissue engineering, *Journal of Membrane Science*, Vol. 379, 341-352
- De Napoli IE, Zanetti EM, Fragomeni G, Giuzio E, Audenino AL, Catapano G (2014) Transport modeling of convection-enhanced hollow fiber membrane bioreactors for therapeutic applications, *Journal of Membrane Science*, Vol. 471, 347-361
- Diban N, Ramos-Vivas J, Remuzgo-Martinez S, Ortiz I, Urtiaga A (2014) Poly(ϵ -caprolactone) films with favourable properties for neural cell growth, *Current Topics in Medicinal Chemistry*, Vol. 14, Issue 23, 2743-2749
- Diban N, Stamatialis D (2014) Polymeric hollow fiber membranes for bioartificial organs and tissue engineering applications, *Journal of Chemical Technology and Biotechnology*, Vol. 89, Issue 5, 633-643
- Dietz P, Hansma PK, Inacker O, Lehmann HD, Herrmann KH (1992) Surface pore structures of micro- and ultrafiltration membranes imaged with the atomic force microscope, *Journal of Membrane Science*, Vol.65, 101-111
- Dionne KE, Cain BM, Li RH, Bell WJ, Doherty EJ, Rein DH, Lysaght MJ, Gentile FT (1996) Transport characterization of membranes for immunoisolation, *Biomaterials*, Vol. 17, Issue 3, 257-266
- Dollimore D, Heal GR (1964) An improved method for the calculation of pore size distribution from adsorption data, *Journal of Applied Chemistry*, Vol.14, Issue 3, 109-114
- Donati D, Zolezzi C, Tomba P, Vigano A (2007) Bone grafting: historical and conceptual review, starting with an old manuscript by Vittorio Putti, *Acta Orthopaedica*, Vol. 78, Issue 1, 19-25
- Dong Y, Gao WY, Man S, Zuo B, Wang J, Huang L, Xiao P (2013) Effect of bioreactor angle and aeration rate on growth and hydromechanics parameters in bioreactor culture of ginseng suspension cells, *Acta Physiologiae Plantarum*, Vol. 35, Issue 5, 1497-1501
- Dullien FAL (1975) Prediction of "tortuosity factors" from pore structure data, *American Institute of Chemical Engineers Journal*, Vol. 21, Issue 4, 820-822

- Dykhuizen RC, Casey WH (1989) An analysis of solute diffusion in rocks, *Geochimica et Cosmochimica Acta*, Vol.53, 2797-2805
- Einstein A (1905) Investigations on the theory of brownian movement, *Annalen der Physik*, Vol. 17, 549-560
- Ellis MJ, Chaudhuri JB (2007) Poly(lactic-co-glycolic acid) hollow fibre membranes for use as a tissue engineering scaffold, *Biotechnology and Bioengineering*, Vol. 96, Issue 1, 177-187
- Ellis MJ, Chaudhuri JB (2008) Human bone derived cell culture on PLGA flat sheet membranes of different lactide:glycolide ratio, *Biotechnology and Bioengineering*, Vol. 101, Issue 2, 369-377
- Ellis SJ, Velayutham M, Velan SS, Petersen EF, Zweier JL, Kuppusamy P, Spencer RGS (2001) EPR oxygen mapping (EPROM) of engineered cartilage grown in a hollow-fiber bioreactor, *Magnetic Resonance in Medicine*, Vol. 46, Issue 4, 819-826
- Fang L, Liang B, Yang G, Hu Y, Zhu Q, Ye X (2014) Study of glucose biosensor lifetime improvement in 37°C serum based on PANI enzyme immobilization and PLGA biodegradable membrane, *Biosensors and Bioelectronics*, Vol. 56, 91-96
- Felder RM, Huvard GS (1980) *Methods of experimental physics*, Academic Press, NY, Vol. 16, 315
- Fiedler T, Belova IV, Murch GE, Poologasundarampillai G, Jones JR, Roether JA, Boccaccini AR (2014) A comparative study of oxygen diffusion in tissue engineering scaffolds, *Journal of Materials Science: Materials in Medicine*, Vol. 25, Issue 11, 2573-2578
- Florczyk SJ, Wang K, Jana S, Wood DL, Sytsma SK, Sham JG, Kievit FM, Zhang M (2013) Porous chitosan-hyaluronic acid scaffolds as a mimic of glioblastoma micronenvironment ECM, *Biomaterials*
- Freed LE, Vunjak-Novakovic G (1998) Culture of organized cell communities, *Advanced Drug Delivery Reviews*, Vol. 33, Issues 1-2, 15-30
- Freed LE, Vunjak-Novakovic G, Langer R (1993) Cultivation of cell-polymer cartilage implants in bioreactors, *Journal of Cellular Biochemistry*, Vol. 51, Issue 3, 257-264

- Galban CJ, Locke BR (1999) Analysis of cell growth kinetics and substrate diffusion in a polymer scaffold, *Biotechnology and Bioengineering*, Vol. 65, Issue 2, 121-132
- Gao X, da Costa JCD, Bhatia SK (2014) Understanding the diffusional tortuosity of porous materials: an effective medium theory perspective, *Chemical Engineering Science*, Vol. 110, 55-71
- Garcia-Abuin A, Gomez-Diaz D, Losada M, Navaza JM (2013) Oxygen absorption in polymer + surfactant aqueous solutions, *Chemical Engineering Journal*, Vol. 225, 76-83
- Gardel LS, Serra LA, Reis RL, Gomes ME (2014) Use of perfusion bioreactors and large animal models for long bone tissue engineering, *Tissue Engineering: Part B*, Vol. 20, Issue 2, DOI: 10.1089/ten.teb.2013.0010
- George KA, Wentrup-Byrne E, Hill DJT, Whittaker AK (2004) Investigation into the diffusion of water into HEMA-co-MOEP hydrogels, *Biomacromolecules*, Vol. 5, Issue 4, 1194-1199
- Goodyer CE, Bunge AL (2012) Mass transfer through membranes with surface roughness, *Journal of Membrane Science*, Vol. 409-410, 127-136
- Grayson WL, Fröhlich M, Yeager K, Bhumiratana S, Chan M, Cannizzaro C, Wan LQ, Liu XS, Guo XE, Vunjak-Novakovic G (2010) Engineering anatomically shaped human bone grafts, *Proceedings of the National Academy of Sciences of the United States of America*, Vol. 107, Issue 8, 3299-3304
- Grayson WL, Marolt D, Bhumiratana S, Fröhlich M, Guo XE, Vunjak-Novakovic G (2011) Optimizing the medium perfusion rate in bone tissue engineering bioreactors, *Biotechnology and Bioengineering*, Vol. 108, Issue 5, 1159-1170
- Gregg SJ, Sing KSW (1982) Adsorption, surface area and porosity, Academic Press, London
- Guaccio A, Borselli C, Oliviero O, Netti PA (2008) Oxygen consumption of chondrocytes in agarose and collagen gels: a comparative analysis, *Biomaterials*, Vol. 29, Issue 10, 1484-1493
- Guan S, Zhang XL, Lin XM, Liu TQ, Ma XH, Cui ZF (2013) Chitosan/gelatin porous scaffolds containing hyaluronic acid and heparan sulfate for neural tissue

engineering, *Journal of Biomaterials Science, Polymer Edition*, Vol. 24, Issue 8, 999-1014

Guo BL, Ma PX (2014) Synthetic biodegradable functional polymers for tissue engineering: a brief review, *Science China Chemistry*, Vol. 57, Issue 4, 490-500

Gutenwik J, Nilsson B, Axelsson A (2004) Determination of protein diffusion coefficients in agarose gel with a diffusion cell, *Biochemical Engineering Journal*, Vol. 19, Issue 1, 1-7

Hamburger V (1997) Wilhelm Roux: visionary with a blind spot, *Journal of the History of Biology*, Vol. 30, Issue 2, 229-238

Han B, Zhang D, Shao Z, Kong L, Lv S (2013) Preparation and characterization of cellulose acetate/carboxymethyl cellulose acetate blend ultrafiltration membranes, *Desalination*, Vol.311, 80-89

Han R (2013) Formation and characterization of (melamine-TMC) based thin film composite NF membranes for improved thermal and chlorine resistances, *Journal of Membrane Science*, Vol.425-426, 176-181

Hannoun BJM, Stephanopoulos G (1986) Diffusion coefficients of glucose and ethanol in cell-free and cell-occupied calcium alginate membranes, *Biotechnology and Bioengineering*, Vol.28, Issue 6, 829-835

Harrison RG (1907) Observations on the living developing nerve fiber, *Proceedings of the Society for Experimental Biology and Medicine*, Vol. 4, 140-143

Hebrard G, Zeng J, Loubiere K, Effect of surfactants on liquid side mass transfer coefficients: a new insight, *Chemical Engineering Journal*, Vol. 148, Issue 1, 132-138

Henke L, Nagy N, Krull UJ (2002) An AFM determination of the effects of surface roughness caused by cleaning of fused silica and glass substrates in the process of optical biosensor preparation, *Biosensors and Bioelectronics*, Vol. 17, Issues 6-7, 547-555

Hernandez A, Calvo JI, Pradanos P, Tejerina F (1996) Pore size distributions in microporous membranes. A critical analysis of the bubble point extended method, *Journal of Membrane Science*, Vol.112, 1-12

- Hewitt I, Chernyavsky I, Middleton A, Fozard J, Bailey C, Please C, King J, Halliday I, Ward J, Breward C (2008) Multiscale modelling of bioreactors for growing bone tissue, <http://www.maths-in-medicine.org/uk/2008/bioreactors>
- Holzwarth JM, Ma PX (2011) 3D nanofibrous scaffolds for tissue engineering, *Journal of Materials Chemistry*, Vol. 21, 10243-10251, DOI: 10.1039/c1jm10522a
- Hossain MS, Bergstrom DJ, Chen XB (2015) Modelling and simulation of the chondrocyte cell growth, glucose consumption and lactate production within a porous tissue scaffold inside a perfusion bioreactor, *Biotechnology Reports*, Vol. 55, 55-62
- Hossain MS, Chen XB, Bergstrom DJ (2012) Investigation of the *in vitro* culture process for skeletal-tissue-engineered constructs using computational fluid dynamics and experimental methods, *Journal of Biomechanical Engineering*, Vol. 134, Issue 12, 1-11
- Hutmacher DW (2001) Scaffold design and fabrication technologies for engineering tissues – state of the art and future perspectives, *Journal of Biomaterials Science*, Vol. 12, Issue 1, 107-124
- Idris A, Zain NM, Noordin MY (2007) Synthesis, characterization and performance of asymmetric polyethersulfone (PES) ultrafiltration membranes with polyethylene glycol of different molecular weights as additives, *Desalination*, Vol. 207, Issues 1-3, 324-339
- Jamnongwong M, Loubiere K, Dietrich N, Hebrard G (2010) Experimental study of oxygen diffusion coefficients in clean water containing salt, glucose or surfactant: consequences on the liquid-side mass transfer coefficients, *Chemical Engineering Journal*, Vol. 165, Issue 3, 758-768
- Jeon G, Yang SY, Kim JK (2012) Functional nanoporous membranes for drug delivery, *Journal of Materials Chemistry*, Vol. 22, 14814-14834
- Jin R, Hiemstra C, Zhong Z, Feijen J (2007) Enzyme-mediated fast in situ formation of hydrogels from dextran-tyramine conjugates, *Biomaterials*, Vol.28, 2791-2800
- Jin R, Teixeira LSM, Dijkstra PJ, Zhong Z, van Blitterswijk CA, Karperien M, Feijen J (2010) Enzymatically crosslinked dextran-tyramine hydrogels as injectable

scaffolds for cartilage tissue engineering, *Tissue Engineering: Part A*, Vol.16, 2429-2440, DOI: 10.1089/ten.tea.2009.0764

Kang HG, Kim SY, Lee YM (2006) Novel porous gelatin scaffolds by overrun/particle leaching process for tissue engineering applications, *Journal of Biomedical Materials Research Part B Applied Biomaterials*, Vol. 79B, Issue 2, 388-397

Kang TY, Kang HW, Hwang CM, Lee SJ, Park J, Yoo JJ, Cho DW (2011) The realistic prediction of oxygen transport in a tissue-engineered scaffold by introducing time-varying effective diffusion coefficients, *Acta Biomaterialia*, Vol. 7, Issue 9, 3345-3353

Kang Y, Yao Y, Yin G, Huang Z, Liao X, Xu X, Zhao G (2009) A study on the *in vitro* degradation properties of poly(L-lactic acid)/ β -tricalcium phosphate (PLLA/ β -TCP) scaffold under dynamic loading, *Medical Engineering & Physics*, Vol. 31, Issue 5, 589-594

Karageorgiou V, Kaplan D (2005) Porosity of 3D biomaterial scaffolds and osteogenesis, *Biomaterials*, Vol. 26, Issue 27, 5474-5491

Karande TS, Ong JL, Agrawal CM (2004) Diffusion in musculoskeletal tissue engineering scaffolds: design issues related to porosity, permeability, architecture, and nutrient mixing, *Annals of Biomedical Engineering*, Vol. 32, Issue 12, 1728-1743

Kellner K, Liebsch G, Klimant I, Wolfbeis OS, Blunk T, Schulz MB, Gopferich A (2002) Determination of oxygen gradients in engineered tissue using a fluorescent sensor, *Biotechnology and Bioengineering*, Vol. 80, Issue 1, 73-83

Keogh MB, O'Brien FJ, Daly JS (2010) Substrate stiffness and contractile behaviour modulate the functional maturation of osteoblasts on a collagen-GAG scaffold, *Acta Biomaterialia*, Vol. 6, Issue 11, 4305-4313

Khademi R, Mohebbi-Kalhari D, Hadjizadeh A (2014) Computational study of culture conditions and nutrient supply in a hollow membrane sheet bioreactor for large-scale bone tissue engineering, *Journal of Artificial Organs*, Vol. 17, Issue 1, 69-80

- Khaled A-RA, Vafai K (2003) The role of porous media in modeling flow and heat transfer in biological tissues, *International Journal of Heat and Mass Transfer*, Vol.46, 4989-5003
- Khaled EG, Saleh M, Hindocha S, Griffin M, Khan WS (2011) Tissue engineering for bone production – stem cells, gene therapy and scaffolds, *The Open Orthopaedics Journal*, Vol. 5, 289-295
- Khanafer K, Vafai K (2006) The role of porous media in biomedical engineering as related to magnetic resonance imaging and drug delivery, *Heat Mass Transfer*, Vol.42, 939-953, DOI 10.1007/s00231-006-0142-6
- Kim J, der Bruggen BV (2010) The use of nanoparticles in polymeric and ceramic membrane structures: review of manufacturing procedures and performance improvement for water treatment, *Environmental Pollution*, Vol.158, Issue 7, 2335-2349
- Kim J, Ryu S, Ju YM, Yoo JJ, Atala A (2014) Amniotic fluid-derived stem cells for bone tissue engineering, *Perinatal Stem Cells*, 107-114
- Kim JY, Lee JW, Lee SJ, Park EK, Kim SY, Cho DW (2007) Development of a bone scaffold using HA nanopowder and micro-stereolithography technology, *Microelectronic Engineering*, Vol. 84, Issues 5-8, 1762-1765
- Kim S, Cho YI, Hogenauer WN, Kensey KR (2002) A method of isolating surface tension and yield stress effects in a U-shaped scanning capillary-tube viscometer using a Casson model, *Journal of Non-Newtonian Fluid Mechanics*, Vol. 103, Issues 2-3, 205-219
- Kimelman-Bleich N, Seliktar D, Kallai I, Helm GA, Gazit Z, Gazit D, Pelled G (2011) The effect of ex vivo dynamic loading on the osteogenic differentiation of genetically engineered mesenchymal stem cell method, *Journal of Tissue Engineering and Regenerative Medicine*, Vol. 5, Issue 5, 384-393
- Klein E, Holland FF, Donnaud A, Lebeouf A, Eberle K (1977) Diffusive and hydraulic permeabilities of commercially available cellulosic hemodialysis films and hollow fibers, *Journal of Membrane Science*, Vol. 2, 349-364

- Kleinstreuer C, Agarwal SS (1986) Analysis and simulation of hollow-fiber bioreactor dynamics, *Biotechnology and Bioengineering*, Vol. 28, Issue 8, 1233-1240
- Koponen A, Kataja M, Timonen J (1996) Tortuous flow in porous media, *Physical Review E*, Vol. 54, Issue 1, 406-410
- Kwak S, Lafleur M (2003) NMR self-diffusion measurements of molecular and macromolecular species in dextran solutions and gels, *Macromolecules*, Vol. 36, Issue 9, 3189-3195
- Laatikainen M, Heinonen J, Sainio T (2011) Modeling of chromatographic separation of concentrated-acid hydrolysates, *Separation and Purification Technology*, Vol. 80, Issue 3, 610-619
- Langer R (2009) Perspectives and challenges in tissue engineering and regenerative medicine, *Advanced Materials*, Vol. 21, Issue 32-33, 3235-3236
- Langer R, Vacanti JP (1993) Tissue engineering, *Science*, Vol. 260, Issue 5110, 920-926
- Leddy HA, Awad HA, Guilak F (2004) Molecular diffusion in tissue-engineered cartilage constructs: Effects of scaffold material, time, and culture conditions, *Journal of Biomedical Materials Research Part B: Applied Biomaterials*, Vol. 70B, Issue 2, 397-406
- L'Heureux N, Dusserre N, Marini A, Garrido S, de la Fuente L, McAllister T (2007) Technology insight: the evolution of tissue-engineered vascular grafts-from research to clinical practice, *Nature Clinical Practice Cardiovascular Medicine*, Vol. 4, 389-395
- Li CKN (1982) The glucose distribution in 9l rat brain multicell tumor spheroids and its effect on cell necrosis, *Cancer*, Vol. 50, Issue 10, 2066-2073
- Li M, Wang D, Xiao R, Sun G, Zhao Q, Li H (2013) A novel high flux poly(trimethylene terephthalate) nanofiber membrane for microfiltration media, *Separation and Purification Technology*, Vol.116, 199-205
- Li MZ, Li JH, Shao XS, Miao J, Wang JB, Zhang QQ, Xu XP (2012) Grafting zwitterionic brush on the surface of PVDF membrane using physisorbed free radical grafting technique, *Journal of Membrane Science*, Vol.405-406, 141-148

- Li RH, Altreuter DH, Gentile FT (1996) Transport characterization of hydrogel matrices for cell encapsulation, *Biotechnology and Bioengineering*, Vol.50, Issue 4, 365-373
- Li ST, Liu Y, Zhou Q, Lue RF, Song L, Dong SW, Guo P, Branko K (2014) A novel axial-stress bioreactor system combined with a substance exchanger for tissue engineering of 3D constructs, *Tissue Engineering Part C: Methods*, Vol. 20, Issue 3, DOI: 10.1089/ten.tec.2013.0173
- Li X, Zhang G, Xu D, Zhao C, Na H (2007) Morphology study of sulfonated poly (ether ether ketone ketone)s (SPEEKK) membranes: the relationship between morphology and transport properties of SPEEKK membranes, *Journal of Power Sources*, Vol.165, 701-707
- Liabastre AA, Orr C (1978) An evaluation of pore structure by mercury penetration, *Journal of Colloid and Interface Science*, Vol.64, Issue 1, 1-18
- Liang S, Xu J, Weng L, Dai H, Zhang X, Zhang L (2006) Protein diffusion in agarose hydrogel in situ measured by improved refractive index method, *Journal of Controlled Release*, Vol.115, Issue 2, 189-196
- Lin DJ, Chang CL, Chen TC, Cheng LP (2002) Microporous PVDF membrane formation by immersion precipitation from water/TEP/PVDF system, *Desalination*, Vol.145, Issue 1-3, 25-29
- Lindh M, Lindgren K, Carlstrom A, Masson P (1982) Electrochemical interferences with the YSI glucose analyser, *Clinical Chemistry*, Vol. 28, Issue 4, 726-727
- Little RJ, Versteeg GF, van Swaaij WPM (1992) Diffusivity measurements in some organic solvents by a gas-liquid diaphragm cell, *Journal of Chemical & Engineering Data*, Vol. 37, Issue 1, 42-45
- Liu C, Abedian R, Meister R, Haasper C, Hurschler C, Krettek C, Lewinski GV, Jagodzinski M (2012) Influence of perfusion and compression on the proliferation and differentiation of bone mesenchymal stromal cells seeded on polyurethane scaffolds, *Biomaterials*, Vol. 33, Issue 4, 1052-1064
- Liu H, Beauvoit B, Kimura M, Chance B (1996) Dependence of tissue optical properties on solute-induced changes in refractive index and osmolarity, *Journal of Biomedical Optics*, Vol.1, Issue 2, 200-211

- Liu J, Hilderink J, Groothuis TA, Otto C, van Blitterswijk CA, Boer JD (2013) Monitoring nutrient transport in tissue-engineered grafts, *Journal of Tissue Engineering and Regenerative Medicine*, DOI: 10.1002/term.1654
- Liu J, Li P, Li Y, Xie L, Wang S, Wang Z (2009) Preparation of PET threads reinforced PVDF hollow fiber membrane, *Desalination*, Vol.249, Issue 2, 453-457
- Liu Y, Lim J, Teoh SH (2013) Review: development of clinically relevant scaffolds for vascularised bone tissue engineering, *Biotechnology Advances*, Vol. 31, 688-705
- Liu Y, Teoh SH, Chong MSK, Yeow CH, Kamm RD, Choolani M, Chan JKY (2012) Contrasting effects of vasculogenic induction upon biaxial bioreactor stimulation of mesenchymal stem cells and endothelial progenitor cells cocultures in three-dimensional scaffolds under *in vitro* and *in vivo* paradigms for vascularized bone tissue engineering, *Tissue Engineering Part A*, Vol. 19, Issue 7-8, 893-904
- Loeb L (1897) *Über die entstehung von bindegewebe, leukocyten und roten blutkörperchen aus epithel und über eine method, isolierte gewebsteile zu zuchten*, Stern
- Longworth LG (1952) Diffusion measurements, at 1°, of aqueous solutions of amino acids, peptides and sugars, *Journal of the American Chemical Society*, Vol. 74, Issue 16, 4155-4159
- Longworth LG (1953) Diffusion measurements, at 25-degrees, of aqueous solutions of amino acids, peptides and sugars, *Journal of the American Chemical Society*, Vol. 75, Issue 22, 5705-5709
- Lonsdale HK, Merten U, Riley RL (1965) Transport properties of cellulose acetate osmotic membranes, *Journal of Applied Polymer Science*, Vol.9, 1341-1362
- Lu JP, Tan FW, Tang Q, Jiang TC (2013) Novel method for indirect determination of iodine in marine products by atomic fluorescence spectrometry, *Chemical Research in Chinese Universities*, Vol. 29, Issue 1, 26-29
- Madaeni SS, Bakhtiari L (2012) Thermodynamic-based predictions of membrane morphology in water/dimethylsulfoxide/polyethersulfone systems, *Polymer*, Vol.53, Issue 20, 4481-4488
- Maier JS, Walker SA, Fantini S, Franceschini MA, Gratton E (1994) Possible correlation between blood glucose concentration and the reduced scattering

coefficient of tissues in the near infrared, *Optics Letters*, Vol.19, Issue 24, 2062-2064

Malda J, Rouwkema J, Martens DE, le Comte EP, Kooy FK, Tramper J, van Blitterswijk CA, Riesle J (2004a) Oxygen gradients in tissue-engineered PEGT/PBT cartilaginous constructs: measurement and modelling, *Biotechnology and Bioengineering*, Vol. 86, Issue 1, 9-18

Malda J, Woodfield TBF, van der Vloodt F, Kooy FK, Martens DE, Tramper J, van Blitterswijk CA, Riesle J (2004b) The effect of PEGT/PBT scaffold architecture on oxygen gradients in tissue engineered cartilaginous constructs, *Biomaterials*, Vol. 25, Issue 26, 5773-5780

Martin AN (1993) *Physical Pharmacy: physical chemical principles in the pharmaceutical sciences*, Lea and Febiger, Philadelphia, 337

Mauck RL, Hung CT, Ateshian GA (2003) Modeling of neutral solute transport in a dynamically loaded porous permeable gel: implications for articular cartilage biosynthesis and tissue engineering, *Journal of Biomechanical Engineering*, Vol. 125, Issue 5, 602-614

Mauret E, Renaud M (1997) Transport phenomena in multi-particle systems-I. Limits of applicability of capillary model in high voidage beds-application to fixed beds of fibers and fluidized beds of spheres, *Chemical Engineering Science*, Vol. 52, Issue 11, 1807-1817

McCain KS, Schluesche P, Harris JM (2004) Poly(amidoamine) dendrimers as nanoscale diffusion probes in sol-gel films investigated by total internal reflection fluorescence spectroscopy, *Analytical Chemistry*, Vol. 76, Issue 4, 939-946

McDuff RE, Ellis RA (1979) Determining diffusion coefficients in marine sediments: a laboratory study of the validity of resistivity techniques, *American Journal of Science*, Vol.279, 666-675

Meneghello G, Parker DJ, Ainsworth BJ, Perera SP, Chaudhuri JB, Ellis MJ, De Bank PA (2009) Fabrication and characterization of poly(lactic-co-glycolic acid)/polyvinyl alcohol blended hollow fibre membranes for tissue engineering applications, *Journal of Membrane Science*, Vol. 344, 55-61

- Mey-Marom A, Katz MG (1986) Measurement of active pore size distribution of microporous membranes – a new approach, *Journal of Membrane Science*, Vol.27, 119-130
- Mills R (1957) The self-diffusion of chloride ion in aqueous alkali chloride solutions at 25°, *Journal of Physical Chemistry*, Vol.61, Issue 12, 1631-1634
- Misener R, Gari MF, Rende M, Velliou E, Panoskaltsis N, Pistikopoulos EN, Mantalaris A (2014) Global superstructure optimisation of red blood cell production in a parallelised hollow fibre bioreactor, *Computers & Chemical Engineering*, Vol. 71, 532-553
- Miyagi A, Nabetani H, Nakajima M (2012) Analysis of transport mechanism of binary organic solvent system through a PDMS-based dense membrane using a regular solution model combined with a solution-diffusion model, *Separation and Purification Technology*, Vol.88, 216-226
- Mohammadi T, Saljoughi E (2009) Effect of production conditions on morphology and permeability of asymmetric cellulose acetate membranes, *Desalination*, Vol.243, Issue 1-3, 1-7
- Mohebbi-Kalhari D, Behzadmehr A, Doillon CJ, Hadjizadeh A (2012) Computational modeling of adherent cell growth in a hollow-fiber membrane bioreactor for large-scale 3-D bone tissue engineering, *International Journal of Artificial Organs*, Vol. 15, 250-265
- Mohebbi-Kalhari D, Hadjizadeh A (2010) Porous hollow membrane sheet for tissue engineering applications, *Journal of Biomedical Materials Research Part A*, Vol. 93A, Issue 3, 1140-1150
- Mosier NS, Ladisch CM, Ladisch MR (2002) Characterization of acid catalytic domains for cellulose hydrolysis and glucose degradation, *Biotechnology and Bioengineering*, Vol. 79, Issue 6, 610-618
- Morgan SM, Tilley S, Perera S, Ellis MJ, Kanczler J, Chaudhuri JB, Oreffo ROC (2007) Expansion of human bone marrow stromal cells on poly-(DL-lactide-co-glycolide) (P_{DL}LGA) hollow fibres designed for use in skeletal tissue engineering, *Biomaterials*, Vol. 28, 5332-5343

- Nair LS, Laurencin CT (2007) Biodegradable polymers as biomaterials, *Progress in Polymer Science*, Vol. 32, Issues 8-9, 762-798
- Nakao S (1994) Determination of pore size and pore size distribution, *Journal of Membrane Science*, Vol.96, 131-165
- Napoli IED, Scaglione S, Giannoni P, Quarto R, Catapano G (2011) Mesenchymal stem cell culture in convection-enhanced hollow fibre membrane bioreactors for bone tissue engineering, *Journal of Membrane Science*, Vol. 379, Issues 1-2, 341-352
- Napoli IED, Zanetti EM, Fragomeni G, Giuzio E, Audenino AL, Catapano G (2014) Transport modeling of convection-enhanced hollow fiber membrane bioreactors for therapeutic applications, *Journal of Membrane Science*, Vol. 471, 347-361
- Nauth A, McKee MD, Einhorn TA, Watson JT, Li R, Schemitsch EH (2011) Managing bone defects, *Journal of Orthopaedic Trauma*, Vol. 25, Issue 8, 462-466
- Nichol JL, Morozowich NL, Allcock HR (2013) Biodegradable alanine and phenylalanine alkyl ester polyphosphazenes as potential ligament and tendon tissue scaffolds, *Polymer Chemistry*, Vol. 4, 600-606, DOI: 10.1039/c2py20631e
- Nishi M, Matsumoto R, Dong J, Uemura T (2013) Engineered bone tissue associated with vascularization utilizing a rotating wall vessel bioreactor, Vol. 101A, Issue 2, 421-427
- Norimoto M, Ohtori S, Eguchi Y, Inoue G, Orita S, Yamauchi K, Aoki Y, Nakamura J, Ishikawa T, Miyagi M, Kamoda H, Suzuki M, Kubota G, Sakuma Y, Oikawa Y, Inage K, Sainoh T, Sato J, Toyone T, Takahashi T (2014) Teriparatide accelerates lumbar posterolateral fusion in a patient with risk factors for bone fusion: a case report, *Chiba Medical Journal* 90, Issue 2, 7-12
- O'Brien FJ, Harley BA, Yannas IV, Gibson LJ (2005) The effect of pore size on cell adhesion in collagen-GAG scaffolds, *Biomaterials*, Vol. 26, Issue 4, 433-441
- Ochoa NA, Pradanos P, Palacio L, Pagliero C, Marchese J, Hernandez A (2001) Pore size distributions based on AFM imaging and retention of multidisperse polymer solutes: characterisation of polyethersulfone UF membranes with dopes

containing different PVP, Journal of Membrane Science, Vol. 187, Issues 1-2, 227-237

O'Dea RD, Byrne HM, Waters SL (2013) Continuum modelling of *in vitro* tissue engineering: a review, Computational Modeling in Tissue Engineering Studies in Mechanobiology, Tissue Engineering and Biomaterials, Vol. 10, 229-266

Omae H, Sun YL, An KN, Amadio PC, Zhao C (2012) Engineered tendon with decellularized xenotendon slices and bone marrow stromal cells: an *in vivo* animal study, Journal of Tissue Engineering and Regenerative Medicine, Vol. 6, Issue 3, 238-244

Ouerfelli N, Das D, Latrous H, Ammar H, Oliver J (2014) Transport behaviour of the lanthanide $^{152}\text{Eu(III)}$, $^{153}\text{Gd(III)}$ and $^{170}\text{Tm(III)}$ and transplutonium element $^{254}\text{Es(III)}$, $^{244}\text{Cm(III)}$, $^{241}\text{Am(III)}$, $^{249}\text{Cf(III)}$ and $^{249}\text{Bk(III)}$ ions in aqueous solutions at 298 K, Journal of Radioanalytical and Nuclear Chemistry, Vol.300, Issue 1, 51-55

Ouyang L, Randaccio L, Rulis P, Kurmaev EZ, Moewes A, Ching WY (2003) Electronic structure and bonding in vitamin B₁₂, cyanocobalamin, Journal of Molecular Structure: THEOCHEM, Vol. 622, Issue 3, 221-227

Page H, Flood P, Reynaud EG (2013) Three-dimensional tissue cultures: current trends and beyond, Cell and Tissue Research, Vol. 352, Issue 1, 123-131

Palacio L, Pradanos P, Calvo JI, Hernandez A (1999) Porosity measurements by a gas penetration method and other techniques applied to membrane characterization, Thin Solid Films, Vol.348, 22-29

Papenburg BJ, Vogelaar L, Bolhuis-Versteeg LAM, Lammertink RGH, Stamatialis D, Wessling M (2007) One-step fabrication of porous micropatterned scaffolds to control cell behavior, Biomaterials, Vol.28, Issue 11, 1998-2009

Parizek M, Douglas TEL, Novotna K, Kromka A, Brady MA, Renzing A, Voss E, Jarosova M, Palatinus L, Tesarek P, Ryparova P, Lisa V, Santos AMD, Bacakova L (2012) Nanofibrous poly(lactide-co-glycolide) membranes loaded with diamond nanoparticles as promising substrates for bone tissue engineering, International Journal of Nanomedicine, Vol. 7, 1931-1951

- Park DY, Mun CH, Kang E, No DY, Ju J, Lee SH (2014) One-stop microfiber spinning and fabrication of a fibrous cell-encapsulated scaffold on a single microfluidic platform, *Biofabrication*, Vol. 6, 1-7
- Patrick CW, Mikos AG, McIntire LV (1998) Prospects of tissue engineering, *Frontiers in Tissue Engineering*, Elsevier Science Ltd, Oxford, 3-11
- Paulose M, Peng L, Popat KC, Varghese OK, LaTempa TJ, Bao N, Desai TA, Grimes CA (2008) Fabrication of mechanically robust, large area, polycrystalline nanotubular/porous TiO₂ membranes, *Journal of Membrane Science*, Vol. 319, Issues 1-2, 199-205
- Pearson NC, Shipley RJ, Waters SL, Oliver JM (2013) Multiphase modelling of the influence of fluid flow and chemical concentration on tissue growth in a hollow fibre membrane bioreactor, *Mathematical Medicine and Biology*, 1-38, DOI: 10.1093/imammb/dqt015
- Peppas NA, Wright SL (1996) Solute diffusion in poly (vinyl alcohol)/poly (acrylic acid) interpenetrating networks, *Macromolecules*, Vol. 29, Issue 27, 8798-8804
- Peter M, Ganesh N, Selvamurugan N, Nair SV, Furuike T, Tamura H, Jayakumar R (2010) Preparation and characterization of chitosan-gelatin/nanohydroxyapatite composite scaffolds for tissue engineering applications, *Carbohydrate Polymers*, Vol. 80, Issue 3, 687-694
- Petersen EE (1958) Diffusion in a pore of varying cross section, *American Institute of Chemical Engineers Journal*, Vol.4, 343-345
- Phanthong C, Somasundrum M (2003) The steady state current at a microdisk biosensor, *Journal of Electroanalytical Chemistry*, Vol. 558, 1-8
- Pleitez MA, Hertzberg O, Bauer A, Seeger M, Lieblein T, v Lilienfeld-Toal H, Mantele W (2015) Photothermal deflectometry enhanced by total internal reflection enables non-invasive glucose monitoring in human epidermis, *Analyst*, Vol. 140, 483-488, DOI: 10.1039/C4AN01185F
- Pluen A, Netti PA, Jain RK, Berk DA (1999) Diffusion of macromolecules in agarose gels: comparison of linear and globular configurations, *Biophysical Journal*, Vol. 77, Issue 1, 542-552
- Provin C, Takano K, Sakai Y, Fujii T, Shirakashi R (2008) A method for the design of 3D scaffolds for high-density cell attachment and

determination of optimum perfusion culture conditions, *Journal of Biomechanics*, Vol. 41, Issue 7, 1436-1449

Podichetty JT, Bhaskar PR, Singarapu K, Madihally SV (2014) Multiple approaches to predicting oxygen and glucose consumptions by HepG2 cells on porous scaffolds in an axial-flow bioreactor, *Biotechnology and Bioengineering*, DOI: 10.1002/bit.25355

Provin C, Takano K, Sakai Y, Fujii T, Shirakashi R (2008) A method for the design of 3D scaffolds for high-density cell attachment and determination of optimum perfusion culture conditions, *Journal of Biomechanics*, Vol.41, Issue 7, 1436-1449

Rahimpour A, Jahanshahi M, Khalili S, Mollahosseini A, Zirepour A, Rajaeian B (2012) Novel functionalized carbon nanotubes for improving the surface properties and performance of polyethersulfone (PES) membrane, *Desalination*, Vol.286, 99-107

Regional data of the US Scientific Registry for transplant recipients, donor and wait-listed patients from 2000 to 2012, United Network for Organ Sharing, Richmond, Virginia, www.unos.org

Ribeiro ACF, Barros MCF, Verissimo LMP, Lobo VMM, Valente AJM (2014) Binary diffusion coefficients for aqueous solutions of L-aspartic acid and its respective monosodium salt, *Journal of Solution Chemistry*, Vol.43, Issue 1, 83-92

Ribeiro ACF, Ortona O, Simoes SMN, Santos CIAV, Prazeres PMRA, Valente AJM, Lobo VMM, Burrows HD (2006) Binary mutual diffusion coefficients of aqueous solutions of sucrose, lactose, glucose and fructose in the temperature range from (298.15 to 328.15) K, *Journal of Chemical Engineering Data*, Vol.51, 1836-1840

Riedel C, Spohr R (1980) Transmission properties of nuclear track filters, *Journal of Membrane Science*, Vol.7, 225-234

Robinson RA, Stokes RH, *Electrolyte solutions: the measurement and interpretation of conductance, chemical potential and diffusion in solutions of simple electrolytes*, second edition, Butterworths, London, 1959

- Rong Z, Cheema U, Vadgama P (2006) Needle enzyme electrode based glucose diffusive transport measurement in a collagen gel and validation of a simulation model, *The Analyst*, Issue 7, 816-821, DOI: 10.1039/b600334f
- Sachlos E, Czernuszka JT (2003) Making tissue engineering scaffolds work. Review on the application of solid freeform fabrication technology to the production of tissue engineering scaffolds, *European Cells and Materials*, Vol. 5, 29-40
- Sadighi S, Bahmani M, Mohadecy SRS (2013) Effect of pore size distribution and temperature on the catalyst tortuosity, *Chemical Engineering Research Bulletin*, Vol. 16, 61-72
- Sahlin JJ, Peppas NA (1996) Investigation of polymer diffusion in hydrogel laminates using near-field FTIR microscopy, *Macromolecules*, Vol. 29, Issue 22, 7124-7129
- Sanni SA, Hutchison HP (1968) The diaphragm cell method for diffusion measurements at temperatures up to 60°C, *Journal of Physics E: Scientific Instruments*, Vol. 1, Issue 11, 1101-1104
- Schulz RM, Wustneck N, van Donkelaar CC, Shelton JC, Bader A (2008) Development and validation of a novel bioreactor system for load- and perfusion-controlled tissue engineering of chondrocyte-constructs, *Biotechnology and Bioengineering*, Vol. 101, Issue 4, 714-728
- Sequeira SJ, Soscia DA, Oztan B, Mosier AP, Jean-Gilles R, Gadre A, Cady NC, Yener B, Castracane J, Larsen M (2012) The regulation of focal adhesion complex formation and salivary gland epithelial cell organization by nanofibrous PLGA scaffolds, *Biomaterials*, Vol. 33, Issue 11, 3175-3186
- Setiawan L, Wang R, Li K, Fane AG (2011) Fabrication of novel poly(amide-imide) forward osmosis hollow fiber membranes with a positively charged nanofiltration-like selective layer, *Journal of Membrane Science*, Vol.369, Issue 1-2, 196-205
- Shanbhag S, Lee JW, Kotov N (2005) Diffusion in three-dimensionally ordered scaffolds with inverted colloidal crystal geometry, *Biomaterials*, Vol.26, Issue 27, 5581-5585

- Sharma RR, Chellam S (2005) Temperature effects on the morphology of porous thin film composite nanofiltration membranes, *Environmental Science & Technology*, Vol. 39, Issue 13, 5022-5030
- Shaw M, Schy A (1981) Diffusion coefficient measurement by the 'stop-flow' method in a 5% collagen gel, *Biophysical Journal*, Vol. 34, Issue 3, 375-381
- Shen L, Chen Z (2007) Critical review of the impact of tortuosity on diffusion, *Chemical Engineering Science*, Vol.62, 3748-3755
- Sherwood TK, Brian PLT, Fisher RE (1967) Desalination by reverse osmosis, *Industrial and Engineering Chemistry Fundamentals*, Vol.6, Issue 1, 2-12
- Shi C, Wright GJ, Ex-Lubeskie CL, Bradshaw AD, Yao H (2013) Relationship between anisotropic diffusion properties and tissue morphology in porcine TMJ disc, *Osteoarthritis and Cartilage*, Vol.21, 625-633
- Simon KA, Park KM, Mosadegh B, Subramaniam AB, Mazzeo AD, Ngo PM, Whitesides GM (2014) Polymer-based mesh as supports for multi-layered 3D cell culture and assays, *Biomaterials*, Vol. 35, Issue 1, 259-268
- Skalak R, Fox CF (1988) Tissue engineering: proceedings of a workshop held at Granlibakken, Lake Tahoe, CA, New York, 26-29
- Soraruf D, Roosen-Runge F, Grimaldo M, Zanini F, Schweins R, Seydel T, Zhang F, Roth R, Oettel M, Schreiber F (2014) Protein cluster formation in aqueous solution in the presence of multivalent metal ions – a light scattering study, *Royal Society of Chemistry*, Vol.10, 894-902
- Stamatialis DF, Papenburg BJ, Girones M, Saiful S, Bettahalli SNM, Schmitmeier S, Wessling M (2008) Medical applications of membranes: drug delivery, artificial organs and tissue engineering, *Journal of Membrane Science*, Vol. 308, Issues 1-2, 1-34
- Starecki M, Schwartz JA, Grande DA (2014) Evaluation of amniotic-derived membrane biomaterial as an adjunct for repair of critical sized bone defects, *Advances in Orthopedic Surgery*, Vol. 2014, 1-4
- Suhaimi H, Das DB (2015c) Glucose diffusivity in cell-seeded tissue engineering scaffolds, *Chemical Engineering Journal* (submitted)

- Suhaimi H, Wang S, Das DB (2015a) Glucose diffusivity in cell culture medium, *Chemical Engineering Journal*, Vol. 269, 323-327, DOI: 10.1016/j.cej.2015.01.130
- Suhaimi H, Wang S, Thornton T, Das DB (2015b) On glucose diffusivity of tissue engineering membranes and scaffolds, *Chemical Engineering Science*, Vol. 126, 244-256, DOI: 10.1016/j.ces.2014.12.029
- Sukitpaneemit P, Chung TS (2009) Molecular elucidation of morphology and mechanical properties of PVDF hollow fiber membranes from aspects of phase inversion, crystallization and rheology, *Journal of Membrane Science*, Vol.340, Issue 1-2, 192-205
- Sun Z, Tang X, Cheng G (2013) Numerical simulation for tortuosity of porous media, *Microporous and Mesoporous Materials*, Vol. 173, 37-42
- Sweerts JP, Kelly CA, Rudd JW, Hesslein R, Cappenberg TE (1991) Similarity of whole-sediment molecular diffusion coefficients in freshwater sediments of low and high porosity, *Limnology Oceanography*, Vol.36, 335-342
- Tabata Y (2014) Positioning of tissue engineering in regenerative medicine, *Inflammation and Regeneration*, Vol. 34, Issue 1, 1-3
- Tham MK, Walker Jr RD, Modell JH (1973) Diffusion coefficients of O₂, N₂ and CO₂ in fluorinated ethers, *Journal of Chemical and Engineering Data*, Vol.18, Issue 4, 411-412
- Travascio F, Jackson AR, Brown MD, Gu WY (2009) Relationship between solute transport properties and tissue morphology in human annulus fibrosus, *Journal of Orthopaedic Research*, Vol.27, Issue 12, 1625-1630
- Trichet AAP, Foster J, Omori NE, James D, Dolan PR, Hughes GM, Vallance C, Smith JM (2014) Open-access optical microcavities for lab-on-a-chip refractive index sensing, *Lab Chip*, Vol. 14, 4244-4249, DOI: 10.1039/C4LC00817K
- Tsuru T, Toyosada T, Yoshioka T, Asaeda M (2001) Photocatalytic reactions in a filtration system through porous titanium dioxide membranes, *Journal of Chemical Engineering of Japan*, Vol.34, Issue 6, 844-847
- Tuchin VV, Maksimova IL, Zimnyakov DA, Kon IL, Mavlutov AH, Mishin AA (1997) Light propagation in tissues with controlled optical properties, *Journal of Biomedical Optics*, Vol.2, Issue 4, 401-417

- Turhan M, Desai MA, Vadgama P, Mutlu M (1995) Estimation of liquid diffusivities of biosolutes by using diaphragm cell method with defined pore characteristics, *Biotechnology Techniques*, Vol.9, Issue 6, 413-416
- Tyrrell HJV, Harris KR, *Diffusion in liquids: a theoretical and experimental study*, Butterworths, London, 2013
- Uehara S, Hanasaki I, Arai Y, Nagai T, Kawano S (2014) Statistical characterisation of single-stranded DNA motion near glass surface beyond diffusion coefficient, *Micro and Nano Letters*, Vol.9, Issue 4, 257-260
- Ullah H, Ahmed E, Ikram M (2014) Monitoring of glucose levels in mouse blood with noninvasive optical methods, *Laser Physics*, Vol. 24, Issue 2, 1-8, DOI: 10.1088/1054-660X/24/2/025601
- Umecky T, Ehara K, Omori S, Kuga T, Yui K, Funazukuri T (2013) Binary diffusion coefficients of aqueous phenylalanine, tyrosine isomers, and aminobutyric acids at infinitesimal concentration and temperatures from (293.2 to 333.2) K, *Journal of Chemical & Engineering Data*, Vol. 58, 1909-1917
- Van Cappellen P, Gaillard JF (1996) Biogeochemical dynamics in aquatic systems, *Reviews in Mineralogy*, Vol.34, 335-376
- Van Winkle AP, Gates ID, Kallos MS (2012) Mass transfer limitations in embryoid bodies during human embryonic stem cell differentiation, *Cells, Tissues, Organs*, Vol. 196, Issue 1, 34-47, DOI: 10.1159/000330691
- Vargas G, Chan KF, Thomsen SL, Welch AJ (2001) Use of osmotically active agents to alter optical properties of tissue: effects on the detected fluorescence signal measured through skin, *Lasers in Surgery and Medicine*, Vol. 29, Issue 3, 213-220
- Viateau V, Manassero M, Petite H, Logeart-Avramoglou D, Sladkova M, Oudina K, Bensidhoum M (2014) Perfusion bioreactor for engineering bone constructs: bone regeneration in sheep using coral scaffold and autologous mesenchymal stem cells, *The Bone & Joint Journal*, Vol. 96B, Issue 11, 114
- Vindigni V, Abatangelo G, Bassetto F (2011) New developments in tissue engineering of microvascular prostheses (Chapter 21), *Biomaterials Science and Engineering*, InTech publisher

- Wang J, Musameh M (2003) Enzyme-dispersed carbon-nanotube electrodes: a needle microsensor for monitoring glucose, *Royal Society of Chemistry*, Vol.128, 1382-1385, DOI: 10.1039/B309928H
- Wang N, Krishna W, Burugapalli K, Song W, Halls J, Moussy F, Zheng Y, Ma Y, Wu Z, Li K (2013). Tailored fibro-porous structure of electrospun polyurethane membranes, their size-dependent properties and trans-membrane glucose diffusion, *Journal of Membrane Science*, Vol. 427, Issue 5, 207–217
- Wang RK (2000) Modelling optical properties of soft tissue by fractal distribution of scatterers, *Journal of Modern Optics*, Vol.47, Issue 1, 103-120
- Wang S, Liu W, Han B, Yang L (2009) Study on a hydroxypropyl chitosan-gelatin based scaffold for corneal stroma tissue engineering, *Applied Surface Science*, Vol. 255, Issue 20, 8701-8705
- Wang Z, Ma J (2012) The role of nonsolvent in-diffusion velocity in determining polymeric membrane morphology, *Desalination*, Vol. 286, 69-79
- Wartella KA, Wayne JS (2009) Bioreactor for biaxial mechanical stimulation to tissue engineered constructs, *Journal of Biomechanical Engineering*, Vol. 131, Issue 4, Article ID 044501
- Washburn EW (1921) The dynamics of capillary flow, *Physical Review*, Vol.17, Issue 3, 273-283
- Washburn EW (1926) International critical tables of numerical data, physics, chemistry and technology, Vol. 5, 63
- Wendt RP, Shamim M (1970) Isothermal diffusion in the system water-magnesium chloride-sodium chloride as studied with the rotating diaphragm cell, *Journal of Physical Chemistry*, Vol.74, Issue 14, 2770-2783
- Weng L, Liang S, Zhang L, Zhang X, Xu J (2005) Transport of glucose and poly(ethylene glycol)s in agarose gels studies by the refractive index method, *Macromolecules*, Vol.38, 5236-5242
- Weng LH, Liang SM, Zhang L, Zhang XM, Xu J (2005) Transport of glucose and poly(ethylene glycol)s in agarose gels studied by the refractive index method, *Macromolecules*, Vol. 38, Issue 12, 5236-5242

- Westrin BA, Axelsson A (1991) Diffusion in gels containing immobilized cells: a critical review, *Biotechnology and Bioengineering*, Vol. 38, Issue 5, 439-446
- Wilke CR, Chang P (1955) Correlation of diffusion coefficients in dilute solutions, *American Institute of Chemical Engineers Journal*, Vol. 1, Issue 2, 264-270
- Wu X, Li SH, Lou LM, Chen ZR (2013) The effect of the microgravity rotating culture system on the chondrogenic differentiation of bone marrow mesenchymal stem cells, *Molecular Biotechnology*, Vol. 54, Issue 2, 331-336
- Wu X, Liu Y, Li X, Wen P, Zhang Y, Long Y, Wang X, Guo Y, Xing F, Gao J (2010) Preparation of aligned porous gelatin scaffolds by unidirectional freeze-drying method, *Acta Biomaterialia*, Vol. 6, Issue 3, 1167-1177
- Wu YS, van Vliet LJ, Frijlink HW, van der Voort Maarschalk K (2006) The determination of relative path length as a measure for tortuosity in compacts using image analysis, *European Journal of Pharmaceutical Sciences*, Vol. 28, Issue 5, 433-440
- Wung N, Acott SM, Tosh D, Ellis MJ (2014) Hollow fibre membrane bioreactors for tissue engineering applications, *Biotechnology Letters*, Vol. 36, Issue 12, 2357-2366
- Xiong Z, Yan Y, Wang S, Zhang R, Zhang C (2002) Fabrication of porous scaffolds for bone tissue engineering via low-temperature deposition, *Scripta Materialia*, Vol. 46, Issue 11, 771-776
- Xue CH, Wang D, Xiang B, Chiou BS, Sun G (2010) Controlled and high throughput fabrication of poly(trimethylene terephthalate) nanofibers via melt extrusion of immiscible blends, *Materials Chemistry and Physics*, Vol.124, Issue 1, 48-51
- Yang S, Leong KF, Du Z, Chua CK (2001) The design of scaffolds for use in tissue engineering. Part I. Traditional factors, *Tissue Engineering*, Vol. 7, Issue 6, 679-689, DOI: 10.1089/107632701753337645
- Yao L, Cheng H, Luo Q, Zhang W, Zeng S, Tuchin VV (2002) Control of rabbit dura mater optical properties with osmotical liquids, *Society of Photo-Optical Instrumentation Engineers Proceedings* 4536, *International Workshop on Photonics and Imaging in Biology and Medicine*, 147-152, DOI:10.1117/12.462541

- Yaroshchuk A, Martinez-Llado X, Llenas L, Rovira M, de Pablo J (2011) Solution-diffusion-film model for the description of pressure-driven trans-membrane transfer of electrolyte mixtures: one dominant salt and trace ions, *Journal of Membrane Science*, Vol.368, Issues 1-2, 192-201
- Ye H, Das DB, Triffitt JT, Cui Z (2006) Modelling nutrient transport in hollow fibre membrane bioreactors for growing three-dimensional bone tissue, *Journal of Membrane Science*, Vol. 272, Issues 1-2, 169-178
- Ye H, Xia Z, Ferguson DJP, Triffitt JT, Cui Z (2007) Studies on the use of hollow fibre membrane bioreactors for tissue generation by using rat bone marrow fibroblastic cells and a composite scaffold, *Journal of Materials Science: Materials in Medicine*, Vol. 18, Issue 4, 641-648
- Ye X, Farinha JPS, Oh JK, Winnik MA, Wu C (2003) Polymer diffusion in PBMA latex films using a polymerizable benzophenone derivative as an energy transfer acceptor, *Macromolecules*, Vol. 36, Issue 23, 8749-8760
- Yoo EH, Lee SY (2010) Glucose biosensors: an overview of use in clinical practice, *Sensors*, Vol. 10, 4558-4576
- Yu HY, Liu LQ, Tang ZQ, Yan MG, Gu JS, Wei XW (2008) Surface modification of polypropylene microporous membrane to improve its antifouling characteristics in an SMBR: air plasma treatment, *Journal of Membrane Science*, Vol. 311, Issues 1-2, 216-224
- Yui K, Yamazaki N, Funazukuri T (2013) Infinite dilution binary diffusion coefficients for compounds derived from biomass in water at 0.1 MPa and temperatures from (298.2 to 353.2) K, *Journal of Chemical & Engineering Data*, Vol. 58, 183-186
- Zhang Q, Jiang Y, Zhang Y, Ye Z, Tan W, Lang M (2013) Effect of porosity on long-term degradation of poly(ϵ -caprolactone) scaffolds and their cellular response, *Polymer Degradation and Stability*, Vol. 98, Issue 1, 209-218
- Zhang WM, Gaberman I, Ciszowska M (2002) Diffusion and concentration of molecular probes in thermoresponsive poly(N-isopropylacrylamide) hydrogels: Effect of the volume phase transition, *Analytical Chemistry*, Vol. 74, Issue 6, 1343-1348

- Zhang X, Xiao C, Hu X, Bai Q (2013) Preparation and properties of homogeneous-reinforced polyvinylidene fluoride hollow fiber membrane, *Applied Surface Science*, Vol.264, 801-810
- Zhang Y, Wang R, Yi S, Setiawan L, Hu X, Fane AG (2011) Novel chemical surface modification to enhance hydrophobicity of polyamide-imide (PAI) hollow fiber membranes, *Journal of Membrane Science*, Vol.380, Issue 1-2, 241-250
- Zhang Y, Wei H, Yang H, He Y, Wu G, Xie S, Zhu Z, He R (2013) Noninvasive blood glucose monitoring during oral intake of different sugars with optical coherence tomography in human subjects, *Journal of Biophotonics*, Vol. 6, Issue 9, 699-707
- Zhao F, Ma T (2005) Perfusion bioreactor system for human mesenchymal stem cell tissue engineering: dynamic cell seeding and construct development, *Biotechnology and Bioengineering*, Vol. 91, Issue 4, 482-493
- Zhao S, Wang Z, Wei X, Zhao B, Wang J, Yang S, Wang S (2011) Performance improvement of polysulfone ultrafiltration membrane using PANiEB as both pore forming agent and hydrophilic modifier, *Journal of Membrane Science*, Vol.385-386, 252-262
- Zhao SY, Harrison BS (2015) Morphology impact on oxygen sensing ability of Ru(dpp)₃Cl₂ containing biocompatible polymers, *Materials Science and Engineering: C* (in press), DOI: 10.1016/j.msec.2015.04.001
- Zhu W, Wang M, Fu Y, Castro NJ, Fu SW, Zhang LJ (2015) Engineering a biomimetic three-dimensional nanostructured bone model for breast cancer bone metastasis study, *Acta Biomaterialia*, Vol. 14, 164-174

APPENDIX

Matlab code for the mathematical model of the glucose diffusion in hollow fibre membrane bioreactor

```

function HF1

global C_in Pe lambda Da Dm Ds delta R

tic

%%%%%%%%%%%%%%%%%%%%%%%%%%%%%%%%%%%%%%%%%%%%%%%%%%%%%%%%%%%%%%%%%%%%%%%%

m = 1;
Pe = 8.06;
C_in = 1;
Da = 9.93e-03;
Dm = 0.125;
Ds = 0.226;
delta = 1.25;
R = 3.2;
Z0 = 0;
Z1 = 1;

lambda = get_lambda()

RLM = 1;
RMS = 1+delta;

%%%%%%%%%%%%%%%%%%%%%%%%%%%%%%%%%%%%%%%%%%%%%%%%%%%%%%%%%%%%%%%%%%%%%%%%

% Matlab does not render the surface plot well for a uniform mesh in
% z.
% "umz" is a flag variable such that umz = 1 => uniform mesh in z
% and
% umz <> 1 creates a uniformly expanding mesh such that
% z(i+1)-z(i) = ef.(z(i)-z(i-1)) starting with a given z(1)-z(0) =
% dz0.
% Thus z(i) is a sum of a geometric progression.
% Given dz0, Nz, z(Nz)-z(1) the commands below are aimed at finding
% the expansion factor "ef".

Nz = 51;

umz = 1;

if (umz == 1)
    dz = 1/(Nz-1);
    z = (Z0:dz:Z1-dz);
else
    % Starts with a small step dz0 at z=0 and then subsequent steps are
    % a
    % factor "ef" > 0 times the previous step. We need to find "ef" so
    % that

```



```

% z(Nz) = Z1 (or z(Nz)=1 in the standard scaling). This problem is a
% geometric progression, and to find "ef" we use Newton-Raphson
iteration.
%
% First space-step in z - should be quite small
dz0 = 0.1;
% Newton-Raphson method to find expansion factor ef:
%   initial estimate of expansion factor (must not = 1)
ef = 2;
% Tolerance is a measure of the error, smaller=> more accuracy.
tol = 1e-12;
res = fmesh(ef,dz0,Nz,Z1-Z0);
k = 0;
while (k < 100 && abs(res) > tol)
    ef = ef - res/dfmesh(ef,dz0,Nz,Z1-Z0);
    res = fmesh(ef,dz0,Nz,Z1-Z0);
    k = k+1;
end;
% Having found the expansion factor
z = zeros(1,Nz);
z(1) = Z0;
for k = 2:Nz-1
    z(k) = Z0 + dz0*(ef^(k-1)-1)/(ef-1);
end;
end;
z(Nz) = Z1;

%
% Uniform mesh for the lumen,membrane and scaffold in r direction

NrL = 20;
drL = 1/(NrL-1);
rL = (0:drL:RLM);

NrM = 10;
drM = (RMS-RLM)/NrM;
rM = (RLM+drM:drM:RMS);

NrS = 20;
drS = (R-RMS)/NrS;
rS = (RMS+drS:drS:R);

%%%%%%%%%%%%%%%%%%%%%%%%%%%%%%%%%%%%%%%%%%%%%%%%%%%%%%%%%%%%%%%%%%%%%%%%
%%%%%%%%%%%%%%%%%%%%%%%%%%%%%%%%%%%%%%%%%%%%%%%%%%%%%%%%%%%%%%%%%%%%%%%%

% Solving for the lumen, using pde solver pdepe

sol = pdepe(m,@pdex4pde,@pdex4ic,@pdex4bc,rL,z);
cL = sol(:, :, 1);

% use second order accurate approximation for dc/dr at r = 1
cL1 = cL(:,NrL,1);
cLr1 = (3*cL(:,NrL)-4*cL(:,NrL-1)+cL(:,NrL-2))/(2*drL);

% Solving for the membrane and scaffold

% For z=0, cL = 1 does not satisfy the equations.
% At z=0, we impose cM(1)=1 and continuity of cM=cS
% and Dm dcM/dr = Ds dcS/dr at r = 1+delta.

```

```

cS0 = get_cS(rS);
cM = zeros(Nz,NrM);
cS = zeros(Nz,NrS);
for k = 1:Nz
    cM(k,:) = cL1(k) + cLr1(k)*log(rM)/Dm;
    cS(k,:) = (cL1(k) + log((1+delta))*cLr1(k)/Dm)*cS0;
end;

% Setting up variables for display

Nr = NrL+Nrm+NrS;
r = [rL, rM, rS];
c = [cL, cM, cS];
rmx = r(end);

%%%%%%%%%%%%%%%%%%%%%%%%%%%%%%%%%%%%%%%%%%%%%%%%%%%%%%%%%%%%%%%%%%%%%%%%
%%%%%%%%%%%%%%%%%%%%%%%%%%%%%%%%%%%%%%%%%%%%%%%%%%%%%%%%%%%%%%%%%%%%%%%%

npx = 1;
npy = 3;

figure(1)

% Chosen orientation of r and z => transpose of c is being plotted
subplot(npx,npy,1)
surf(z,r,c')
view(110,10)
%shading flat
shading interp
axis([0.9 Z1 0.94 R 0.94 1])
title('c(r,z)')
xlabel('z/Z')
ylabel('r/R')

subplot(npx,npy,2)
cla
hold on
axis([0.94 rmx 0.94 1])
plot(r,c(1,:), 'b')
for k = 1:10:Nz
    plot(r,c(k,:), 'r')
    xlabel('r/R')
    ylabel('c/c0')
end
hold off;

subplot(npx,npy,3)
cla
hold on
for k = 1:5:Nr
    plot(z,c(:,k), 'r')
    xlabel('z/Z')
    ylabel('c/c0')
end
hold off;

toc;

% -----
% -----

```

```

% Determine lambda

function val = get_lambda()
    global Da Dm Ds delta R
    K0d = besselk(0,sqrt(Da)*(1+delta));
    I0d = besseli(0,sqrt(Da)*(1+delta));
    K1R = besselk(1,sqrt(Da)*R);
    I1R = besseli(1,sqrt(Da)*R);
    K1d = besselk(1,sqrt(Da)*(1+delta));
    I1d = besseli(1,sqrt(Da)*(1+delta));
    l1 = (1+delta)*(K1d*I1R - K1R*I1d)*sqrt(Da)*Ds;
    l2 = Dm*(K1R*I0d+K0d*I1R);
    val = Dm*l1/(l2+log(1+delta)*l1);

% Calculate c in scaffold

function val = get_cS(r)
    global Da delta R
    K0d = besselk(0,sqrt(Da)*(1+delta));
    I0d = besseli(0,sqrt(Da)*(1+delta));
    K1R = besselk(1,sqrt(Da)*R);
    I1R = besseli(1,sqrt(Da)*R);
    l1 = K1R*besseli(0,sqrt(Da)*r)+I1R*besselk(0,sqrt(Da)*r);
    l2 = K1R*I0d+I1R*K0d;
    val = l1/l2;

% Calculate dc/dr in scaffold (not used)

function val = get_cSr(r)
    global Da delta R
    K0d = besselk(0,sqrt(Da)*(1+delta));
    I0d = besseli(0,sqrt(Da)*(1+delta));
    K1R = besselk(1,sqrt(Da)*R);
    I1R = besseli(1,sqrt(Da)*R);
    l1 = sqrt(Da)*(K1R*besseli(1,sqrt(Da)*r)-
    I1R*besselk(1,sqrt(Da)*r));
    l2 = K1R*I0d+I1R*K0d;
    val = l1/l2;

% -----

% Routines to calculate the expansion factor for the mesh in
% the z direction. The idea is to solve for x in the geometric
% progression formula  $d \cdot (x^{(N-1)} - 1) / (x - 1) = z$ .
% fmesh evaluates the function  $d \cdot (x^{(N-1)} - 1) - z \cdot (x - 1)$ 
% upon which we wish to find x so that fmesh ~ 0.
% dfmesh is d(fmesh)/dx for the Newton-Raphson iteration.

function val = fmesh(x,d,N,z)
    val = d*(x^(N-1)-1)-z*(x-1);

function val = dfmesh(x,d,N,z)
    val = d*(N-1)*x^(N-2)-z;

% -----

% pdepe routines for PDE in the lumen

```

```
function [c,f,s] = pdex4pde(r,z,u,DuDr)
    global Pe
    c = Pe*(1-r^2);
    f = DuDr(1);
    s = 0;

% -----

% pdepe routine that prescribes lumen concentration at z=0

function u0 = pdex4ic(r)
    global C_in
    u0 = C_in;

% -----

% pdepe routine that prescribes boundary conditions at z=0 and 1

function [p0,q0,p1,q1] = pdex4bc(r0,u0,r1,u1,z)
    global lambda
    p0 = 0;
    q0 = 1;
    p1 = lambda*u1(1);
    q1 = 1;
```